AD-A133 947 DEFORMATION AND FATIGUE OF AIRCRAFT STRUCTURAL ALLOYS 1/2
(U) ROCKWELL INTERNATIONAL THOUSAND OAKS CA SCIENCE
CENTER J A WERT ET AL. JUL 83 SC5254.2FR
UNCLASSIFIED AFOSR-TR-83-0745 F49620-80-C-0030 F/G 11/6 NL

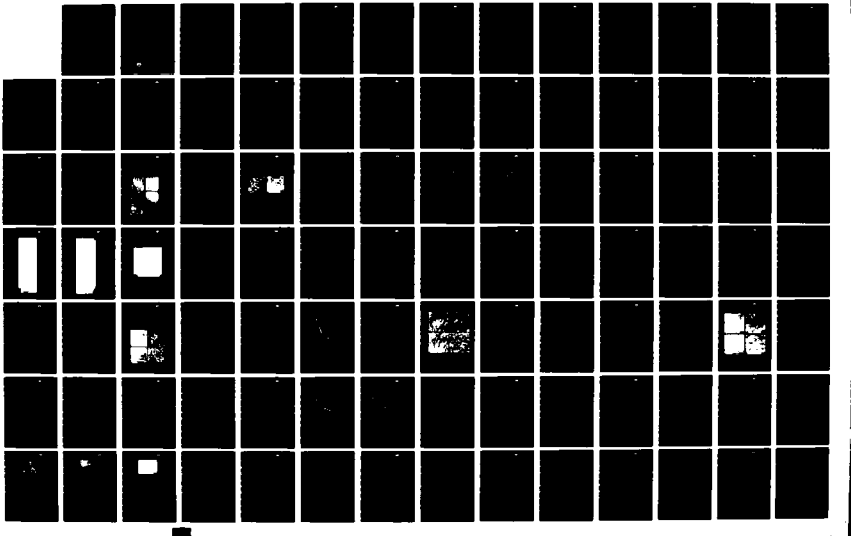

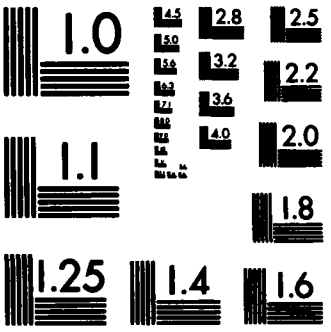

(12)

SC5254.2FR

Copy No. 6

DEFORMATION AND FATIGUE OF AIRCRAFT STRUCTURAL ALLOYS

FINAL REPORT FOR THE PERIOD
January 1, 1980 through December 31, 1982

CONTRACT NO. F49620-80-C-0030

Prepared for

Air Force Office of Scientific Research
Building 410
Bolling AFB, DC 20332

J. A. Wert
J. C. Chesnutt
M. R. Mitchell

JULY 1983

Approved for public release; distribution unlimited

Rockwell International
Science Center

UNCLASSIFIED

SECURITY CLASSIFICATION OF THIS PAGE (When Data Entered)

REPORT DOCUMENTATION PAGE		READ INSTRUCTIONS BEFORE COMPLETING FORM
1. REPORT NUMBER AFOSR-TR- 83-0745	2. GOVT ACCESSION NO. AD-A133947	3. RECIPIENT'S CATALOG NUMBER
4. TITLE (and Subtitle) DEFORMATION AND FATIGUE OF AIRCRAFT STRUCTURAL ALLOYS		5. TYPE OF REPORT & PERIOD COVERED FINAL REPORT No. 1 for the period 01/01/80 - 12/31/82
		6. PERFORMING ORG. REPORT NUMBER SC5254.2FR
7. AUTHOR(s) J. A. Wert, J. C. Chesnutt, M. R. Mitchell		8. CONTRACT OR GRANT NUMBER(s) F49620-80-C-0030
9. PERFORMING ORGANIZATION NAME AND ADDRESS Rockwell International Science Center 1049 Camino Dos Rios Thousand Oaks, CA 91360		10. PROGRAM ELEMENT, PROJECT, TASK AREA & WORK UNIT NUMBERS 2306/A1 61102F
11. CONTROLLING OFFICE NAME AND ADDRESS Air Force Office of Scientific Research Building 410 Bolling AFB, DC 20332		12. REPORT DATE July 1983
		13. NUMBER OF PAGES 46
14. MONITORING AGENCY NAME & ADDRESS(if different from Controlling Office)		15. SECURITY CLASS. (of this report) Unclassified
		15a. DECLASSIFICATION DOWNGRADING SCHEDULE

16. DISTRIBUTION STATEMENT (of this Report)

Approved for public release; distribution unlimited.

17. DISTRIBUTION STATEMENT (of the abstract entered in Block 20, if different from Report)

18. SUPPLEMENTARY NOTES

19. KEY WORDS (Continue on reverse side if necessary and identify by block number)

Titanium, superplastic, fatigue.

20. ABSTRACT (Continue on reverse side if necessary and identify by block number)

This final report describes the results obtained in a basic research program to study two aspects of aircraft structural alloys. In Part I, titanium alloys specifically designed for improved superplastic forming capability have been investigated. The frequently used alloy Ti-6Al-4V displays extensive superplasticity at 927°C, but lower superplastic forming temperatures would be desirable. This study was conducted with the goal of modifying the composition of the Ti-6Al-4V alloy to lower the optimum superplastic forming temperature. Computer modeling results and previous experimental data

DD FORM 1 JAN 73 1473

UNCLASSIFIED

SECURITY CLASSIFICATION OF THIS PAGE (When Data Entered)

suggested that additions to Ti-6Al-4V of beta-stabilizing elements which have high diffusivity in the beta-phase would permit lower superplastic forming temperatures. A series of modified alloys with 2 wt% additions of Fe, Co and Ni was prepared for experimental evaluation. The modified alloys achieved desirable microstructures for superplasticity at 815°C, i.e., the grain size was approximately 5 μm and roughly equal volume fractions of the alpha- and beta-phases were present at the deformation temperature. The superplastic properties of the modified alloys were measured at 815°C. The modified alloys produced values of flow stress, strain rate sensitivity and total elongation at 815°C approaching those of the base Ti-6Al-4V alloy at its standard superplastic forming temperature of 927°C. In addition to lowering the superplastic forming temperature, the β-stabilizing additions also increased room temperature strength levels above those normally found for Ti-6Al-4V. Based on the room temperature and elevated temperature tensile properties, additions of selected beta-stabilizing elements to Ti-6Al-4V simultaneously raise resistance to deformation at room temperature and lower resistance to deformation at elevated temperatures. This reversal in behavior is explained by considering the effect of beta-stabilizer additions on the deformation mechanisms at room temperature and at elevated temperatures.

In Part II of the program, several aspects of fatigue behavior of Ti-6Al-4V have been investigated. The influence of microstructure on low cycle fatigue (LCF) properties have been evaluated. Smooth bar and notched bar LCF properties have been fully evaluated for the three microstructural conditions; the notch fatigue ranking of the three microstructures is different from the smooth bar ranking. Fatigue crack growth behavior of the three microstructural conditions has been measured in both laboratory air and wet air. Only in the case of the recrystallization annealed microstructural condition did humidity have any significant effect on crack propagation behavior.

The low cycle fatigue properties and a microstructural parameter have been used to predict fatigue crack growth behavior of the three microstructural conditions in laboratory air. Excellent agreement between the predicted curve and the experimental data was found for each microstructural condition by using a microstructural parameter which was characteristic of the slip length or deformation character of that particular microstructure. Low cycle fatigue properties have also been used to perform cumulative fatigue damage modeling under spectrum loading conditions. A load spectrum for an F-15 instrument-navigation mission was used to predict fatigue life of smooth and notched specimen configurations.

TABLE OF CONTENTS

TABLE OF CONTENTS

LIST OF ILLUSTRATIONS

LIST OF ILLUSTRATIONS

LIST OF ILLUSTRATIONS

LIST OF ILLUSTRATIONS

LIST OF TABLES

LIST OF TABLES

1. Summary

This final report describes the results obtained in a basic research program to study two aspects of aircraft structural alloys. In Part I, titanium alloys specifically designed for improved superplastic forming capability have been investigated. The frequently used alloy Ti-6Al-4V displays extensive superplasticity at 927°C, but lower superplastic forming temperatures would be desirable. This study was conducted with the goal of modifying the composition of the Ti-6Al-4V alloy to lower the optimum superplastic forming temperature. Computer modeling results and previous experimental data suggested that additions to Ti-6Al-4V of beta-stabilizing elements which have high diffusivity in the beta-phase would permit lower superplastic forming temperatures. A series of modified alloys with 2 wt% additions of Fe, Co and Ni was prepared for experimental evaluation. The modified alloys achieved desirable microstructures for superplasticity at 815°C, i.e., the grain size was approximately 5 μm and roughly equal volume fractions of the alpha- and beta-phases were present at the deformation temperature. The superplastic properties of the modified alloys were measured at 815°C and 871°C. The modified alloys produced values of flow stress, strain rate sensitivity and total elongation at 815°C approaching those of the base Ti-6Al-4V alloy at its standard superplastic forming temperature of 927°C. In addition to lowering the superplastic forming temperature, the β-stabilizing additions also increased room temperature strength levels above those normally found for Ti-6Al-4V. Based on the room temperature and elevated temperature tensile properties, additions of selected beta-stabilizing elements to Ti-6Al-4V simultaneously raise resistance to deformation at room temperature and lower resistance to deformation at elevated temperatures. This reversal in behavior is explained by considering the effect of beta-stabilizer additions on the deformation mechanisms at room temperature and at elevated temperatures.

In part II of the program, several aspects of fatigue behavior of Ti-6Al-4V have been investigated. The influence of microstructure on low cycle fatigue (LCF) properties has been evaluated. Smooth bar and notched bar LCF properties have been fully evaluated for the three microstructural conditions;

the notch fatigue ranking of the three microstructures is different from the smooth bar ranking. Fatigue crack growth behavior of the three microstuctural conditions has been measured in both laboratory air and wet air. Only in the case of the recrystallization annealed microstructural condition did humidity have any significant effect on crack propagation behavior.

The low cycle fatigue properties and a microstructural parameter have been used to predict fatigue crack growth behavior of the three microstructural conditions in laboratory air. Excellent agreement between the predicted curve and the experimental data was found for each microstructural condition by using a microstructural parameter which was characteristic of the slip length or deformation character of that particular microstructure. Low cycle fatigue properties have also been used to perform cumulative fatigue damage modeling under spectrum loading conditions. A load spectrum for an F-15 instrument-navigation mission was used to predict fatigue life of smooth and notched specimen configurations.

2. Introduction

This final report describes results obtained during the course of a two-part basic research program addressing problems of airframe structural materials. Both areas of investigation concentrated on deformation of α-β titanium alloys. In Part I, superplasticity of two-phase titanium alloys was investigated, with the goal of improving the superplastic forming capabilities through alloy modifications. Part II of this program concentrated on understanding the early stages of fatigue crack initiation and propagation in titanium alloys.

A basic understanding of the deformation of the individual α and β phases in titanium alloys can lead to optimization of deformation processing of titanium alloys. The goal of Part I of this rsearch program was to modify the composition of a Ti-6Al-4V* base alloy for improved superplastic forming capability, while maintaining adequate room temperature strength. Thus, the program sought to enhance superplastic formability, and to improve room temperature strength of an α - β titanum alloy. Although this sort of optimization is frequently impossible, there was reason to believe that improvements could be obtained in both areas. Enhanced superplastic forming capability can be achieved by alloy modifications that increase the volume fraction of β phase, and that increase the rates of creep processes that contribute to superplastic deformation. At the same time, solid solution strengthening of both α and β phases can achieve higher room temperature strength.

Experiments conducted during the first year of this program showed that modest additions of certain β-stabilizing elements to the base Ti-6Al-4V alloy produce approximately equal volume fractions of α and β phases at 815°C (1500°F). This is the same phase mixture present int he base alloy at the usual forming temperature of 927°C (1700°F). Based on this work, six modified alloy compositions were produced in sheet form. In the second year of the program, the superplastic properties of the modified alloys were evaluated at several temper-

*Except were specified, compositions are given in weight percent.

atures. Two of the modified alloys have superplastic properties at 815°C that are very similar to the superplastic properties of the base alloy at the usual forming temperature of 927°C. The room temperature tensile properties of the modified alloys have also been measured. In all cases, the modified alloys have yield strengths higher than that of the base alloy; the ductilities are slightly lower, as would be expected.

In the third year of this program, efforts on Part I were devoted to completion of room temperature tensile testing, computer modeling of the superplastic flow properties, and investigation of cavitation during superplastic forming. The computer modeling results are particularly interesting because they resolve a controversial aspect of alloy selection for enhanced superplastic properties. There was uncertainty about the relative importance of β-phase stabilization and high diffusivity of the β-stabilizers in producing enhanced superplasticity. The computer modeling results show that both β-phase stabilization and high diffusivity are needed, but that the diffusivity makes the largest contribution to enhanced superplasticity in the alloys used in this investigation.

In Part II, a similar approach of employing fundamental knowledge of the deformation of α - β titanium alloys was utilized in understanding the early stages of fatigue crack initiation and propagation in titanium alloys. Considerable understanding of mechanical deformation of titanium alloys has been generated under previous AFOSR sponsorship and could be applied in the current program to problems involving fatigue crack initiation and propagation. One example is modeling aimed at predicting fatigue crack propagation (FCP) from low-cycle fatigue (LCF) properties and a microstructural parameter. Selection of such a microstructural parameter required knowledge of the deformation behavior of each microstructural condition. A cumulative damage approach to fatigue life prediction has also reached a stage of considerable reliability in its application to steel and aluminum structural materials. However, this approach has not previously been applied to titanium alloys, partly because of the relative complexity of these alloy systems, and partly because the understanding

of the mechanical deformation of titanium alloys was not available. Much of the fatigue life of aircraft structures is consumed in the early stages of initiation and propagation at very low growth rates. For this reason, a study of this regime of fatigue behavior is of extreme importance in predicting the life of real structures. Of further importance is a means by which life can be predicted under spectrum loading conditions, and the modeling approach described in this report is precisely the type which can be used under conditions of varying load always encountered in service.

3. Part I - Enhanced Superplasticity and Strength in Modified Ti-6Al-4V Alloys

3.1 Background

Ti-6Al-4V is superplastic at temperatures between approximately 875°C and 950°C [1]. Full scale components of this alloy are frequently formed at temperatures near 927°C, where the α- and β-phases coexist in approximately equal volume fractions. Partitioning of the substitutional alloying elements between the α- and β-phases slows grain coarsening when substantial volume fractions of both phases are present [2]. At higher temperatures, the volume fraction of α-phase is lower, allowing more rapid grain coarsening. As a result of rapid grain coarsening, superplastic properties of Ti-6Al-4V degrade as the forming temperature increases above 927°C. At temperatures substantially below 927°C, the deformation processes that produce superplastic behavior do not proceed sufficiently rapidly to permit superplasticity. Consequently, superplasticity in Ti-6Al-4V occurs only in the temperature range where the α- and β-phases are present in similar volume fractions, and where creep temperature deformation processes proceed at sensible rates. Similar observations have been made for other alloys with duplex microstructures [3-6].

Lower superplastic forming temperatures would be desirable for a number of reasons, among them reduced oxidation, shorter forming cycle times, and lower cost die materials. Alloy modifications designed to lower the optimum superplastic forming temperature of Ti-6Al-4V must alter two characteristics of the alloy [7]. First, a substantial volume fraction of β-phase is required for superplastic deformation of titanium alloys [8,9]. Consequently, alloy additions should stabilize the β-phase, thereby increasing the volume fraction of β-phase at temperatures below the conventional superplastic forming temperature. Second, the creep processes essential to superplastic deformation proceed too slowly at temperatures substantially below 927°C for superplasticity to occur at reasonable strain rates. Alloy additions with high diffusivity accelerate the rates of processes that compose superplastic deformation [4]. Based on these arguments, additions of strong β-stabilizers with rapid diffusion rates to Ti-6Al-4V are expected to lower the optimum superplastic forming temperature of this alloy.

Previous investigations of lowering superplastic forming temperatures for titanium alloys have been conducted by Paton and Hall [7] and by Hammond [4]. Paton and Hall studied the effect of Fe additions to Ti-6Al-4V on superplastic properties, as well as room temperature strength. Their results showed, for example, that addition of 2 wt% Fe to Ti-6Al-4V lowered the flow stress required for deformation at 871°C and at a strain rate of 2×10^{-4} s^{-1}. They also found that addition of the slowly diffusing element Mo to Ti-6Al-4V substantially increased the flow stress required for deformation under the same conditions. Hammond reported the effect of different levels of Co and Ni additions to Ti-6Al-4V on superplastic properties at 750°C [4]. He showed that increasing the level of Co or Ni addition from 0.25 wt% to 2.0 wt% enhanced the superplastic properties. Not only was the flow stress lower for larger Co and Ni additions, the slope of the log (flow stress) vs log (strain rate) curve increased. Hammond suggested that these effects are due to the enhanced mass transport rates produced by the addition of elements with high diffusivities.

This contract report describes the results of a study of composition modifications to Ti-6Al-4V to achieve the following goals:

1. An alloy that is superplastically formable at 815°C at flow stresses and strain rates comparable with those used for Ti-6Al-4V at 927°C

2. An alloy with room temperature yield strength after forming at least equivalent to the yield strength of Ti-6Al-4V before forming.

To achieve these goals, several β-stabilizing elements were added to the Ti-6Al-4V base alloy. The superplastic properties of the modified alloys were measured at various temperatures and microstructural observations were used to interpret the superplastic properties. Room temperature tensile properties were measured for both as-received material and material annealed at the superplastic forming temperature. Section 3.3 of this report contains results

of these tests and observations while Section 3.4 includes a discussion of the effect of the β-stabilizing additions on the temperature dependence of flow stress.

3.2 Experimental Procedures

Six modified Ti-6Al-4V compositions were cast by TIMET for this investigation. Two additional alloys (#5412 and #5483) were provided by TIMET for use on this program. These alloys had been produced for a previous investigation, permission for their inclusion in this program was granted by TIMET. Table I shows the compositions of the modified alloys and of a Ti-6Al-4V alloy that was used for comparison. The 7 kg ingots were broken down in the conventional manner and were finish rolled in the α- plus β-phase field to produce a fine mixture of equiaxed α and β grains. The additional β stabilizers lower the β-transus of the modified alloys, requiring lower finish rolling temperatures than are conventionally used for Ti-6Al-4V. The final sheet thickness was approximately 1.3 mm for each of the alloys.

Table I

Alloy Compositions*

Heat Number	Alloy Designation	Al	V	Fe	Co	Ni
5412	Base	5.94	4.01	0.06	0.07	0.09
5914	Base + 2Fe (5914)	5.86	3.92	2.30	0.01	<0.01
5483	Base + 2Fe (5483)	5.97	4.05	2.00	0.01	0.01
5992	Base + 2Co	5.85	3.98	0.09	2.10	0.01
5993	Base + 2Ni	5.78	3.88	0.08	0.01	2.10
5918	Base + 1Fe + 1Co	5.95	3.90	1.41	1.00	0.08
5107	Base + 1Fe + 1Ni	5.99	3.92	1.44	0.01	1.07
5994	Base + 1Co + 1Ni	6.06	4.11	0.10	1.06	1.06

*Weight percent

Microstructural analysis was carried out on specimen coupons annealed at superplastic forming temperatures. The coupons were enclosed in evacuated silica capsules to avoid contamination during heat treatment, and were water quenched to retain the microstructural features present at the annealing temperature. Standard metallographic preparation and analysis methods were used.

Two types of high temperature tensile tests were conducted to determine the superplastic properties of the modified alloys. The tests were performed in a vacuum of 10^{-4} torr or less using specimens with dimensions: gage length = 12.7 mm, width = 7.9 mm, thickness = full sheet thickness, approximately 1.3 mm. The dependence of flow stress on strain rate was determined using step strain rate tests, discussed in detail by previous investigators [11]. The strain rate was varied from 2×10^{-5} s^{-1} to 2×10^{-2} s^{-1} in the step strain rate tests, resulting in a total accumulated strain of less than 0.5 during the entire test. Data from the step strain rate tests were collected and analysed by computer. In the second type of high temperature tensile test, total elongation to failure was measured for constant strain rate deformation. During these computer-controlled tests, the crosshead displacement rate was adjusted to maintain a constant strain rate. Total elongation was measured from the failed specimens after completion of testing.

Room temperature tensile properties were measured for the modified alloys in the as-received condition, and after annealing cycles designed to produce elevated temperature exposure typical of superplastic forming cycles. Annealing treatments for room temperature tensile specimens were carried out in a vacuum furnace in a vacuum less than 10^{-5} torr. Upon completion of the anneal, the furnace was removed from the evacuated silica tube and the specimens radiantly cooled. The room-temperature tensile specimens had dimensions: gage length = 50.8 mm, gage width = 12.7 mm and thickness = full sheet thickness. These tests were conducted at a crosshead displacement rate of 8.5×10^{-6} $m \cdot s^{-1}$, giving an initial strain rate of 1.7×10^{-4} s^{-1}.

3.3 Results

3.3.1 Selection of β-Stabilizing Additions

As discussed in the introduction, alloy additions designed to lower the optimum superplastic forming temperature should satisfy two criteria.

1. The alloy addition should stabilize the β-phase.
2. The alloy addition should have high diffusivity in β-Ti.

The importance of each factor was studied by a computer modeling method originally developed by Hamilton, Ghosh and Mahoney [8]. The purpose of the model was to calculate the effects of β-phase stabilization and diffusivity on the flow stress-strain rate relationship. The modeling approach is fully described by the original investigators and will only be discussed briefly here.

The flow stress-strain rate behavior of each phase is assumed to be represented by the Ashby-Verrall model [12] as follows:

$$\dot{\varepsilon} = \frac{100\Omega D_v}{kTd^2}\left(\sigma - \frac{0.72\Gamma}{d}\right)\left(1 + \frac{3.3\delta D_b}{dD_v}\right) + \frac{AD_vGb}{kT}\left(\frac{\sigma}{G}\right)^n \qquad (1)$$

$\dot{\varepsilon}$ = strain rate
Ω = atomic volume
σ = applied stress
d = grain size
D_v = bulk diffusivity
D_b = grain boundary diffusivity
δ = grain boundary width
Γ = grain boundary energy
G = shear modulus
b = Burgers vector

n,A = constants
T = temperature

To represent the behavior of the two-phase alloy, Hamilton et al showed that the iso-strain rate assumption closely matched experimental results. Thus, it is further assumed that

$$\dot{\varepsilon}_{total} = \dot{\varepsilon}_{\alpha} = \dot{\varepsilon}_{\beta} \tag{2}$$

and that

$$\sigma_{total} = f_v^{\alpha}\sigma_{\alpha} + f_v^{\beta}\sigma_{\beta} \quad , \tag{3}$$

Using Eqs. (1) to (3), the flow stress-strain rate behavior for the two-phase mixture can be calculated.

Values used in the calculation are listed in Table II. These values are the same as those chosen by Hamilton et al, except the diffusivities at various temperatures were calculated from the values of D_0 and Q in the usual manner. Following the approach of Hamilton et al, grain boundary diffusivities were calculated using $Q_b = 0.6\ Q_v$ and $(D_0)_b = 0.5\ (D_0)_v$, where the subscript b denotes a grain boundary property and the subscript v denotes a bulk property.

Figure 1 shows results of the calculations employing the Ashby-Verrall model. In the figure, curves illustrating the flow stress-strain rate relationship for several different combinations of temperature, volume fraction β-phase and diffusivity are shown. The lowest curve is the calculated dependence of σ on $\dot{\varepsilon}$ for Ti-6Al-4V at 927°C (1200K) where the volume fraction of β-phase is 0.5. When the temperature is lowered to 815°C (1088K), the volume fraction β-phase decreases to approximately 0.2 and the diffusivities decrease; these changes raise the flow stress for each $\dot{\varepsilon}$, producing the highest curve on Fig. 1. To determine the importance of volume fraction of β-phase and diffusivity on the flow stress-strain rate relationship, each factor was varied as shown in the key on the figure while the temperature was fixed at 815°C (1088K).

Table II
Values Used in the Ashby-Verrall Model

Parameter	Alpha Phase	Beta Phase	Units	Reference
D_v at 927°C	2.7×10^{-16}	8.6×10^{-14}	m^2/s	[13]
D_v at 815°C	4.7×10^{-17}	2.2×10^{-14}	m^2/s	See Text
D_b at 927°C	1.2×10^{-13}	8.3×10^{-11}	m^2/s	[13]
D_b at 815°C	4.2×10^{-14}	3.7×10^{-12}	m^2/s	See Text
b	3.0×10^{-10}	3.0×10^{-10}	m	[8]
δ	6.0×10^{-10}	6.0×10^{-10}	m	[8]
Ω	1.7×10^{-29}	3.5×10^{-1}	m^3/mol	[8]
Γ	3.5×10^{-1}	3.5×10^{-1}	N/m	[8]
G	2.9×10^{12}	2.9×10^{12}	N/m^2	[8]
N	4.85	3.78	-	[8]
A	5.5×10^{11}	5.6×10^{6}	-	[8]
d	5×10^{-6}	5×10^{-6}	m	[8]

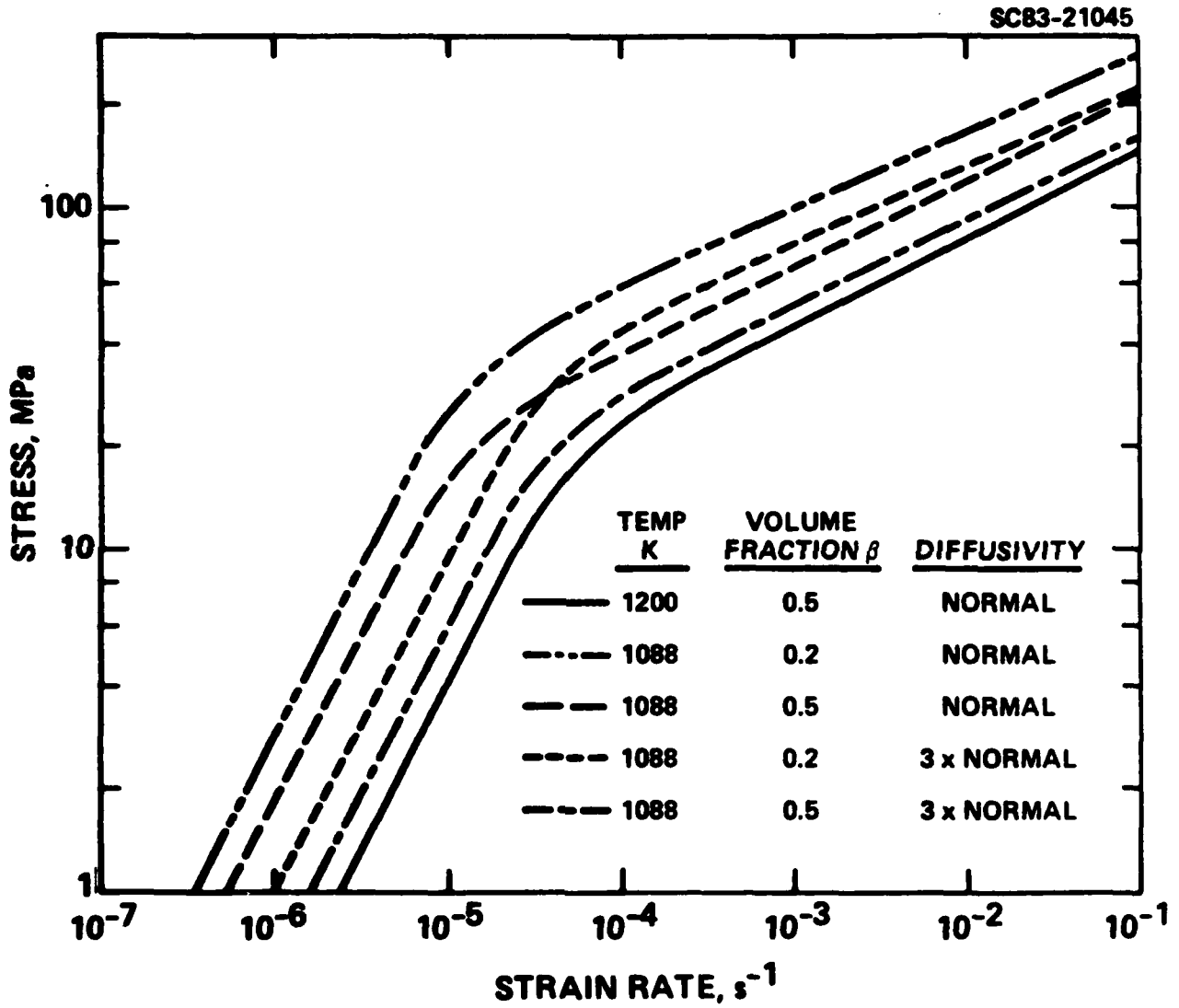

Fig. 1 Calculated flow stress dependence on strain rate for a two-phase Ti alloy. Temperature, β-phase volume fraction and diffusivity were varied as shown on the figure to produce the separate curves.

In one case, the volume fraction of β-phase was increased from 0.2 to 0.5 while the diffusivity values for 815°C (1088K) were retained. A second curve depicts the results for a β-phase volume fraction of 0.2 but an increase in all diffusivity values by a factor of 3.* The third intermediate curve shows the combined effects of β-stabilization and increasing diffusivity.

For the parameters chosen for this series of calculations, the transition from dislocation creep to boundary sliding/diffusional creep occurs at a strain rate between 10^{-5} and 10^{-4} s^{-1}. For strain rates above this transition, β-phase stabilization lowers the flow stress more than the 3-fold increase in diffusivity. In contrast, the 3-fold increase in diffusivity appears to be more effective than β-phase stabilization at lowering the flow stress for strain rates below the transition. For smaller increases in diffusivity, the contributions of enhanced diffusivity and β-phase stabilization are nearly equal. These results demonstrate that both β-phase stabilization and enhanced diffusivity are important in selecting alloy additions to lower the optimum superplastic forming temperature.

The intent of these calculations was to try to establish which alloying element characteristics are important to lower superplastic forming temperatures, not to determine assumptions or parameters providing the best fit with experimental data. Several of the assumptions are crude, for example, assuming parallel, noninteracting diffusive fluxes of Ti and the β-stabilizing elements; ignoring the segregation of β-stabilizing elements to the β-phase and ignoring the presence of Al and V. However, the calculations did serve their purpose of establishing the importance of both β-phase stabilization and enhanced diffusivity in lowering the optimum superplastic forming temperature.

*The factor of 3 was chosen by the following arguments. Beta-stabilizing elements such as Fe, Co and Ni have diffusivities 25 to 90 times higher than Ti in β-Ti. Additions of 1 to 4% of these elements to Ti-6Al-4V were studied in this investigation. Assuming parallel, noninteracting diffusional fluxes of Ti and the β-stabilizing elements in β-Ti, the total flux could be increased 1.25 to 4.5 times by addition of the β-stabilizers.

Figure 2 shows characteristics of candidate alloy additions that pertain to β-phase stabilization and β-phase diffusivity. Depression of the β-transus of Ti per atom percent addition of alloying element was used as a measure of β-stabilizing effectiveness [14]. From Fig. 2, it can be seen that additions of Ni, Fe, Cr, Co and Nb provide more depression of the β-transus than V, with Ni being more potent in this respect than the other elements. Tracer diffusivity of alloying elements in β-Ti, extrapolated to 815°C, was used to assess diffusivity enhancement [15-17]. Figure 2 shows the extrapolated tracer diffusivity at 815°C for each of the candidate alloy additions. As shown in the figure, Ni, Co, Fe, Cr and Cu have more rapid diffusivities in β-Ti than other elements on this list. By combining the two selection criteria, the elements Fe, Co and Ni were selected as the most promising alloying additions to Ti-6Al-4V for the purpose of lowering the optimum superplastic forming temperature.

The size of the Fe, Co and Ni required to significantly lower the optimum superplastic forming temperature of Ti-6Al-4V was established using arc-melted buttons of various compositions. After homogenization, specimens of each alloy were annealed at 871°C and 815°C for 24 hr, then water quenched. Optical metallography was used to determine the volume fraction of β-phase as a function of alloy composition and annealing temperature.

Results from these arc-melted alloys (presented in detail in Ref. 18) showed that a 2 wt% addition of either Fe, Co or Ni to the base alloy, Ti-6Al-4V, was sufficient to stabilize a β-phase volume fraction of approximately 0.5 at 815°C. Based on these results, six ingots were cast and processed as previously described. The chemical composition of the six alloys is shown in Table I. During the final year of this program, a second Ti-6Al-4V-2Fe alloy was provided by TIMET for analysis. The two Base + 2Fe alloys were used to assess the effect of microstructure on superplasticity in the modified alloys. These two alloys will be distinguished by heat number throughout this report.

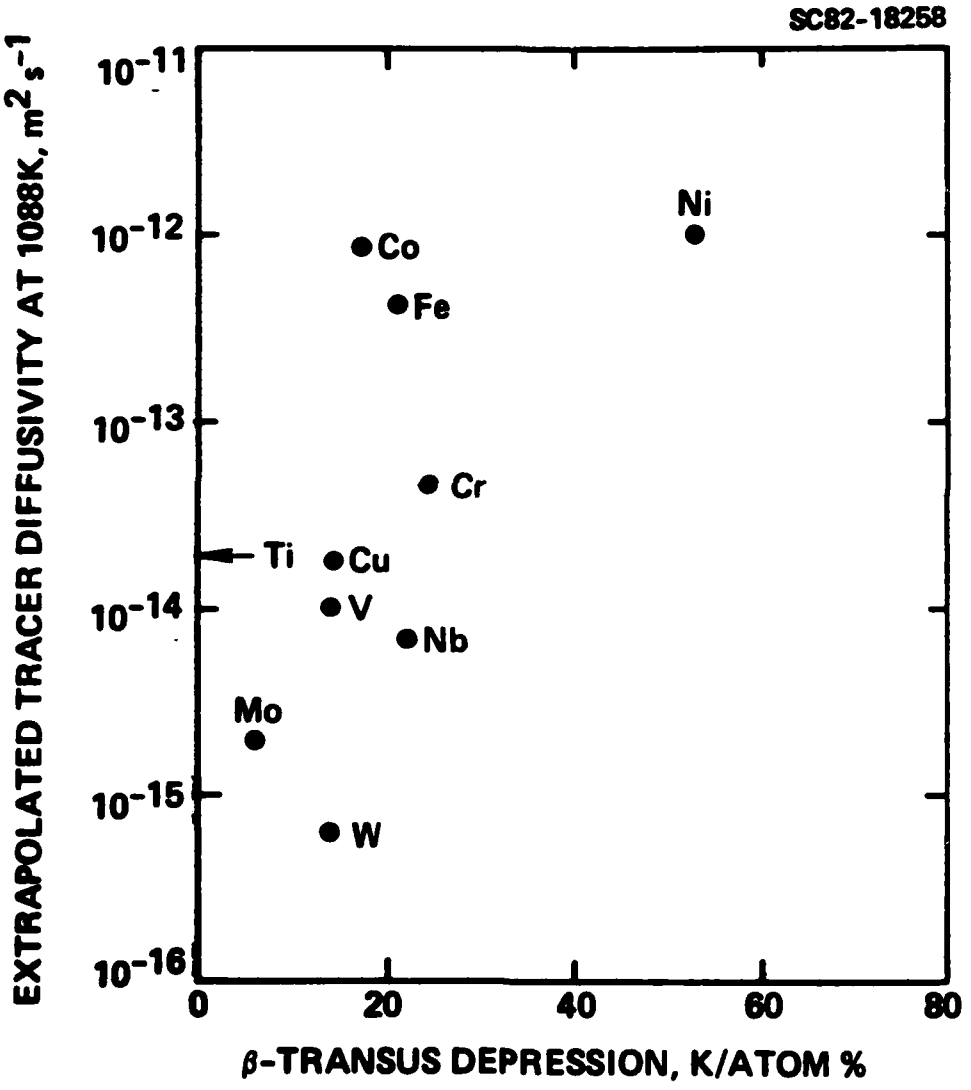

Fig. 2 Extrapolation tracer diffusivity and β-transus depression for various β stabilizing elements in Ti.

3.3.2 Microstructure of the Modified Alloys

The modeling results presented in the previous section, combined with the results of other investigators, show that volume fraction of β-phase and the morphology of the α- and β-phases are among the factors that control superplastic properties [8,11,19,20]. To determine the effect of temperature on phase morphology and β phase volume fraction, (f_v^β), specimens of each alloy were annealed for 1 hr at selected temperatures, and water quenched. The resulting microstructures are similar to microstructures present during the early stages of superplastic forming operation.

Table III lists f_v^β and the mean linear intercept phase sizes (λ^α and λ^β) of the α- and β-phases for each of the modified alloys [21]. Attempts to measure the mean linear intercept grain size did not produce accurate results because the prior β-β grain boundaries could not be reliably located in the transformed β microstructures. The mean linear intercept grain size is always equal to or smaller than the mean linear intercept phase size, so the values of λ^α and λ^β listed in Table III represent upper limits for the grain size.

Table III

Microstructural Characteristics of the Base and Modified Alloys as a Function of Temperature

Alloy	927°C			871°C			815°C		
	f_v^β	λ^α μm	λ^β μm	f_v^β	λ^α μm	λ^β μm	f_v^β	λ^α μm	λ^β μm
Base	0.57	9.0	12	0.38	9.3	5.7	0.22	16	4.6
Base + 2Fe (5914)	-	-	-	-	-	-	-	-	-
Base + 2Fe (5483)	1.00	-	-	0.78	3.5	8.6	0.49	4.0	4.1
Base + 2Co	0.94	4.0	63	0.66	4.1	8.0	0.49	4.3	4.1
Base + 2Ni	0.91	3.5	35	0.65	5.1	9.6	0.47	6.1	5.4
Base + 1Fe + 1Co	1.00	-	-	0.75	3.4	10.0	0.43	3.5	2.7
Base + 1Fe + 1Ni	0.85	3.4	20	0.70	3.8	8.8	0.50	4.2	4.2
Base + 1Co + 1Ni	0.86	3.6	22	0.58	4.5	6.2	0.46	3.4	2.9

Volume Fraction β Phase

The β-phase volume fraction results show that the additions of β-stabilizing elements to Ti-6Al-4V produce approximately equal volume fractions of the α- and β-phases at 815°C. Based on the β-transus depression effects (Fig. 2), the 2 wt% Ni addition was expected to stabilize a larger volume fraction of β-phase than similar additions of either Fe or Co. However, this trend is not reflected in the results listed in Table III for additions of these elements to Ti-6Al-4V. Although depression of β-transus in binary alloys is useful for selection of candidate β-stabilizing additions, the transus depression results cannot be used to predict the volume fraction of β-phase that will be present when the β-stabilizers are added to complex alloys.

There are two possible explanations for the differences observed in β-transus depression and volume fraction results. One explanation stems from possible interactions between alloying elements when β-stabilizers are added to Ti-6Al-4V. If this explanation is correct, volume fraction measurements in binary alloys would correlate with the β-transus depression results shown in Fig. 2. Since β-phase volume fractions were not measured in binary alloys, we are unable to test this explanation. A second explanation arises from the basic differences in the way β-phase stabilization potential is measured. Depression of the β-transus and β-phase volume fraction may measure somewhat different characteristics of β-stabilizing elements. For example, solubility of the β-stabilizer in the α-phase obviously influences f_v^β but does not have a substantial effect on β-transus depression. Volume fraction measurements in binary alloys would also permit evaluation of this explanation.

Phase Size

In addition to β-phase volume fraction, the grain size or phase size is an important factor in superplastic deformation [1,4,11,20]. Table III shows the mean linear intercept phase sizes for each alloy as a function of annealing temperature. At 815°C, the modified alloys all have values of λ^α and λ^β below 7 μm and many values are below 5 μm. Superplasticity has been demonstrated in several titanium alloys when processed to similar α and β grain sizes [4]. The β-phase

volume fraction measurements combined with the mean linear intercept phase sizes indicate that the microstructural conditions required for superplastic deformation at 815°C have been achieved in this set of modified alloys.

Although the mean linear intercept phase sizes at 815°C are near 5 μm, the values of λ^{β} at 927°C are substantially larger. This is more a reflection of the low volume fraction of α-phase at 927°C than of massive β-phase grain growth. As the volume fraction of α decreases, the mean linear intercept β-phase size increases, independent of the β grain size. When the volume fractions of α- and β-phases are nearly equal, the value of λ is close to the grain size in this set of alloys. However, when the volume fraction of α is low, the mean linear intercept β-phase size may be substantially larger than the β grain size.

Phase Morphology

Phase morphology is important to superplastic properties [11-20]. Figure 3 shows the rolling plane microstructures of the base alloy and six of the modified alloys after annealing 1 hr at 815°C and water quenching. The base alloy contains a β-phase volume fraction of only 0.22 after this treatment, primary α grains occupy most of the microstructure. The base alloy microstructure remains nearly equiaxed after annealing at any temperature between 815°C and 927°C.

The modified alloys shown in Fig. 3 contain α grains of two morphologies, as well as β grains, after annealing 1 hr at 815°C. Equiaxed primary α is found in all of the modified alloys, along with various amounts of elongated α grains in some of the alloys. The equiaxed α grains were present during hot rolling in the α + β phase field; production of equiaxed duplex microstructures under these conditons has been previously described [2]. The small, elongated α grains formed during cooling from the hot rolling step or during annealing at 815°C. The elongated grain morphology is not particularly desirable for superplasticity [11]; however, this grain morphology is difficult to alter without further hot deformation or without causing undesirable coarsening of the microstructure. Ideally, the finish rolling temperature for the modified alloys should be near 815°C where approximately equal

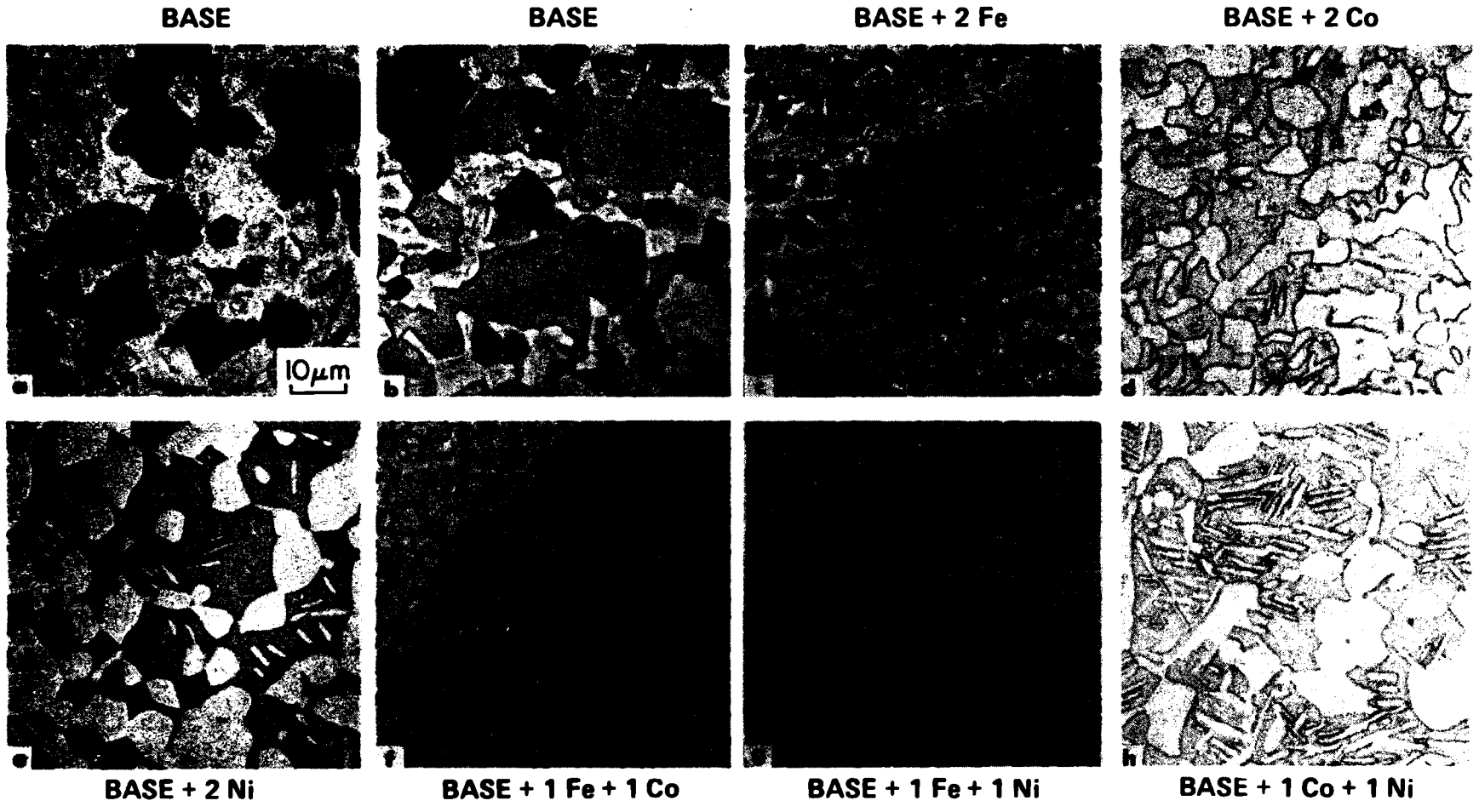

Fig. 3 Microstructures of the base alloy and the modified alloys after being annealed 1 hour at superplastic forming temperatures and water quenched. (a) Base at 927°C. (b) Base at 815°C. (c) Base + 2Fe (5483) alloy at 815°C. (d) through (h) Modified alloys at 815°C.

volume fractions of α and β are present. Finish rolling at 815°C will minimize formation of elongated α grains; higher temperatures will promote formation of the elongated α-phase morphology.

The microstructure of the two Base + 2Fe alloys are shown in Fig. 4. The Base + 2Fe (5483) alloy is composed of an equiaxed mixture of α and β phases at 815°C, this is the same microstructure shown in Fig. 3 for the Base + 2Fe alloy. The second alloy shown in Fig. 4, Base + 2Fe (5914), is composed of a fine mixture of α and β phases that is granular in appearance. A small amount of primary α phase can also be seen in the Base + 2Fe (5914) microstructure. It is believed that the differences in the two Base + 2Fe alloy microstructures are due to different rolling temperatures. Rolling at approximately 815°C produced the equiaxed α + β microstructure shown for the Base + 2Fe (5483) alloy. Rolling at a higher temperature, slightly below the β-transus, produced the small amount of primary α phase found in the Base + 2Fe (5914) alloy; the fine granular microstructure is believed to form during subsequent cooling. Understanding the effect of processing temperature on microstructure for the two Base + 2 Fe alloys further emphasizes the importance of rolling the modified alloys at temperatures near 815°C, where roughly equal volume fractions of α and β phase co-exist.

3.3.3 Superplastic Properties

The dependence of flow stress (σ) on strain rate ($\dot{\varepsilon}$) was determined for each of the modified alloys at 871°C and 815°C. Tests for the base alloy were also conducted to provide data for comparison with the modified alloy test results. Figures 5 and 6 show the flow stress dependence on strain rate for the alloys at 815°C; Figs. 7 and 8 show similar results for 871°C. The lower part of each figure shows the slope of the log σ vs log $\dot{\varepsilon}$ plot, termed m:

$$m = \frac{\partial \log \sigma}{\partial \log \dot{\varepsilon}} \quad . \tag{4}$$

The value of m is used as a measure of the superplastic response of a material, superplastic materials have values of m in the range 0.3 to 1. Previous

SC83-23256

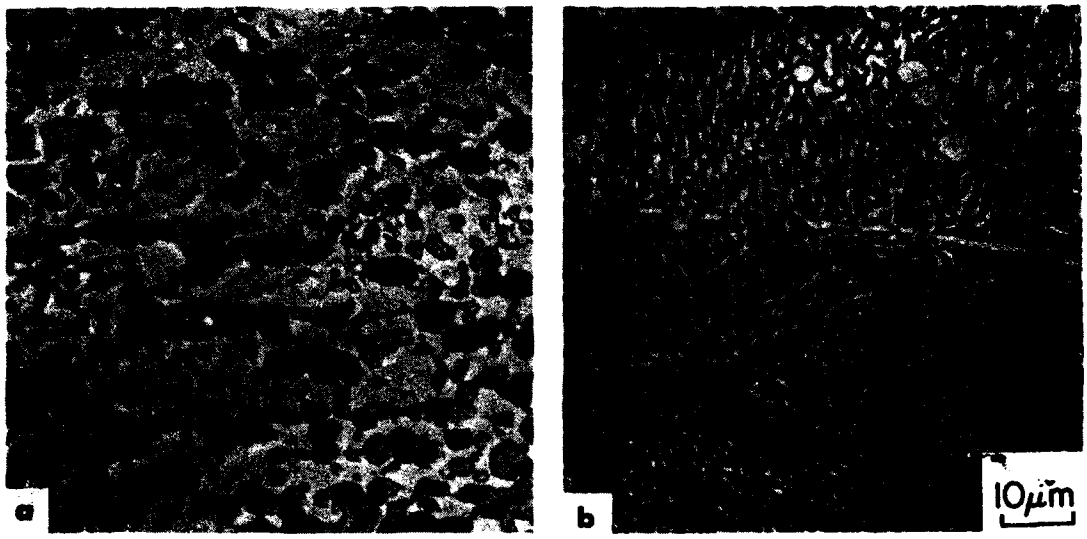

Fig. 4 Comparison of the microstructures of the a) Base + 2Fe (5483) and b) Base + 2Fe (5914) alloys.

SC5254.2FR

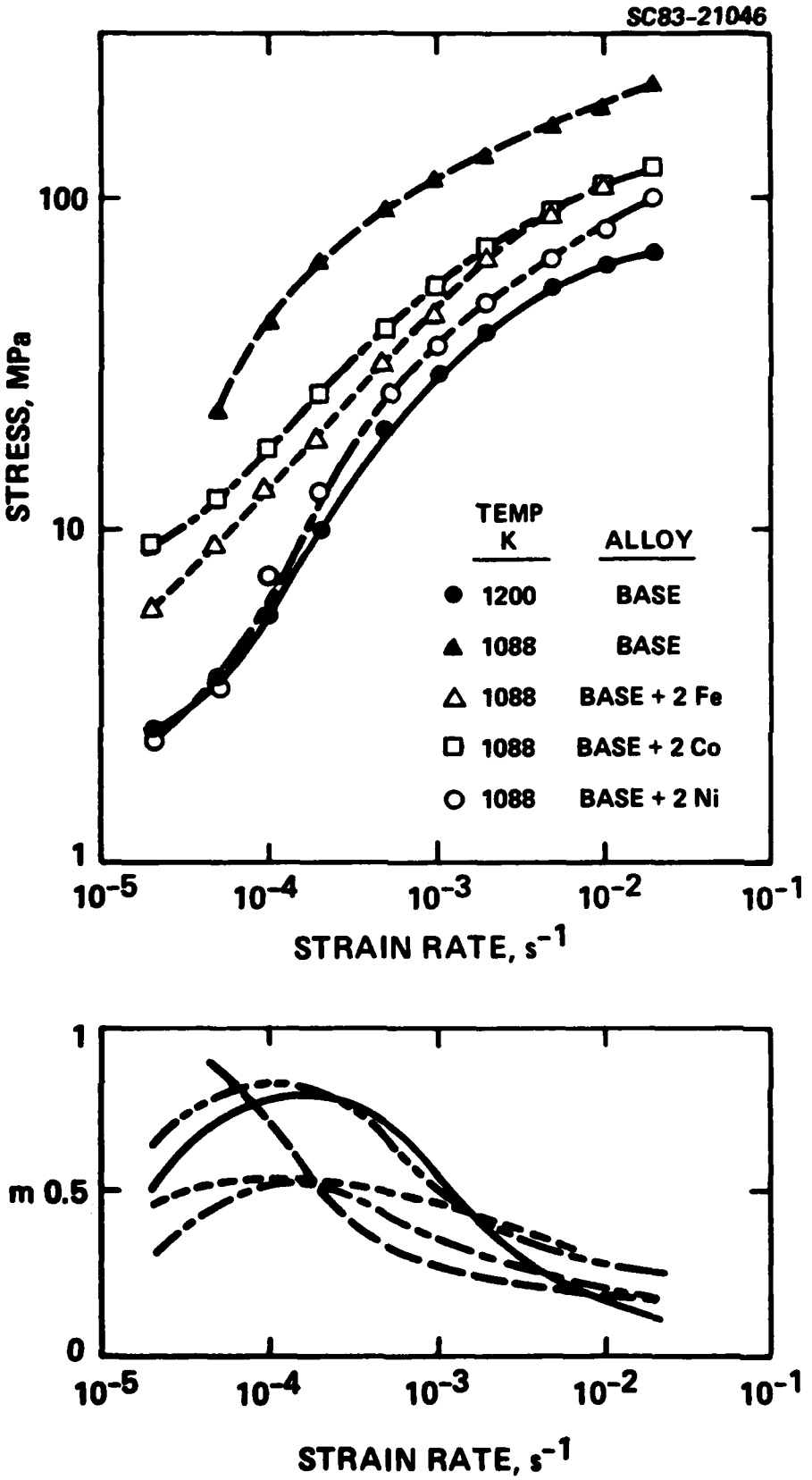

Fig. 5 Flow stress dependence on strain rate for the Base alloy at 927°C (1200K) and 8151C (1088K), and for the Base + 2Fe (5483), Base + 2Co and Base + 2Ni alloys at 815°C (1088K). Lower plot shows corresponding m-values.

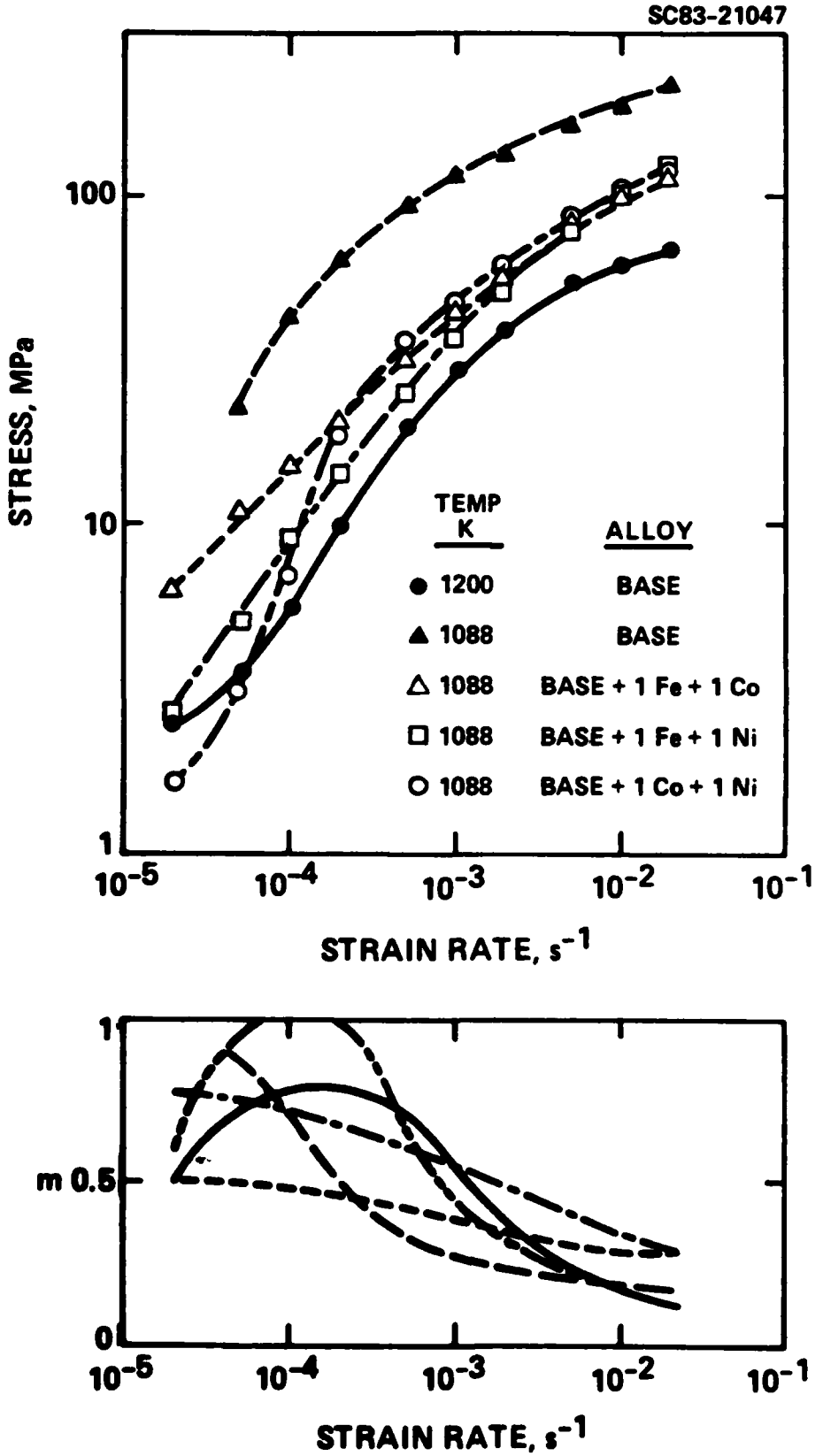

Fig. 6 Flow stress dependence on strain rate for the Base alloy at 927°C (1200K) and 815°C (1088K), and for the Base + 1Fe + 1Co, Base + 1Fe + 1Ni and Base + 1Co + 1Ni alloys at 815°C (1088K). Lower plot shows corresponding m-values.

SC5254.2FR

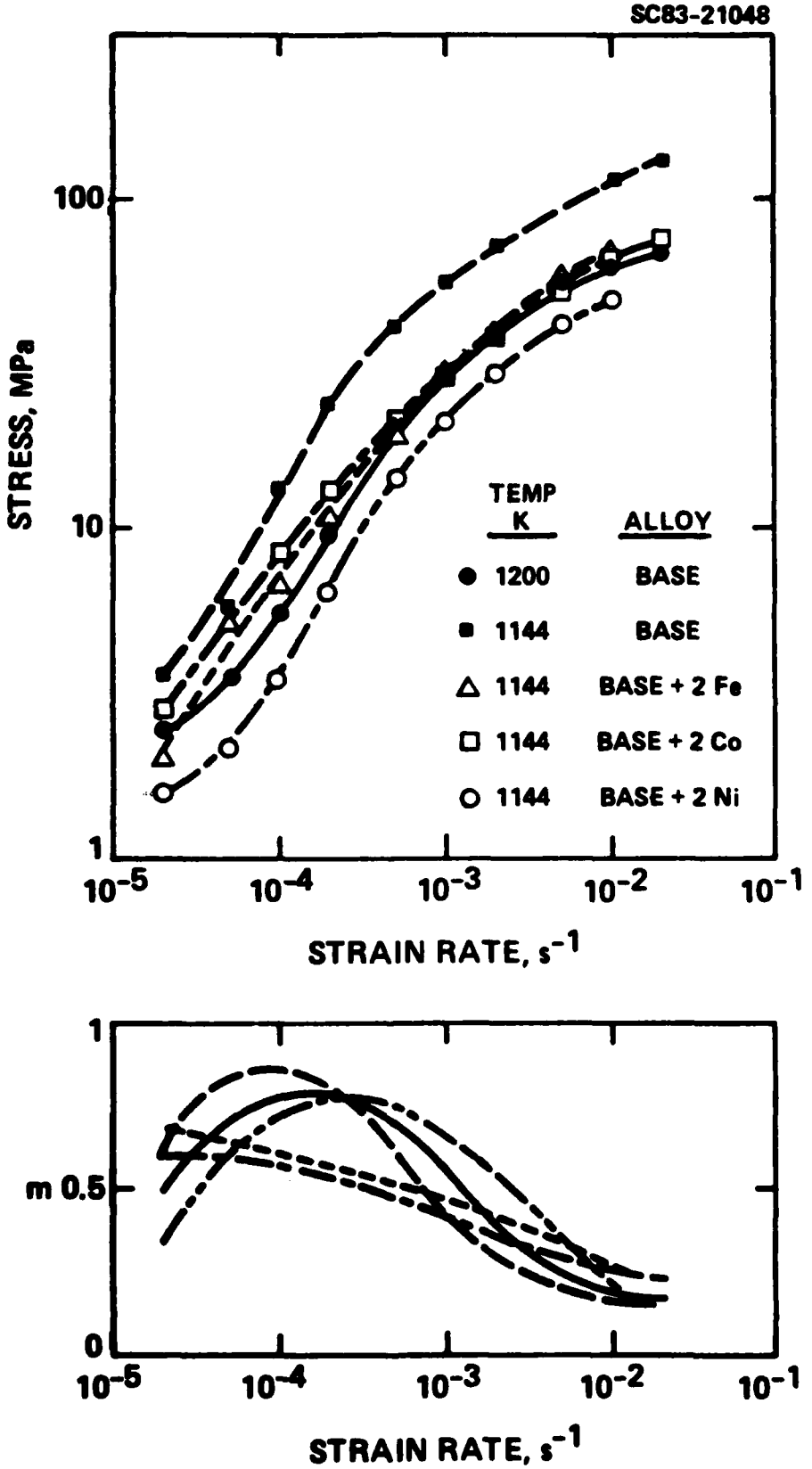

Fig. 7 Flow stress dependence on strain rate for the base alloy at 927°C (1200K) and 871°C (1144K), and for the Base + 2Fe (5483), Base + 2Co and Base + 2Ni alloys at 871°C (1144K). Lower plot shows corresponding m-values.

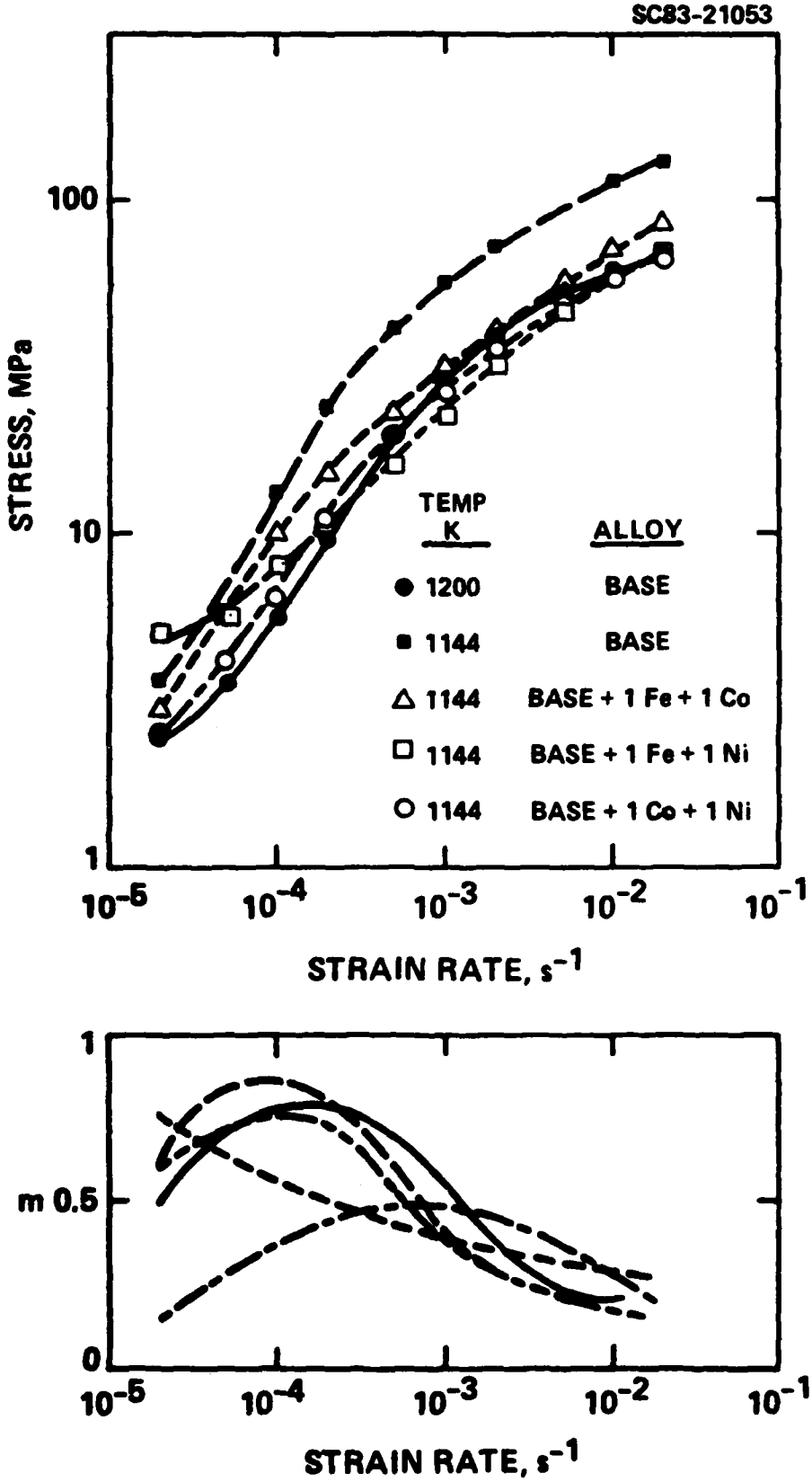

Fig. 8 Flow stress dependence on strain rate for the Base alloy at 927°C (1200K) and 871°C (1144K), and for the Base + 1Fe + 1Co, Base + 1Fe + 1Ni and Base + 1Co + 1Ni alloys at 871°C (1144K). Lower plot shows corresponding m-values.

workers have established an approximate correlation between the value of m and the total elongation achieved in a constant strain rate tensile test [22].

The results show that the flow stress of the modified alloys is lower, at each strain rate, than the flow stress of the base alloy tested at the same temperature. The effect of adding high diffusivity β-stabilizers to Ti-6Al-4V is in good qualitative agreement with the predictions of the model in the following areas:

1. The modified alloys have lower flow stress at any particular strain rate than the base alloy at 815°C and at 871°C.

2. The peak m-value remains approximately the same, but the peak m-value is obtained at substantially higher strain rates for the modified alloys.

3. The modified alloys have slightly higher flow stresses at 815°C than the base alloy at 927°C for the same strain rate. Agreement on this point is probably fortuitous because of the crude assumptions used in the model.

4. The alloy with the highest diffusivity β-stabilizing addition, Ti-6Al-4V-2Ni, has the lowest flow stress of any of the modified alloys at 815°C and at 871°C.

The dependence of flow stress on strain rate for the two Base + 2Fe alloys is shown in Fig. 9 at both 815°C and 871°C. At typical superplastic strain rates, near 2×10^{-4} s^{-1}, the flow stress values for both alloys are nearly equal at each temperature. At higher strain rates, the flow stress values for the two alloys diverge: Base + 2Fe (5914) has the lowest flow stress at 871°C while Base + 2 Fe (5483) has lower flow stress at 815°C. The

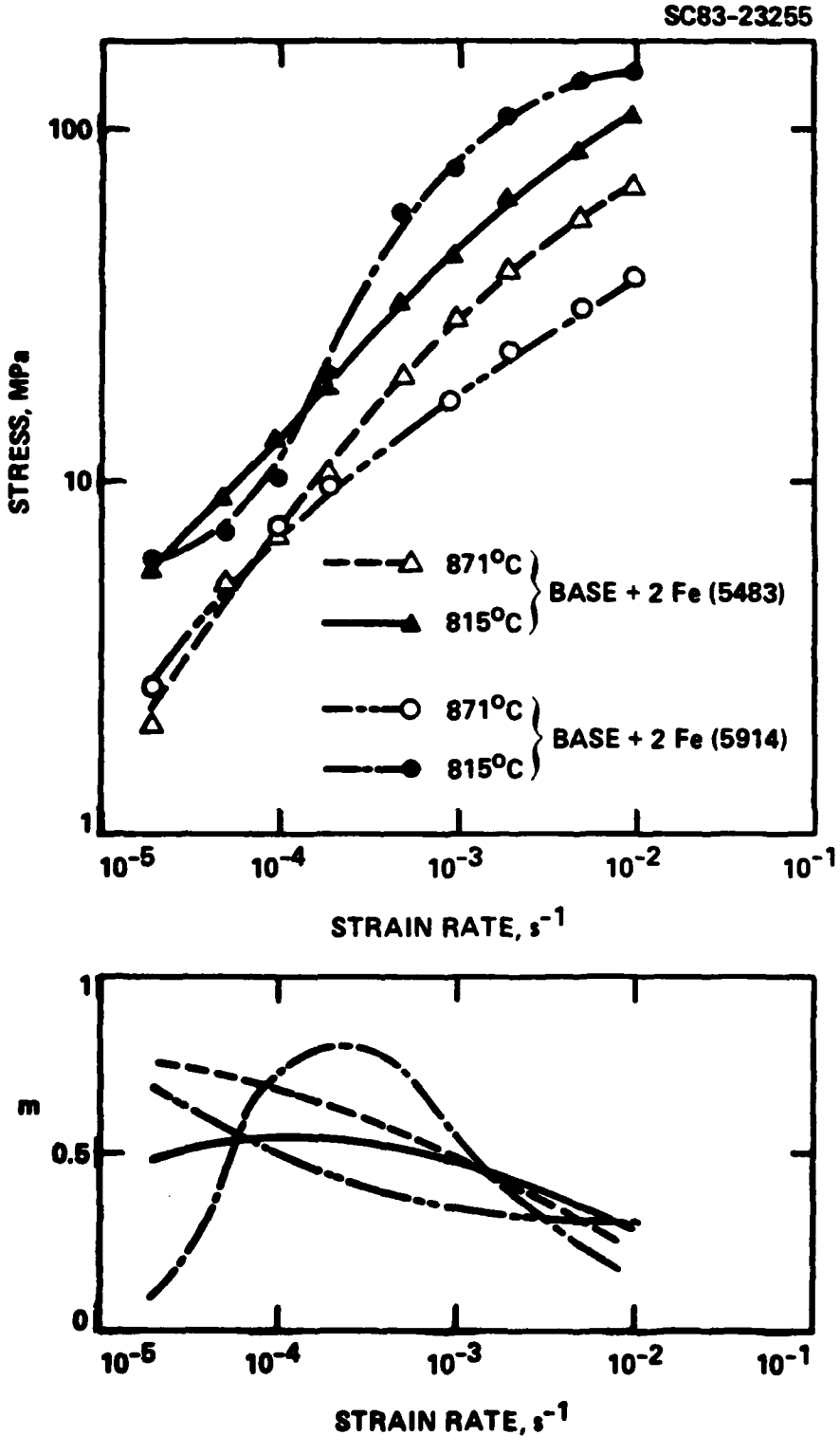

Fig. 9 Flow stress dependence on strain rate for the Base + 2Fe (5483) and Base + 2Fe (5914) alloys at 815°C (1088K) and 871°C (1144K). Lower plot shows corresponding m-values.

link between microstructure and the superplastic properties shown in Fig. 9 is not well understood.

In addition to measuring the flow stress dependence on strain rate, total elongation was measured in constant strain rate tests at 815°C. Results for a strain rate of 2×10^{-4} s^{-1} are listed in Table IV. The values of flow stress and m included in this table were taken from the increasing strain rate tests for a strain rate of 2×10^{-4} s^{-1}, while the total elongations were measured from specimens strained to failure at $\dot{\varepsilon} = 2 \times 10^{-4}$ s^{-1}. The superplasticity parameters for the Base alloy at 927°C are also listed, for comparison. The total elongations for all of the modified alloys at 815°C are similar to the total elongation for the Base alloy at its conventional forming temperature of 927°C.

Table IV
Superplastic Properties of the Modified Alloys
at a Strain Rate of 2×10^{-4} s^{-1}

Alloy	Temperature, °C	m	Flow Stress MPa	Total Elongation Percent
Base	927	0.70	9.6	600
Base	815	0.48	65	225
Base + 2Fe (5914)	815	0.79	20	450
Base + 2Fe (5483)	815	0.54	19	650
Base + 2Co	815	0.53	26	670
Base + 2Ni	815	0.85	13	720
Base + 1Fe + 1Co	815	0.48	21	525
Base + 1Fe + 1Ni	815	0.68	14	550
Base + 1Co + 1Ni	815	0.82	19	550

It is notable that the Base + 2Fe (5914) alloy has a higher m-value but lower total elongation than the Base + 2Fe (5483) alloy under these

deformation conditions. The usual monotonic relationship between m-value and total elongation is not followed in this case, probably as a result of the large microstructural differences between these two alloys.

The superplastic properties of the Base + 2Ni and Base + 2Co alloys are compared in Table V with the superplastic properties of similar alloys investigated by Hammond [4]. Superplastic properties were evaluated at 871°C and 815°C in the present investigation, whereas Hammond measured superplastic properties at 750°C. For the Base + 2Ni alloy, the flow stress values decrease monotonically with increasing temperature, as expected. In contrast, the flow stress values for the Base + 2 Co alloy used in the present investigation are higher than Hammond's data would project. The phase-intercept sizes of the Base + Co alloy used in the present investigation were approximately equal to those of the other modified alloys, suggesting that large grain size did not cause the high flow stresses. Hammond did not report grain sizes, leaving open the possibility that his 2% Co alloy had an unusually fine grain size which produced the lower flow stress values.

Table V
Comparison of Superplastic Properties for Base + 2Co and Base + 2Ni Alloys at $\dot{\varepsilon} = 2 \times 10^{-4}$ s^{-1}

Temperature °C	Base + 2Co		Base + 2Ni		Reference
	Flow Stress MPa	m	Flow Stress MPa	m	
871	20.6	0.48	6.6	0.79	This Investigation
815	27.7	0.53	13.4	0.85	This Investigation
750	23	0.62	27	0.60	4

3.3.4 Cavitation During Superplastic Forming

Previous investigators have reported cavitation during superplastic forming of Ti-6Al-4V when the forming temperature was below 850°C [19]. They suggested that the cavitation was caused by a deformation mechanism that operated below 850°C, although the mechanism was not identified. Since the modified alloys examined in this investigation exhibit substantial superplasticity at temperatures below 850°C, the cavitation behavior of several of the modified alloys was investigated.

Longitudinal cross-sections of superplastic tensile specimens were prepared after the specimens had been strained to failure at 815°C with a strain rate of 2×10^{-4} s^{-1}. Examination in the optical microscope revealed no cavitation at any point along the gage length. Examination of the same specimens in the SEM at higher magnification revealed a small number of tiny cavities near the fracture surface where the highest strains had accumulated during deformation. Figures 10 and 11 show examples of the cavitation that was discovered in the Base + 2Fe (5483) and Base + 1Co + 1Fe alloys. The faint contrast which permits the α and β phases to be seen is due to composition differences between the α and β phases. In the Base + 1Co + 1Fe alloy, cavities were only observed immediately adjacent to the fracture surface. In the Base + 2Fe (5483) alloy, several cavities can be seen adjacent to the fracture surface and several smaller cavities were found further away from the fracture surface, near the right side of Fig. 11a. Figure 11b shows these cavities in greater detail. In parts of the gage section well away from the point of fracture, no cavities were observed in the Base + 2Fe (5483) alloy.

Based on these observations, we conclude that the cavitation behavior of the modified alloys at 815°C is similar to the behavior of Ti-6Al-4V at 927°C. If the suggestion that a particular deformation mechanism promotes cavitation in Ti-6Al-4V is correct, the temperature range where this mechanism operates is below 815°C in the modified alloys. These conclusions are hardly surprising since the microstructures, flow stresses and deformation rates of

Fig. 10 Longitudinal cross-section of failed superplastic tensile specimen of the Base + 2Fe (5483) alloy. Fracture surface is at left side of micrograph.

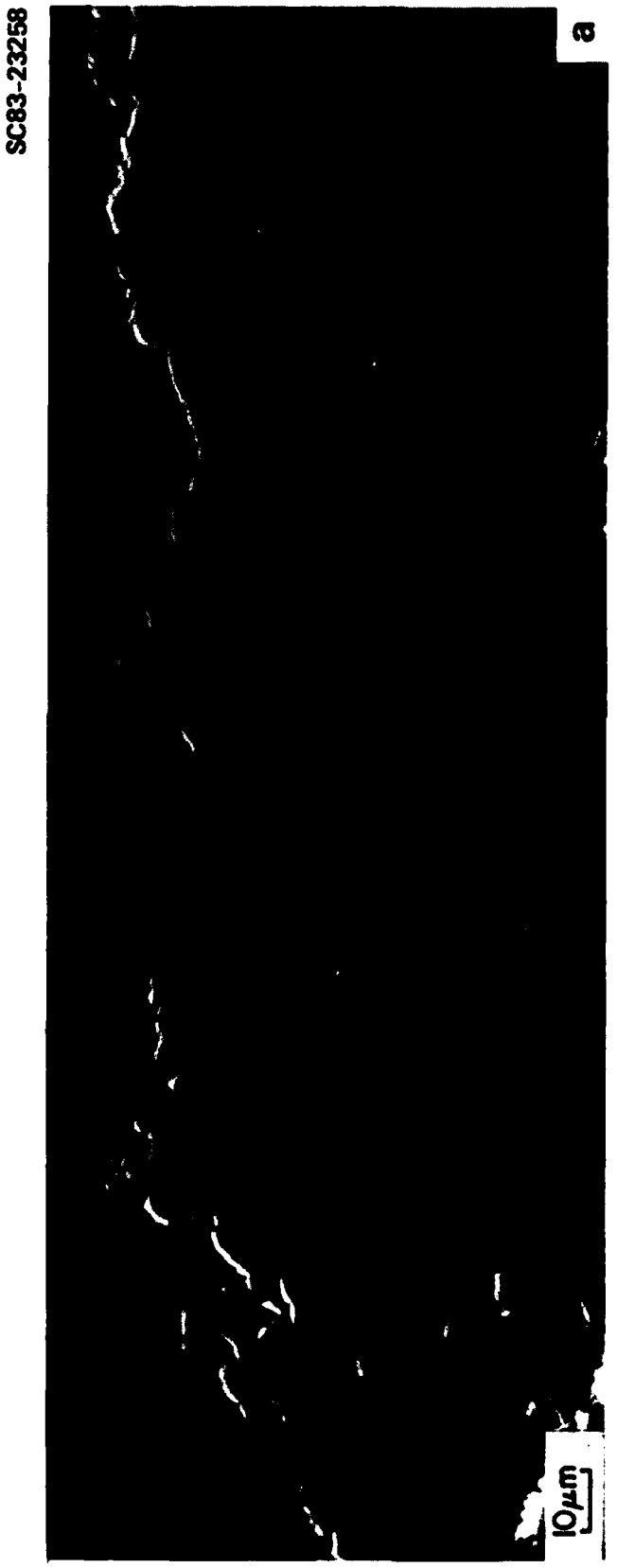

Fig. 11 Longitudinal cross-section of failed superplastic tensile specimen of the Base + 1Fe + 1Co alloy. (a) Region nearest fracture surface, (b) region adjacent to right-hand portion of (a). Fracture surface is at left end of 11a.

SC83-23259

Fig. 11(b)

the modified alloys at 815°C are approximately equal to those values achieved by the base alloy at 927°C

3.3.5 Room Temperature Tensile Properties

Room temperature tensile properties were measured to assess the influence of β-stabilizing additions to Ti-6Al-4V on ambient temperature deformation characteristics. Results for the base and modified alloys in the as-received condition are shown in Table VI. The β-stabilizing additions in the modified alloys generally increase the yield strength over that found for the base alloy. The increase in yield strength produced by the added β-stabilizers is accompanied by a slight drop in ductility, following the usual inverse relationship between strength and ductility.

Table VI
Room Temperature Tensile Properties

Alloy	As-Received			Anneal 815°C, 4 hr Air Cool		
	Yield MPa	Ultimate MPa	RA %	Yield MPa	Ultimate MPa	RA %
Base	931	1020	25	830	886	11
Base + 2Fe (5914)	1060	1070	23	990	1020	19
Base + 2Fe (5483)	992	1050	15	935	1010	20
Base + 2Co	1180	1250	39	1070	1080	17
Base + 2Ni	1070	1140	22	1060	1140	20
Base + 1Fe + 1Co	895	926	34	900	952	28
Base + 1Fe + Ni	1090	1090	27	1080	1160	18
Base + 1Co + 1Ni	1070	1170	30	950	1050	26

The most plausible explanation for the strength increase in the modified alloys is solid solution strengthening produced by the β-stabilizing additions. During annealing at high temperatures, the β-stabilizers partition

to the β-phase, causing the solid solution strengthening to be concentrated primarily in the transformed β products. Strength contributions by other factors, such as lower β-phase transformation temperatures, are also possible.

Addition of eutectoid forming elements such as Co or Ni to titanium is generally accepted to produce very poor ductility due to precipitation of intermetallic compounds [24]. The modified alloys examined in this study did not display the disastrously low ductilities frequently associated with additions of several percent of Ni or Co to titanium. This result indicates that the processing temperature of approximately 815°C was above the eutectoid temperature of the modified alloys. Moreover, precipitation of the intermetallic compounds did not occur during air cooling from 815°C. Thus, the alloys have attractive room temperature tensile properties when processed by conventional methods. However, slow cooling (10°C/hr) of alloys containing Ni additions from 815°C to room temperature produced very poor ductility, as might be expected. Alloys containing only Fe or Co additions were not embrittled by the slow cooling treatment.

3.4 Discussion

3.4.1 Synthesis of Titanium Alloys for Enhanced Superplastic Properties

Theoretical results presented in Section 3.3.1 show that addition to titanium alloys of strong β-stabilizers which also have high diffusivity in the β-phase can substantially lower the optimum superplastic forming temperature, maintaining flow stress and strain rate constant. Experiments in which rapidly diffusing β-stabilizers such as Fe, Co and Ni were added to Ti-6Al-4V qualitatively confirmed the predicted reduction of forming temperature. Several of the modified alloys have superplastic properties at 815°C approximately equal to those of the base alloy at 927°C. Furthermore, the modified alloys have room temperature strength properties higher than the base alloy after equivalent processing.

The alloys developed in this investigation may be useful in applications where the superplastic forming temperature of Ti-6Al-4V must be reduced. In addition, the principles used to develop these alloys are applicable to other titanium alloys. The purpose of this section is to discuss how rapidly diffusing β-stabilizers may be used to change the superplastic forming conditions of titanium alloys. Two cases are considered.

1. Lower Flow Stress, Same SPF Temperature. In this case, additional β-phase stabilization is not required, only accelerated mass transport is necessary. To achieve the goal of lower flow stress at the same SPF temperature, substitution of high diffusivity β-stabilizers for low diffusivity β-stabilizers is sufficient. Substitution of Ni, Co or Fe for some of the V or Mo in a titanium alloy can lower the SPF pressure requirements by lowering the flow stress necessary to drive deformation at a fixed rate.

2. Same Flow Stress, Lower SPF Temperature. This is the case studied theoretically and experimentally in the present investigation. In this case, additional β-phase stabilization and accelerated mass transport are necessary, as shown in earlier sections. To achieve the goal of equal flow stress at lower SPF temperatures, addition of high diffusivity β-stabilizers such as Ni, Co or Fe to an alloy is necessary.

The experimental portion of the present study established that 2% additions of Fe, Co or Ni to Ti-6Al-4V were sufficient to depress the forming temperature from 927°C to 815°C without substantially increasing flow stress. Hammond has shown that superplasticity is found in alloys similar to the Base + 2Co and Base + 2Ni alloys at a temperature of 750°C, although the flow stresses are substantially higher than those found for the Base alloy at 927°C [4]. It is natural to expect that larger additions of these elements would produce further decreases in the superplastic forming temperature. Although this point was not investigated in this program, it is clear that there is a limit to the amount of β-stabilizer that can usefully improve the superplastic properties. This limit is related to the eutectoid temperature of the alloy

in the following manner. The alloy is difficult to superplastically form below the eutectoid temperature because no β-phase is present. The limit to the β-stabilizer addition is that which produces equal volume fractions of α and β phases at the eutectoid temperature. Roughly speaking, the limit is approximately 0.5 of the eutectoid composition. For binary Ti-X alloys, the limits would be approximately 4 wt% Co, 8 wt% Fe or 2 wt% Ni. For the more complex alloys studied in the present investigation, the limits would have to be determined experimentally. Other factors, such as room temperature mechanical properties may pose more severe constraints on the eutectoid forming additions than those stemming from the superplastic forming considerations.

3.4.2 Variation of Flow Stress as a Function of Temperature

By examining the superplasticity data, the flow stress required to deform one of the modified alloys at a particular strain rate, say 2×10^{-4} s^{-1}, can be determined as a function of temperature. Furthermore, the yield strength values shown in Table VI can represent the flow stress at room temperature at $\dot{\varepsilon} = 2 \times 10^{-4}$ s^{-1} since the strain rate for the room temperature tensile tests was nearly equal to 2×10^{-4} s^{-1}. Using these data points, plots of flow stress as a function of temperature at $\dot{\varepsilon} = 2 \times 10^{-4}$ s^{-1} can be constructed for each alloy. Figure 12 is a plot of flow stress vs temperature for the Base and the Base + 2Ni alloys. The notable feature of this plot is the crossing of the curves for the two alloys. Although data were not obtained for a wide range of intermediate temperatures, the flow stress curves for these alloys must cross since the flow stress of the Base + 2 Ni alloy is higher than that of the Base alloy at room temperature and lower at elevated temperatures.

The crossing of the flow stress curves at an intermediate temperature can be explained by the different mechanisms of deformation at ambient and at elevated temperatures. At room temperature (and probably up to approximately 550°C), dislocation slip is the mechanism of deformation. In this temperature regime, the solid solution strengthening provided by the added β-stabilizers

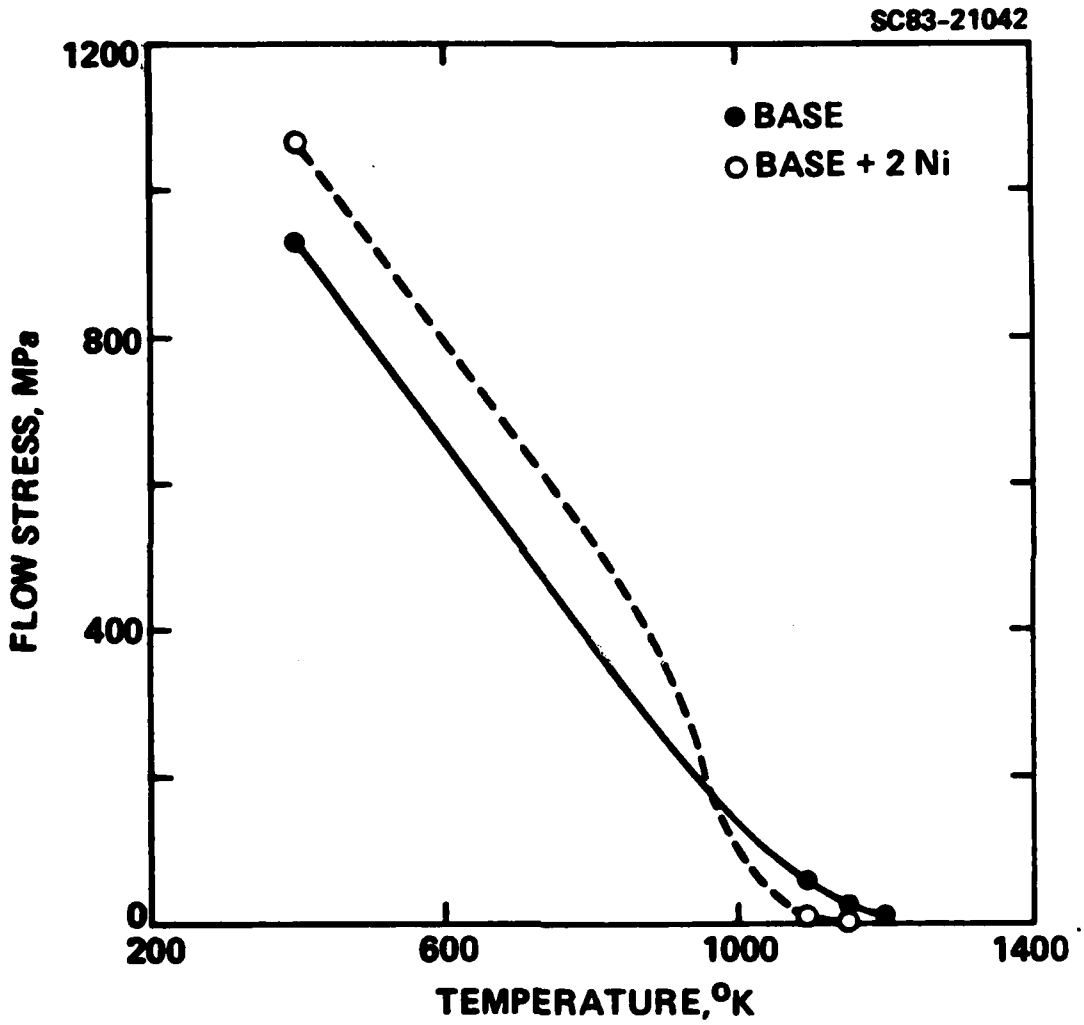

Fig. 12 Longitudinal cross-section of failed superplastic tensile specimen of the Base + 2Fe + 1Co alloy. Right-hand portion of Fig. 11.

raises the flow stress of the modified alloys above that of the base alloy. At temperatures from approximately 750°C to 950°C, where creep processes are the primary mechanisms of deformation, the increased volume fraction of β-phase and accelerated mass transport rates in the modified alloys cause the flow stress of the modified alloys to be lower than that of the base alloy. Addition of a single element which impedes dislocation slip and accelerates mass transport produces higher flow stresses at room temperature and lower flow stresses at elevated temperature.

It is not often that a single element addition to an alloy can simultaneously achieve the goals of increased resistance to deformation at room temperature and decreased resistance to deformation at elevated temperature. By understanding that different deformation mechanisms dominate in the two temperature regimes, and by selection of an alloying addition with the appropriate properties, these counterposed goals were achieved.

3.5 Conclusions

1. Theoretical calculations of the effect of β-phase stabilization and enhanced diffusivity on the flow stress dependence on strain rate and temperature were carried out for two-phase titanium alloys. The results showed the importance of both β-phase stabilization and enhanced diffusivity for lowering the superplastic forming temperature of titanium alloys. Based on these results, Fe, Co and Ni were selected as alloying additions to Ti-6Al-4V for the purpose of lowering the superplastic forming temperature.

2. Modified alloy compositions of Ti-6Al-4V with 2% additions of Fe, Co or Ni were found to contain approximately equal volume fractions of α- and β-phases at 815°C. Obtaining equal volume fractions of the two phases in the Ti-6Al-4V base alloy requires a temperature of approximately 927°C.

3. Flow stress was measured as a function of strain rate for each of the modified alloys at 815°C and 871°C . m-values obtained at a strain rate of 2×10^{-4} s^{-1} for all of the modified alloys at 815°C were equivalent to those obtained for the base alloy at its conventional superplastic forming temperature of 927°C. The flow stress for the Ti-6Al-4V-2Ni modified alloy at 815°C and $\dot{\varepsilon} = 2 \times 10^{-4}$ was approximately equal to that of the base alloy at 927°C and the same strain rate.

4. Total elongations of most of the modified alloys with equiaxed microstructures exceeded 500% when tested at 815°C and a constant strain rate of 2×10^{-4} s^{-1}. This is comparable to the total elongation obtained for the base alloy at its conventional forming temperature and similar strain rates.

5. The effect of microstructure on superplastic properties was evaluated using two Base + 2Fe alloys. The alloy with the equiaxed $\alpha + \beta$ microstructure had lower m-value, equivalent flow stress and higher total elongation than the alloy with a fine "granular" microstructure.

6. Room temperature yield strengths of the modified alloys were generally higher than the yield strength of the base alloy after similar processing treatments.

7. Most of the modified alloys have higher resistance to deformation than the base alloy at room temperature but they have lower resistance to deformation at superplastic forming temperatures. This reversal was explained by considering the effects of high-diffusivity β-stabilizers on deformation processes in the two temperature regimes.

4. Part II - Fatigue of Titanium Alloys

4.1 Background

Considerable progress has been made in recent years in prediction of the initiation fatigue life of aluminum and steel components under conditions of pseudo-random applied load spectra [24-27]. Recently, the effects of both environment and microstructure have been incorporated into these methods and techniques applied to structural design in ground vehicles [25,26] and aircraft [27]. However, this type of analysis and life prediction has not been applied very extensively to titanium alloys.

The first objective of this part of the program is to investigate the cyclic fatigue behavior of three microstructural conditions of Ti-6Al-4V and to incorporate these results and aircraft spectrum loading sequnces into an established cumulative damage model that has been previously employed successfully for aluminum and steel alloy systems. Figure 13 shows the necessary inputs to predictive techniques utilized in the design of critical structural components. As part of any cumulative fatigue damage analysis based on crack initiation concepts, there must be an appropriate description of material properties. The cumulative fatigue damage analysis performed in this study employs strain-life diagrams and the cyclic stress-strain response to describe the cyclic deformation behavior of Ti-6Al-4V in the recrystallization annealed (RA), beta annealed (BA) and solution treated and overaged (STOA) microstructural conditions.

To complete the inputs to the mechanics analysis prior to performing cumulative fatigue damage analysis, geometric factors must then be used to account for local increases of stress and strain (i.e., stress and strain concentration factors). As is known, notches reduce the fatigue resistance of a material but to a lesser degree than predicted from a theoretical stress concentration factor, K_t. Often, a fatigue notch factor, K_f, is employed to describe the reduction in a long life fatigue resistance of a material due to the presence of a geometric notch. K_f is given by the expression:

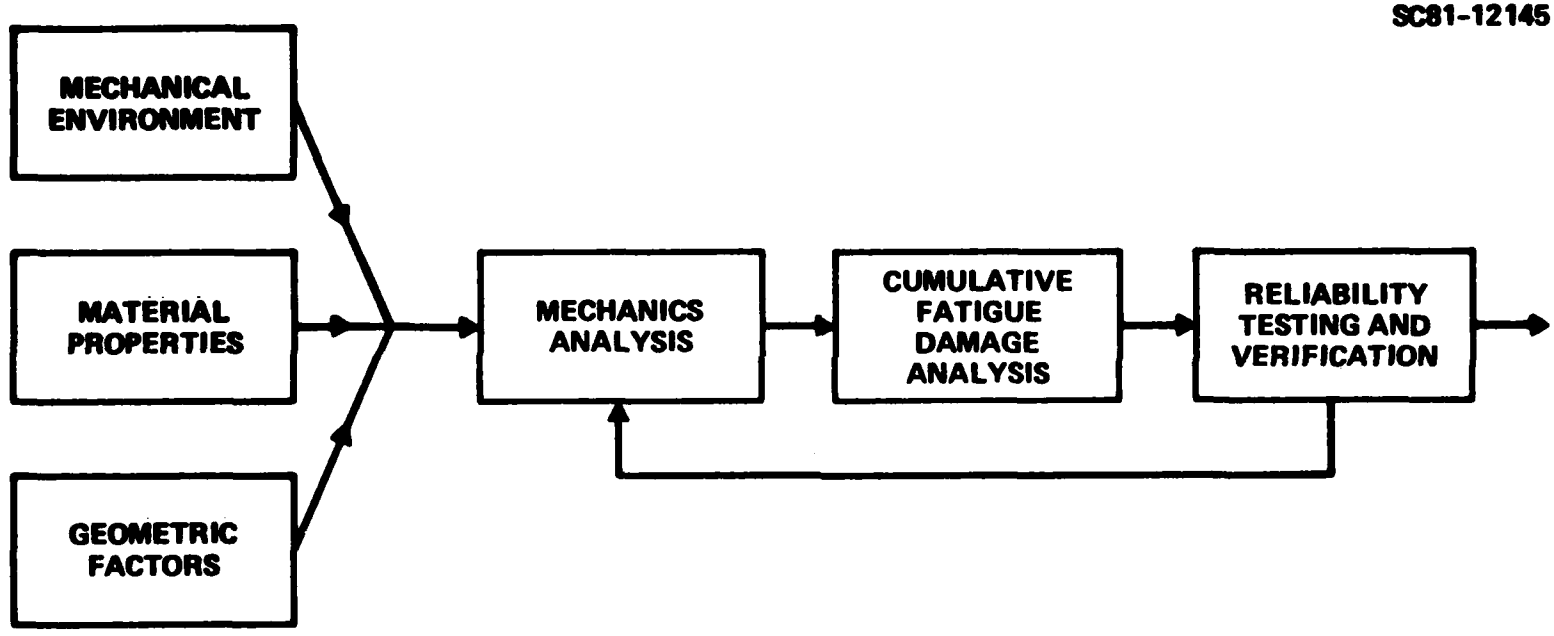

Fig. 13 Cumulative fatigue damage prediction program.

$$K_f \equiv \frac{\text{fatigue strength @ } 10^7 \text{ revs}}{\text{notched fatigue strength @ } 10^7 \text{ revs}} \quad . \tag{5}$$

It is important to realize that three inputs: (1) mechanical environment or duty cycle, (2) material properties or strain-life curves and (3) geometric factors or notches are all necessary for cumulative fatigue analysis. In the mechanics analysis the nominal stresses and strains are translated in a systematic manner into local stresses and strains through the fatigue notch factor, then the damage analysis is performed for life to crack initiation.

The second objective of this part of the program is a study of the effect of microstructure as well as environment on near-threshold fatigue crack propagation in Ti-6Al-4V. Microstructure and environment significantly affect fatigue crack propagation in titanium alloys such as Ti-6Al-4V and Ti-6Al-2Sn-4Zr-6Mo [28]. These effects on fatigue crack growth are generally found to be most pronounced at low crack growth rates associated with low stress intensity factor (ΔK) levels, often referred to as near-threshold fatigue crack propagation. A majority of the crack growth data available for titanium and aluminum alloys is at growth rates greater than 2.5×10^{-6} mm/cycle (10^{-7} in./cycle) and although trends can be inferred from the data, detailed knowledge of microstructural and environmental effects (near ΔK_{th}) has not been investigated.

Methods for predicting fatigue crack propagation behavior from low cycle fatigue properties and microstructural parameters are currently receiving considerable interest. Charkrabortty [29] and Charkrabortty and Starke [30] have utilized low cycle fatigue properties and microstructural parameters to verify fatigue crack propagation behavior of three titanium-vanadium alloys in the crack growth rate range of 10^{-6} to 10^{-3} mm/cycle (4×10^{-8} to 4×10^{-5} in./cycle). The microstructure which Charkrabortty, et al used were single phase beta and beta with precipitated α and/or ω phases. For their study, the fatigue crack propagation behavior could be characterized in terms of the beta grain size for the single phase material or the α particle spacing for the multiphase conditions. The third objective for this part of the program is to extend the predictive method to more complex microstructures such as those produced in Ti-

6Al-4V and to evaluate the applicability of the method to lower crack growth rates (approximately 10^{-7} mm/cycle), a growth rate region in which the crack growth rate (da/dN) vs stress intensity (ΔK) relationship may deviate significantly from linearity.

4.2 Experimental Procedures

Light metallography specimens were prepared by electropolishing using a Buehler recirculating pump cell. Specimens were etched in Kroll's etchant (95% H_2O, 3% HNO_3, 2% HF) or an etchant composed of equal parts of 10% aqueous oxalic acid and 1% aqueous HF solutions. Photomicrographs were taken with a Zeiss Ultraphot Metallograph.

Fatigue crack propagation tests were conducted in accordance with ASTM E647 using compact type (CT) specimens with B = 12.7 mm and W = 50 mm. Tests were conducted in laboratory air (50 - 60% RH) and wet air (~ 100% RH), at R = 0.3 and 30 Hz.

LCF specimens were machined from heat treated blanks of Ti-6Al-4V in the RA, BA and STOA microstructural conditions. All machining to the final dimensions of the gage section of each specimen was accomplished by ever decreasing removal of material ending with a final helical polish using 600 grit carborundum. All specimens were then electropolished and surface residual stresses measured. The maximum surface residual stress determined by x-ray diffraction was approximately -48 MPa (-7 ksi).

All testing was performed in MTS electrohydraulic, closed-loop, test machines. Strain rates for all fatigue tests were ~ $10^{-3}s^{-1}$. A clip-on type extensometer was used to monitor strain for all tests and received calibration prior to a given series of tests via a Schaevitz extensometer calibrator accurate to 0.0001 in.

One set of test data, designated as room temperature-room humidity, was gathered at 20°C/50 - 60% RH.* A second set of test data, designed at 100% RH, was gathered using a specially designed chamber. To maintain saturated water vapor conditions, pressurized air at ~ 100 MPa was bubbled through a water bath prior to entering the test chamber. Both cyclic stress-strain data and strain-life data was generated using these procedures.

4.3 Results

4.3.1 Microstructural Development

The plate obtained for this portion of the program had been purchased by Rockwell International to the high fracture toughness plate specifications for the B-1 aircraft. Plate chemistry, procesing and mechanical properties as reported by the supplier are given in Table VII. Specimen blanks were removed from the plate such that the loading axis of the LCF specimens would be parallel to the T direction and the FCP specimen would have a TL orientation. The blanks were then heat treated and finished machined to specimen configuration. The heat treatments were chosen to produce three distinct microstructures which appear most important for aerospace applications at this time. The heat treatments based on previous experience [28] and adjusted to the beta transus temperature of this plate are given in Table VIII. Microstructures resulting from these heat treatments are shown in Fig. 14. The material had a moderate texture, with basal poles two to four times random in both the rolling direction (L) and the transverse direction (T).

*Relative humidity.

Table VII

Alloy Chemistry and Mechanical Properties

63.5 mm (2.5 in.), Ti-6Al-4V Plate
Composition (wt%)

	Al	V	Fe	Y	C	N	O	H	Bal
RMI Heat No. 802334	6.1	4.0	0.19	<0.005	0.02	0.018	0.122	0.088	Ti

Condition

Hot Rolled, RA Annealed[1] and Pickled

Mechanical Properties

Orient	$\sigma_{0.2}$ MPa (ksi)	σ_u MPa (ksi)	e %	K_{Ic} MPa·$m^{1/2}$	K_{Ic} (ksi$\sqrt{in.}$)
L	846 (122.7)	920 (133.5)	15	85.1	77.4
T	887 (128.7)	934 (135.5)	13	76.3	69.4

1: 941°C (1725°F)/1-1/2 h/AC + 760°C (1400°F)/1 h/AC.

Table VIII

Heat Treatment Schedules

Condition	Heat Treatment
Recrystallization Anneal (RA)	920°C (1700°F)/4 h/cool @ 50°C (90°F) to 760°C (1400°F)/AC
Beta Anneal (BA)	1038°C (1900°F)/1/2 h/AC + 704°C (1300°F)/2 h/AC
Solution Treatment Over Age (STOA)	955°C (1750°F)/1 h/WQ + 593°C (1100°F)/4 h/AC

SC83-23260

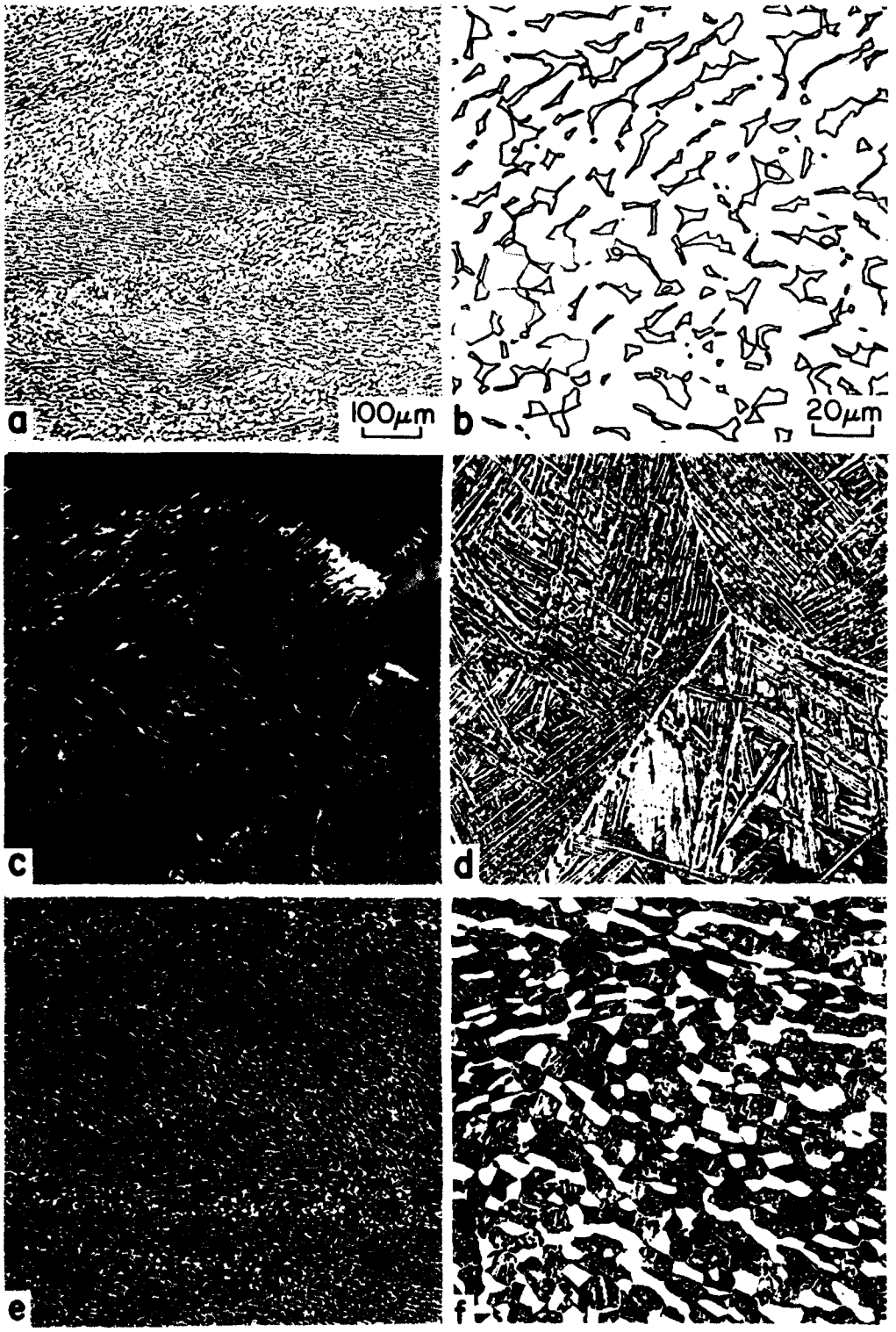

Fig. 14 Microstructures used for the LCF and FCP testing: (a,b) recrystallization annealed (RA), (c,d) beta annealed (BA), and (e,f) solution treated and overaged (STOA).

4.3.2 Fatigue Crack Propagation

All three microstructural conditions were tested in laboratory air and wet air. The fatigue crack propagation behavior of the RA condition is shown in Fig. 15. A fairly smooth curve was obtained with some scatter in the data at ΔK levels between 10 and 20 MPa$\cdot m^{1/2}$. The threshold stress intensity (ΔK_{th}) for this condition is found, by the method of ASSTM E647-78T, to be 5.92 MPa$\cdot m^{1/2}$. Ritchie [31] provides a different definition for the threshold stress intensity (ΔK_o) which he defines as the stress intensity below which no measurable growth (> 0.1 mm) occurs in 10^7 cycles. For the test plotted in Fig. 15b, this criterion was applied, resulting in a value for ΔK_o of 5.71 MPa$\cdot m^{1/2}$, a difference of less than 5%. For the remainder of the tests in this part of the program, the method of ASTM E647-78T was used, a choice which is further justified by the discontinuous nature of crack propagation at near threshold growth rates in titanium alloys, especially for transformed beta microstructures. For these microstructures, a least squares fit of the data in the lowest decade of crack growth, as specified in ASTM E647-78T, should give the most consistent results.

Data from this program for the RA condition is compared to data from a previous progam in Fig. 16. The data are seen to be in good agreement. A trend line has been drawn through the data points and a deviation from the line is observed between ΔK level of ~ 8 and 15 MPa$\cdot m^{1/2}$. The reverse plastic zone size under fatigue loading conditions is given by:

$$r_y^c = 0.033 \left(\frac{\Delta K}{\sigma_y}\right)^2 \qquad (6)$$

and for material with a yield strength of 862 MPa (125 ksi), r_y^c corresponding to these ΔK levels would be 3 and 10 μm respectively. The α grain size of the RA condition is ~ 10 μm and the discontinuity in the curve might be expected to be related to a fracture mode transition as suggested by Yoder and co-workers [32]. Yoder, et al suggest that a sharp transition occurs in growth rate when r_y^c is equal to the mean grain size, $\bar{\ell}$. In this study and work in a previous program [28], the transition has been observed to occur over a range of ΔK. The transition is characterized by a fracture mode transition from

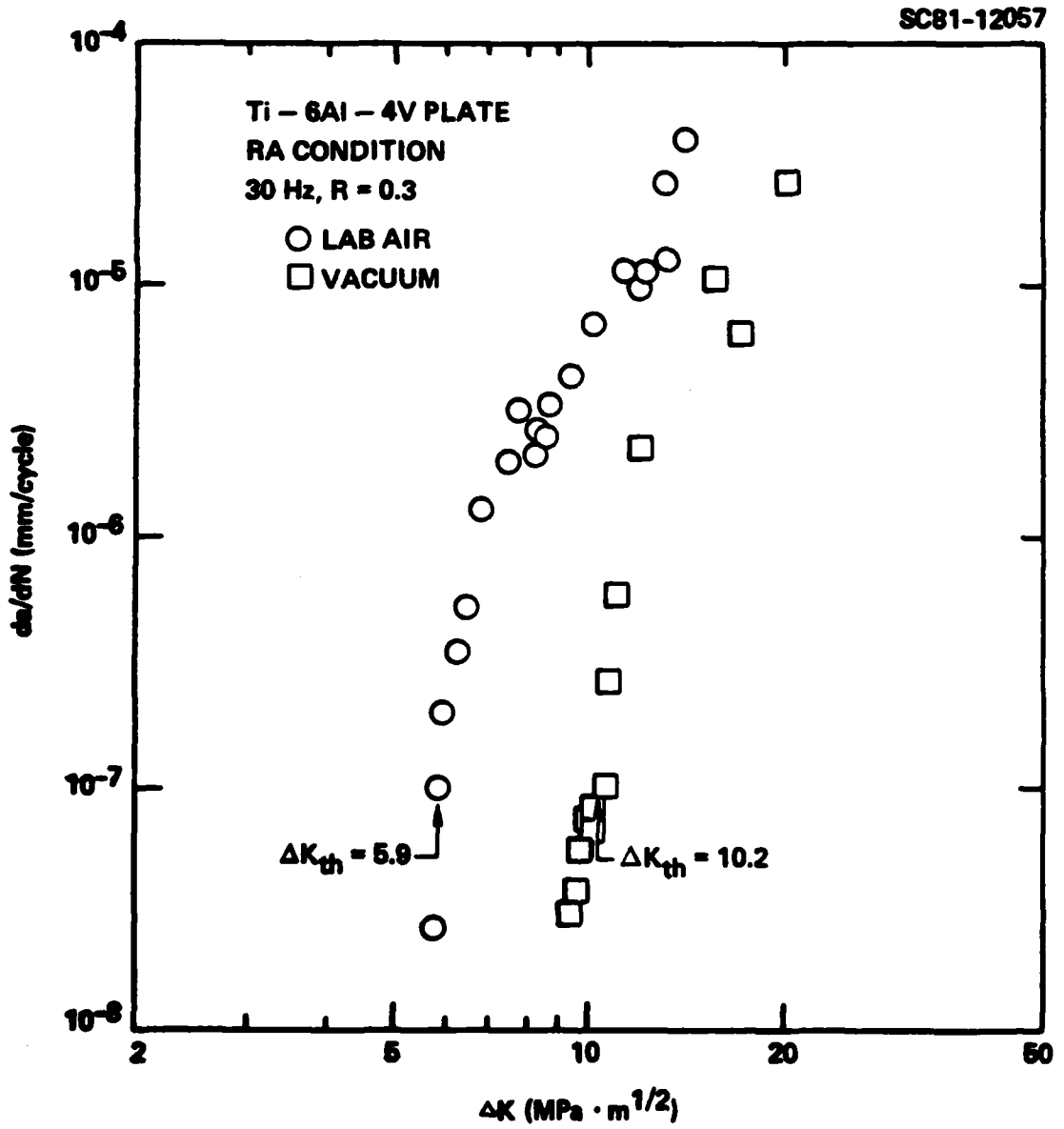

Fig. 15 FCP of Ti-6Al-4V, RA condition, laboratory air, R = 0.3, 30 Hz.

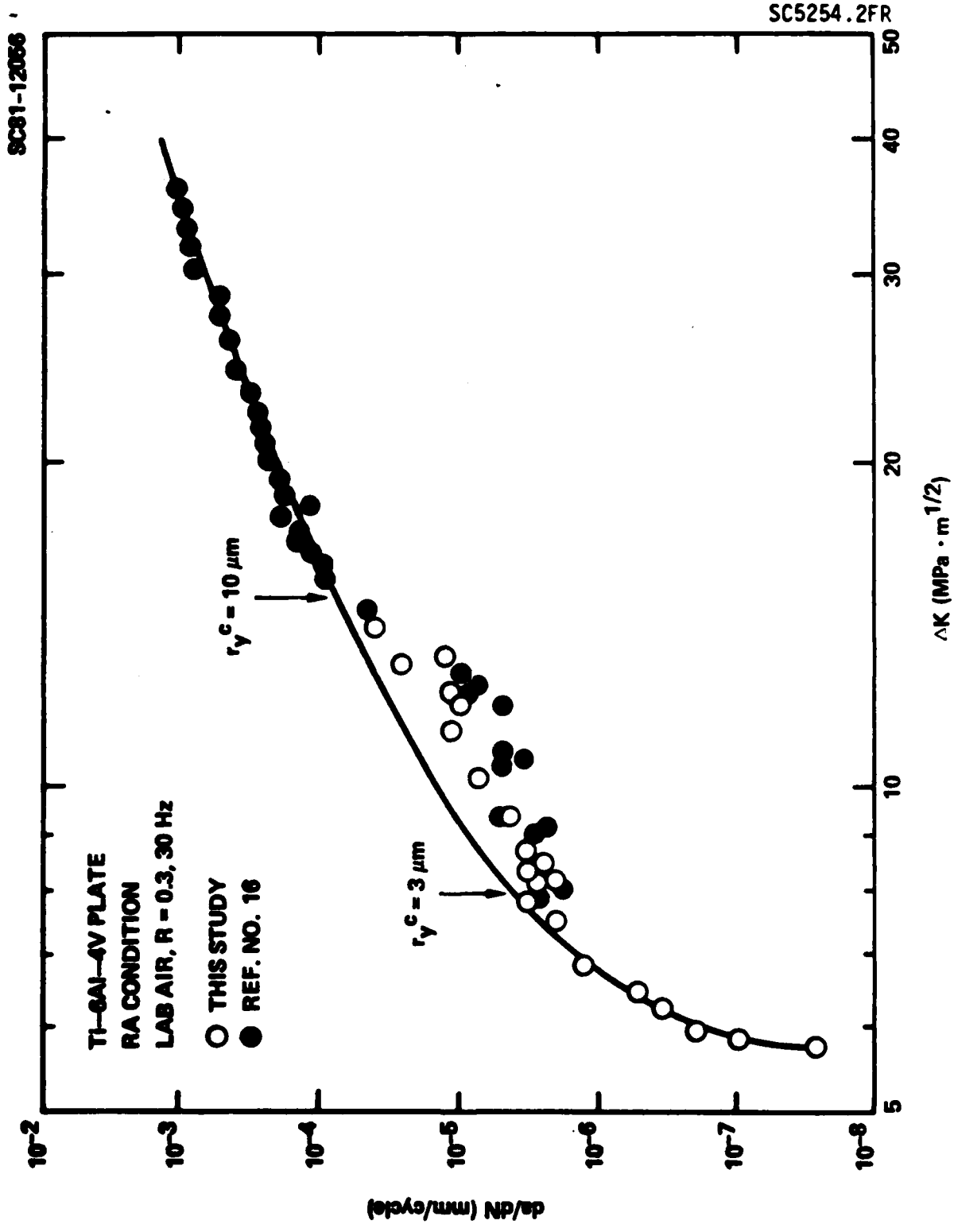

Fig. 16 FCP of Ti-6Al-4V, RA condition, laboratory air, R = 0.3, 30 Hz.

cyclic cleavage to striation formation, with mixed mode propagation occurring over a range of ΔK levels and crack growth rates. Such a fracture mode transition is illustrated in Fig. 17. Transgranular cyclic cleavage of the α-phase is the principal fracture mode at low growth rates where the plastic zone is wholly contained withing the α grains, Fig. 17a. The mixed mode fracture, at higher ΔK levels, can be seen in Fig. 17b and c where $r_y^c < \bar{\ell}$. For ΔK levels where $r_y^c > \bar{\ell}$, Fig. 17d, the absence of cyclic cleavage is noted. Most of the propagation at these higher ΔK levels is by striation formation although the striations are not resolved at this magnification.

Crack propagation behavior in laboratory air for all three microstructural conditions is shown in Fig. 18 with data represented by trend lines. The effect of environment (wet air vs laboratory air) for the three microstructures is shown in Figs. 19, 20 and 21. An environmental effect is observed only in the case of the recrystallization annealed (RA) microstructure. The more rapid propagation rate for wet air at any given ΔK level is associated with a macroscopically flatter fracture. Scanning electron microscopy revealed a greater amount of cleavage in wet air than in laboratory air, cf Fig. 22a and b.

4.3.3 Low Cycle Fatigue

Figures 23, 24 and 25 show the monotonic and cyclic stress-strain curves for the Ti-6Al-4V in the RA, BA and STOA microstructural conditions respectively. Table IX lists the monotonic properties of these materials. As shown, the STOA is superior in true fracture stength, ultimate and yield strength as well as true fracture ductility in comparison with the RA and BA microstructures. This is in general agreement with previously published results [16]. Cyclic stress-strain curves shown in Figs. 23, 24 and 25 were obtained from the locus of tips of stabilized hysteresis loops gathered during companion specimen fatigue-life tests. The results of the controlled strain fatigue tests for the three microstructural conditions are given in Tables X and XI for room temperature/room humidity and 100% RH environments respectively.

SC81-14637

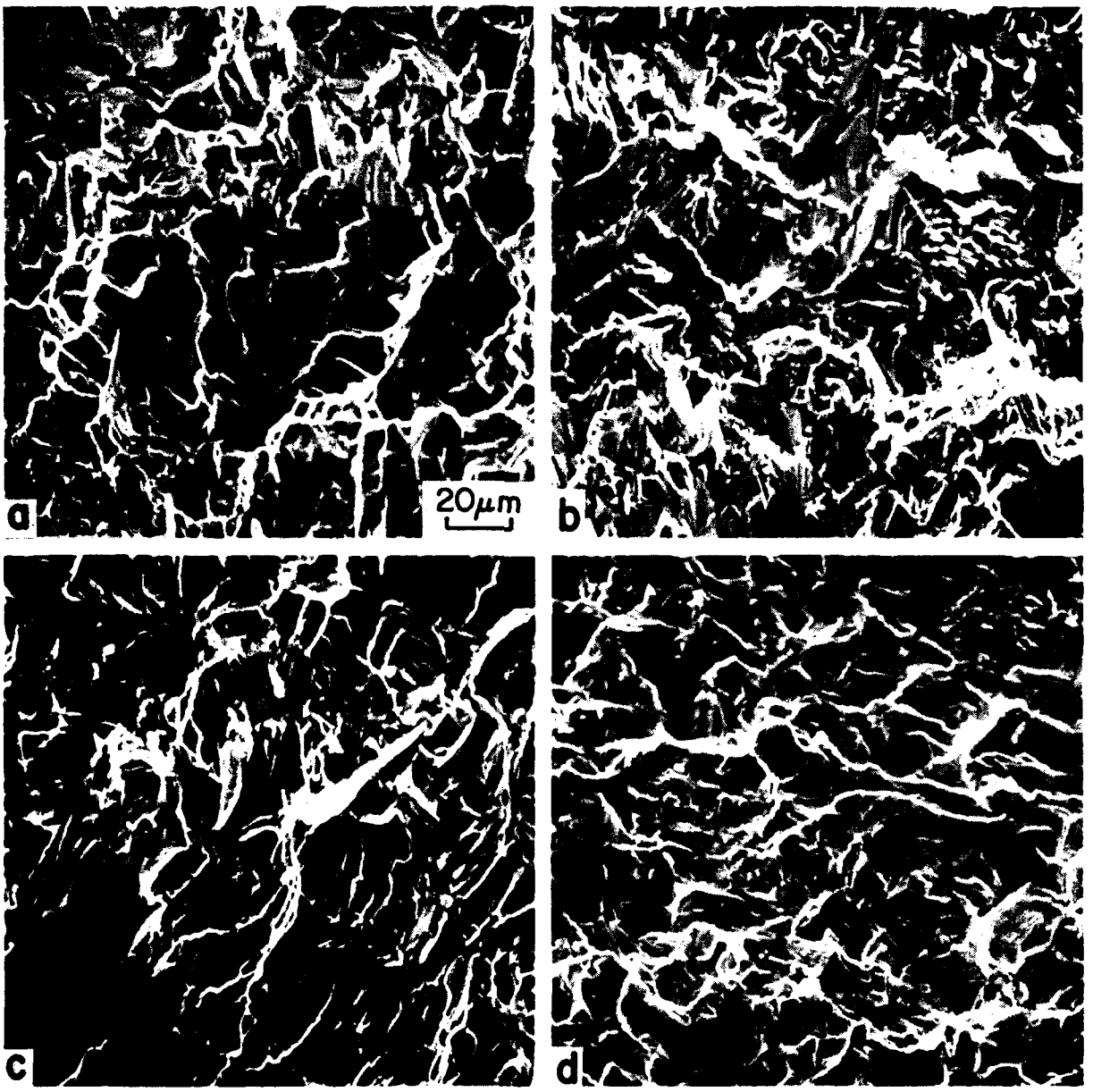

Fig. 17 SEM of Ti-6Al-4V FCP specimen, RA condition, laboratory air, R = 0.3, 30 Hz.
(a) ΔK = 5.5 MPa·$m^{1/2}$, da/dN = 8.5 x 10^{-9} mm/cycle.
(b) ΔK = 8.3 MPa·$m^{1/2}$, da/dN = 2.7 x 10^{-6} mm/cycle.
(c) ΔK = 9.4 MPa·$m^{1/2}$, da/dN = 4.5 x 10^{-6} mm/cycle.
(c) ΔK = 18.7 MPa·$m^{1/2}$, da/dN = 1.8 x 10^{-4} mm/cycle.

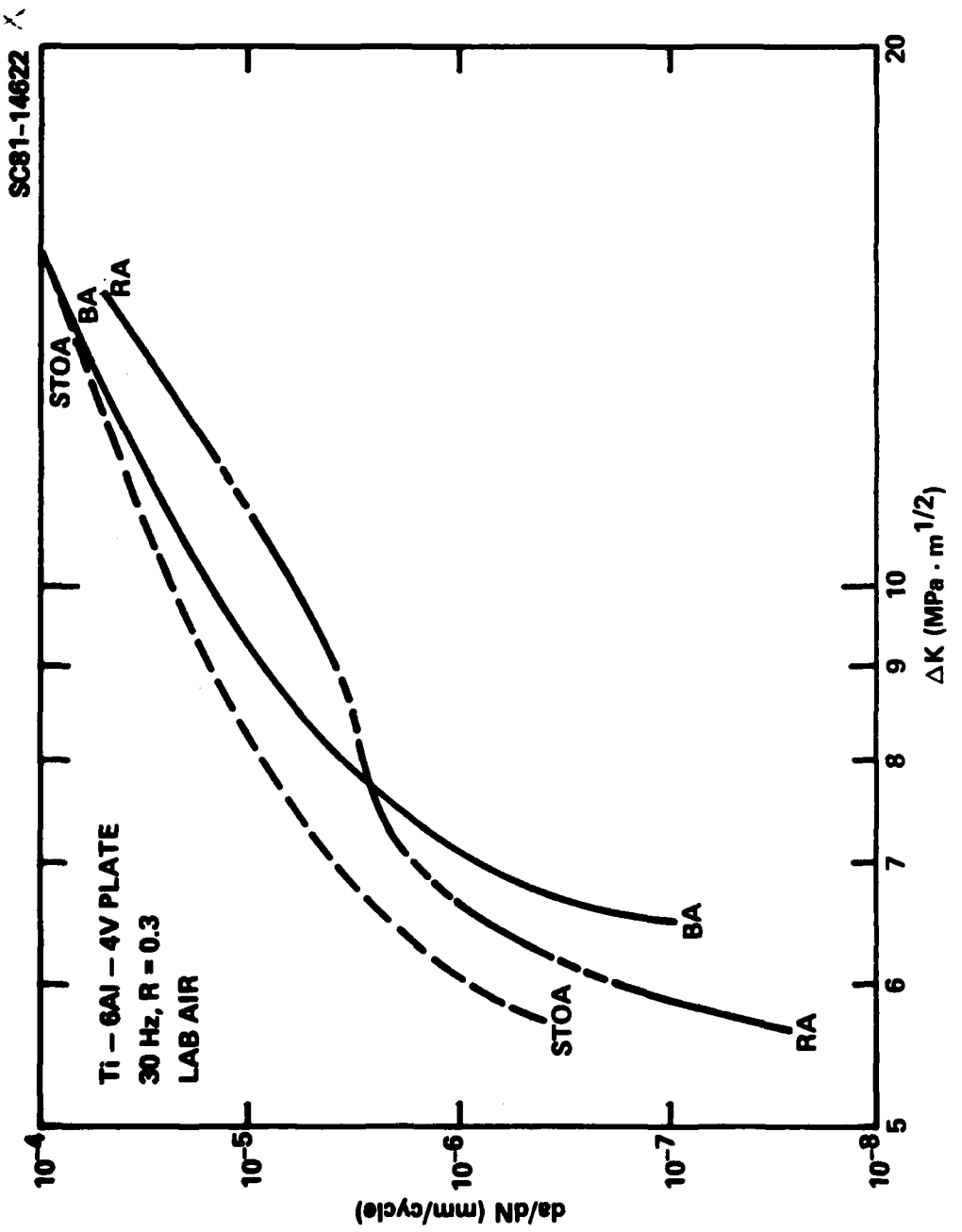

Fig. 18 FCP of Ti-6Al-4V, laboratory air, R = 0.3, 30 Hz.

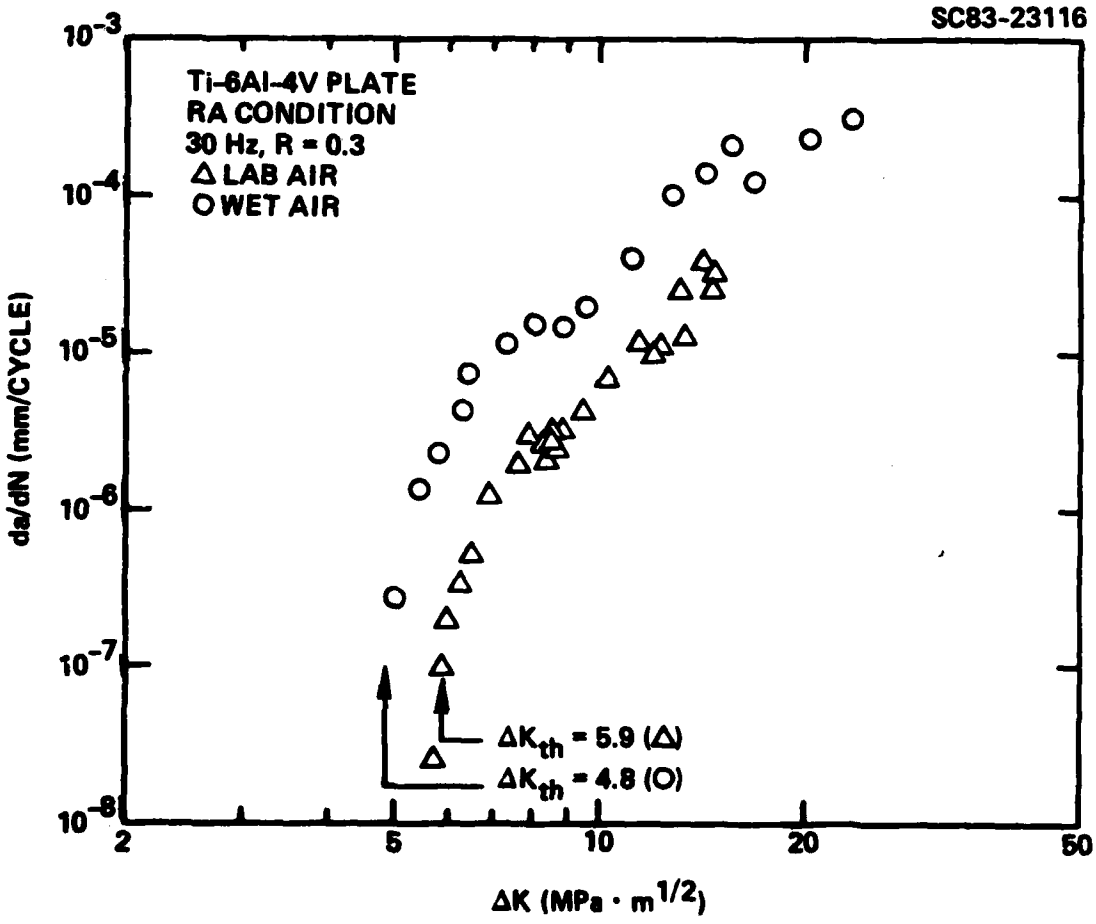

Fig. 19 Effect of humidity on FCP of Ti-6Al-4V, RA condition, R = 0.3, 30 Hz.

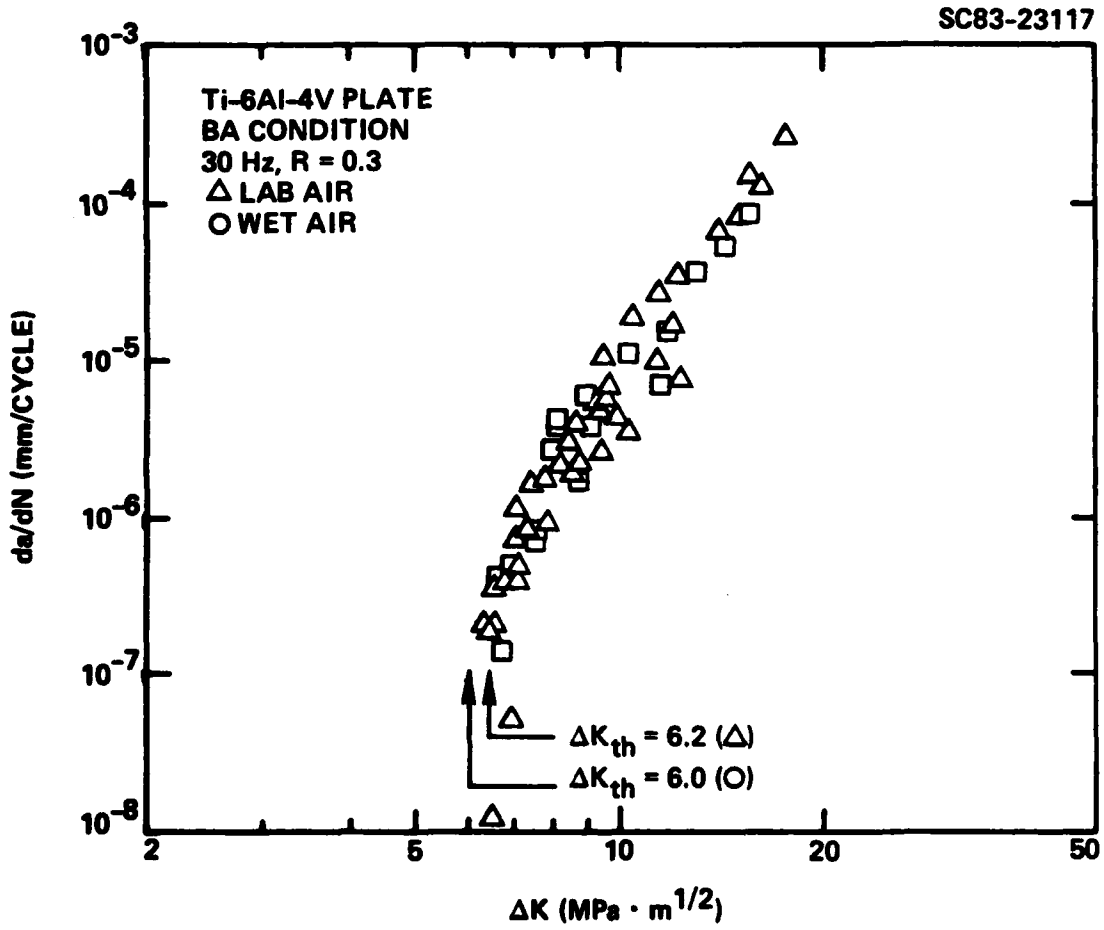

Fig. 20 Effect of humidity on FCP of Ti-6Al-4V, BA condition, R = 0.3, 30 Hz.

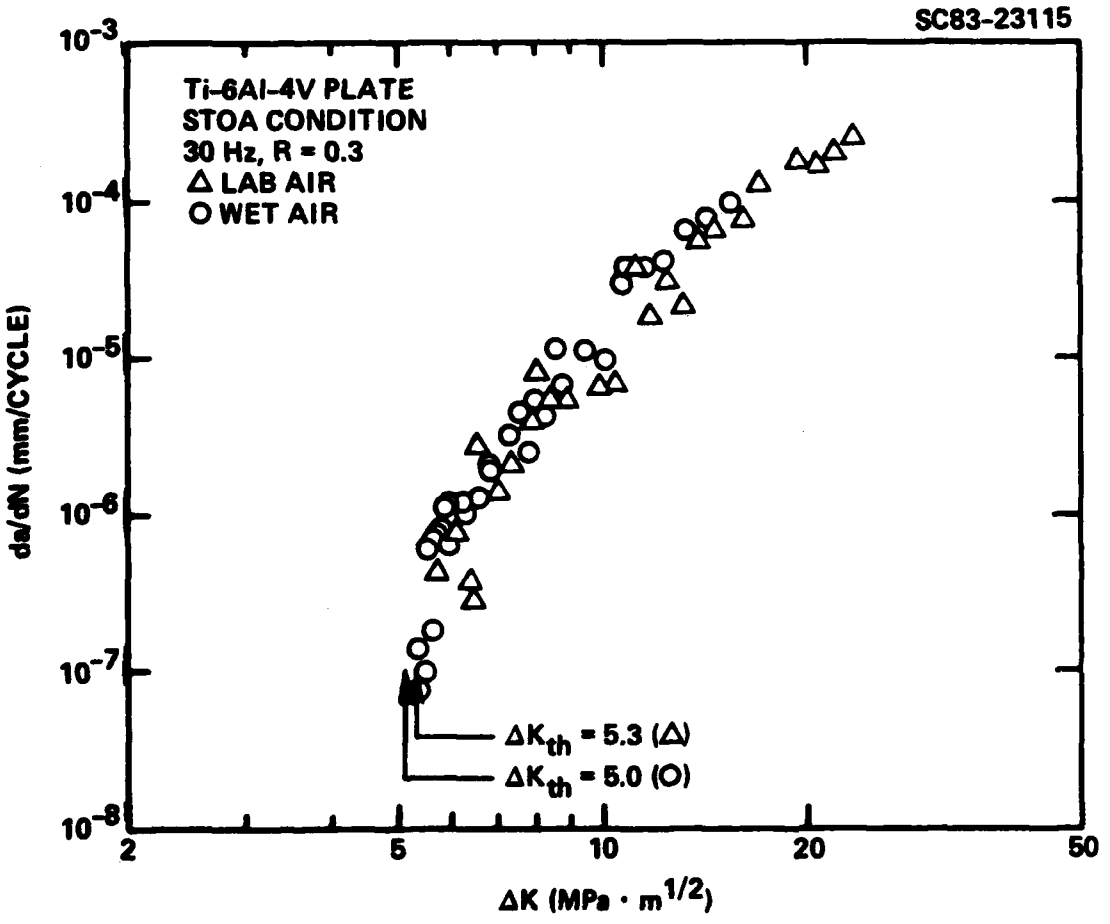

Fig. 21 Effect of humidity on FCP of Ti-6Al-4V, STOA condition, R = 0.3, 30 Hz.

SC83-23261

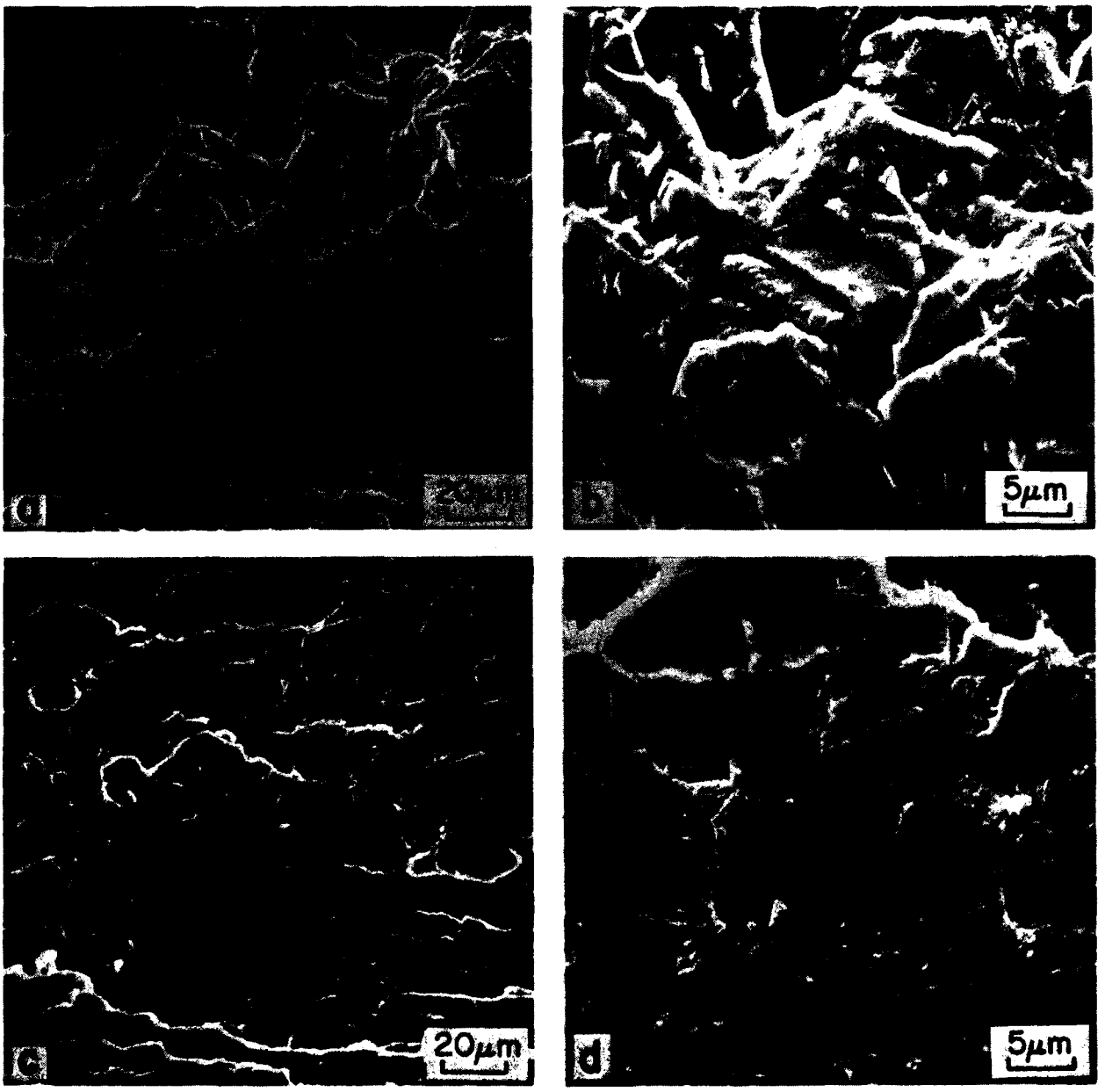

Fig. 22 SEM of Ti-6Al-4V FCP specimens, RA condition, R = 0.3, 30 Hz at $\Delta K = 8.5$ MPa·m$^{1/2}$ (a, b) laboratory air (da/dN = 2.6 x 10^{-6} mm/cycle) (c, d) wet air (da/dN = 1.4 x 10^{-5} mm/cycle.

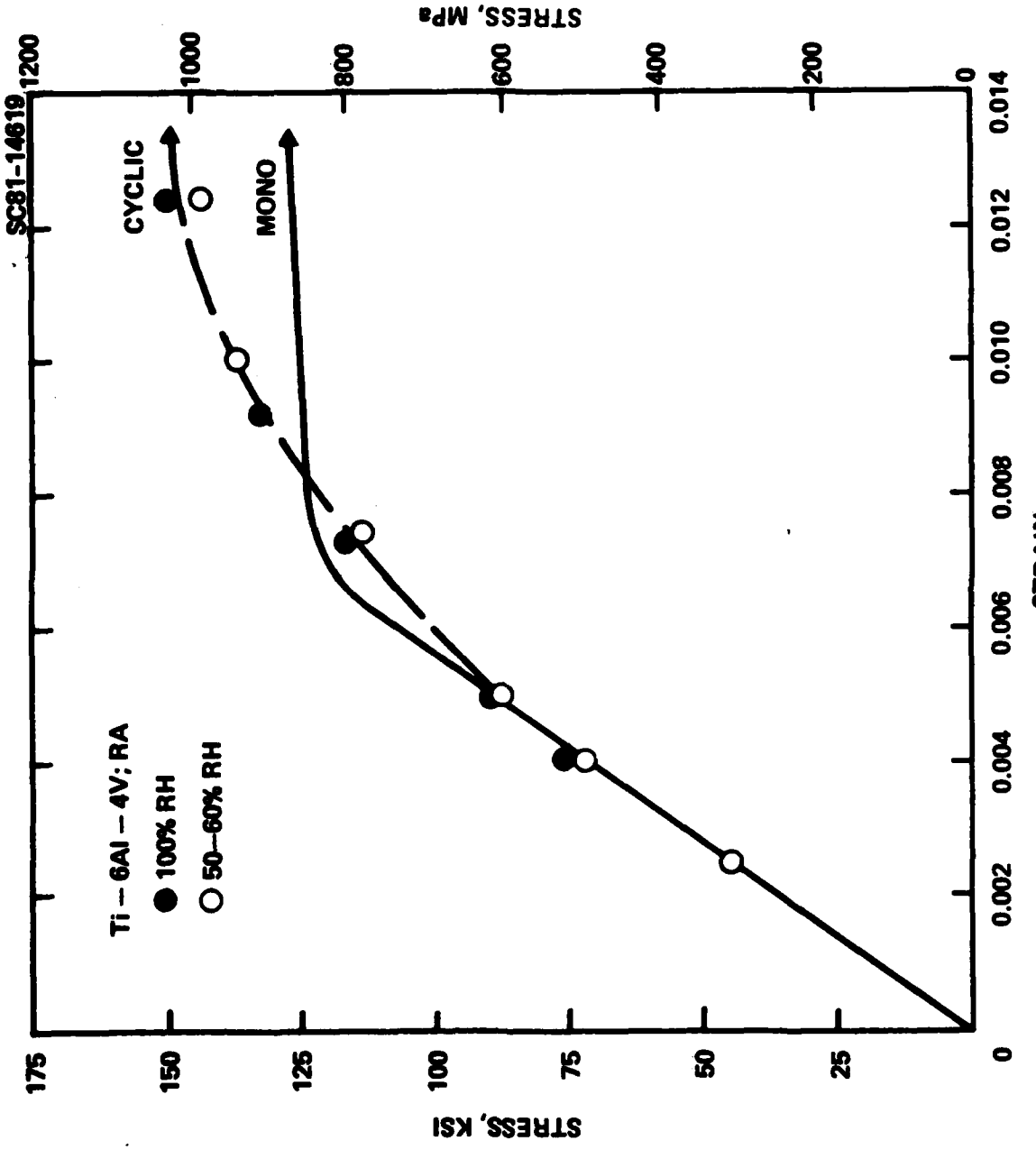

Fig. 23 Monotonic and cyclic stress-strain curves for Ti-6Al-4V, RA condition.

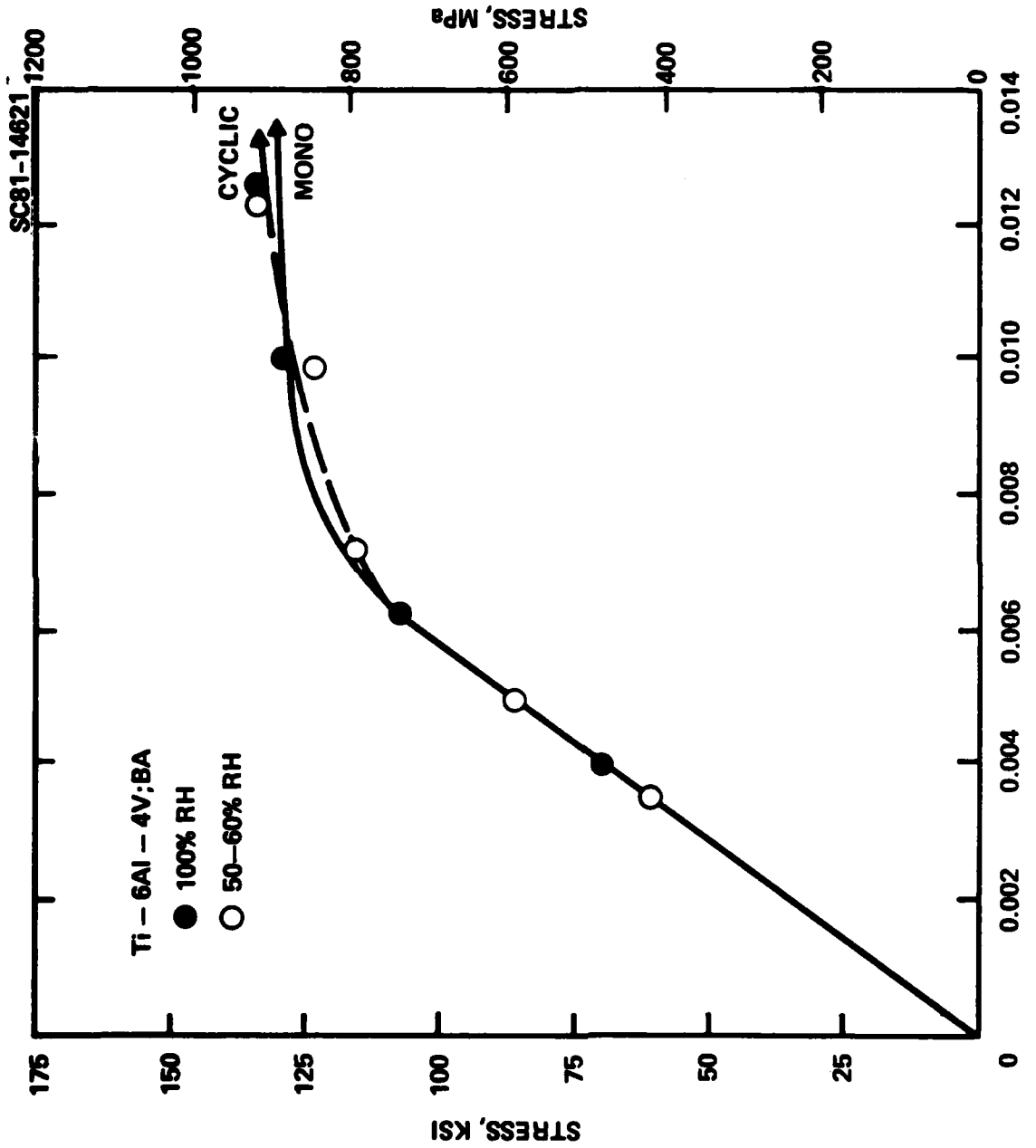

Fig. 24 Monotonic and cyclic stress-strain curves for Ti-6Al-4V, BA condition.

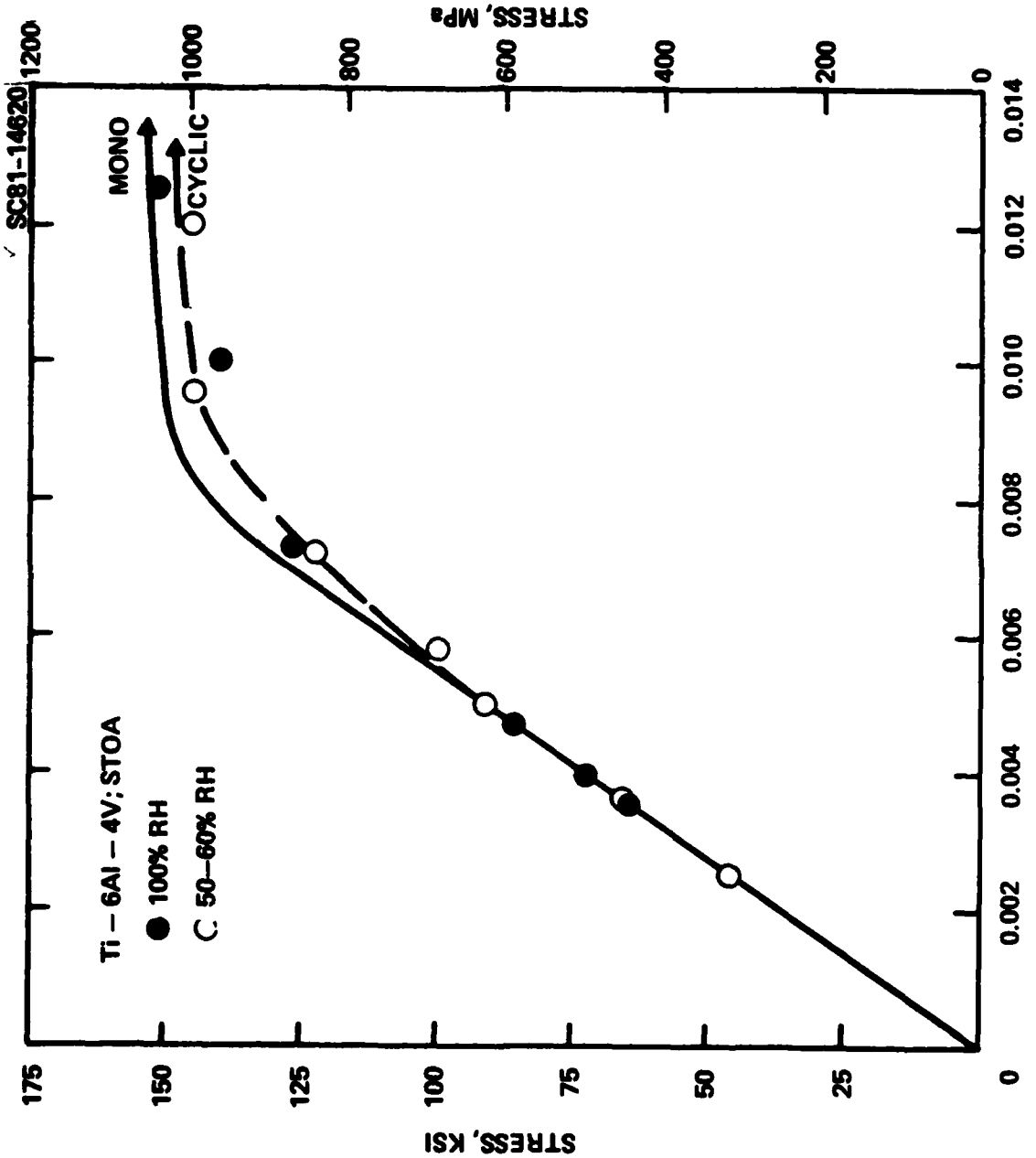

Fig. 25 Monotonic and cyclic stress-strain curves for Ti-6Al-4V, STOA condition.

Note in Fig. 23 that the Ti-6Al-4V in the RA condition cyclically softens at strains less than ~ 0.009 and cyclically hardens at greater strains. The STOA condition cyclic softens slightly and for practical purposes the BA condition remains cyclically stable.

Table IX
Monotonic Tensile Properties of Ti-6Al-4V

Monotonic Properties			RA	BA	STOA
Modulus of Elasticity	E	(GPa)	123.4	120.0	126.2
Yield Strength, 0.2%	S_y	(MPa)	861.8	861.8	1037.7
Ultimate Strength	S_u	(MPa)	910.1	927.3	1081.1
Reduction of Area	%RA		30.1	21.2	34.7
True Fracture Strength	σ_f	(MPa)	1103.2	914.2	1406.6
True Fracture Ductility	ε_f	-	0.36	0.24	0.43
Strain Hardening Exponent	n	-	0.048	0.014	0.057
Strength Coefficient	K	(MPa)	1158.3	932.2	1475.5

Table X

Strain-Life Fatigue Results for Ti-6Al-4V Specimen With Three Microstructural Conditions Tested in Laboratory Air Environment (50 - 60% RH)

Spec. No.	Condition	Strain Amplitude $\Delta\varepsilon/2$	Rev's to Failure $2N_f$	Stabilized Stress Amp. σ_{sat} MPa	Elastic Strain $\varepsilon_e = \frac{\sigma_{sat}}{E}$	Plastic Strain $\varepsilon_p = \varepsilon - \varepsilon_e$
5254-3	RA	0.0122	350	993	0.0080	0.0042
5254-1		0.0102	1,026	945	0.0077	0.0025
5254-6		0.0074	3,200	779	0.0063	0.0011
5254-7		0.005	22,980	600	0.0049	0.0001
5254-2		0.004	41,560	510	0.0040	-
5254-40	STOA	0.0129	950	1000	0.0079	0.0041
5254-37		0.0095	1,560	986	0.0078	0.0017
5254-35		0.0072	6,706	834	0.0066	0.0006
5254-38		0.0058	25,636	676	0.0054	0.0004
5254-41		0.005	56,188	621	0.0049	0.0001
5254-42		0.0036	545,262	455	0.0036	-
5254-26	BA	0.0123	110	924	0.0077	0.0046
5254-22		0.0098	850	848	0.0071	0.0027
5254-27		0.0072	1,014	793	0.0066	0.0006
5254-18		0.0049	20,360	593	0.0049	-

Table XI

Strain-Life Fatigue Results for Ti-6Al-4V Specimens With Three Microstructural Conditions Tested in a 100% RH Environment

Spec. No.	Condition	Strain Amplitude $\Delta\epsilon/2$	Rev's to Failure $2N_f$	Stabilized Stress Amp.* σ_{sat} MPa	Elastic Strain $\epsilon_e = \frac{\sigma_{sat}}{E}$	Plastic Strain $\epsilon_p = \epsilon - \epsilon_e$
5254-9	RA	0.0125	218	1048	0.0085	0.0040
5254-10		0.0092	778	924	0.0075	0.0017
5254-14		0.0073	2,624	800	0.0065	0.0008
5254-16		0.0050	11,120	620	0.0050	-
5254-12		0.0041	25,160	517	0.0041	-
5254-43	STOA	0.0126	370	1048	0.0084	0.0042
5254-44		0.0100	956	956	0.0076	0.0024
5254-48		0.0073	3,500	862	0.0068	0.0005
5254-46		0.0048	23,664	586	0.0046	0.0002
5254-30	BA	0.0126	134	917	0.0076	0.0050
5254-32		0.0100	290	883	0.0074	0.0026
5254-33		0.0063	3,346	731	0.0060	0.0003
5254-34		0.0040	41,270	480	0.0040	-

*Measured at approximately 50% of life to failure.

Figures 26, 27 and 28 show the strain-life curves for Ti-6Al-4V in the three microstructural conditions, RA, BA and STOA, respectively. The results at room temperature/room humidity are designated 50 - 60% RH while those for the saturated water tests are designated 100% RH.

For the 50 - 60% RH results, the total strains have been divided into respective elastic and plastic strain components. Best fit straight lines have been constructed allowing representation of these data by slopes and intercepts through the strain-life equation

$$\frac{\Delta\epsilon}{2} = \frac{\sigma_f'}{E}(2N_f)^b + \epsilon_f'(2N_f)^c \qquad (7)$$

where

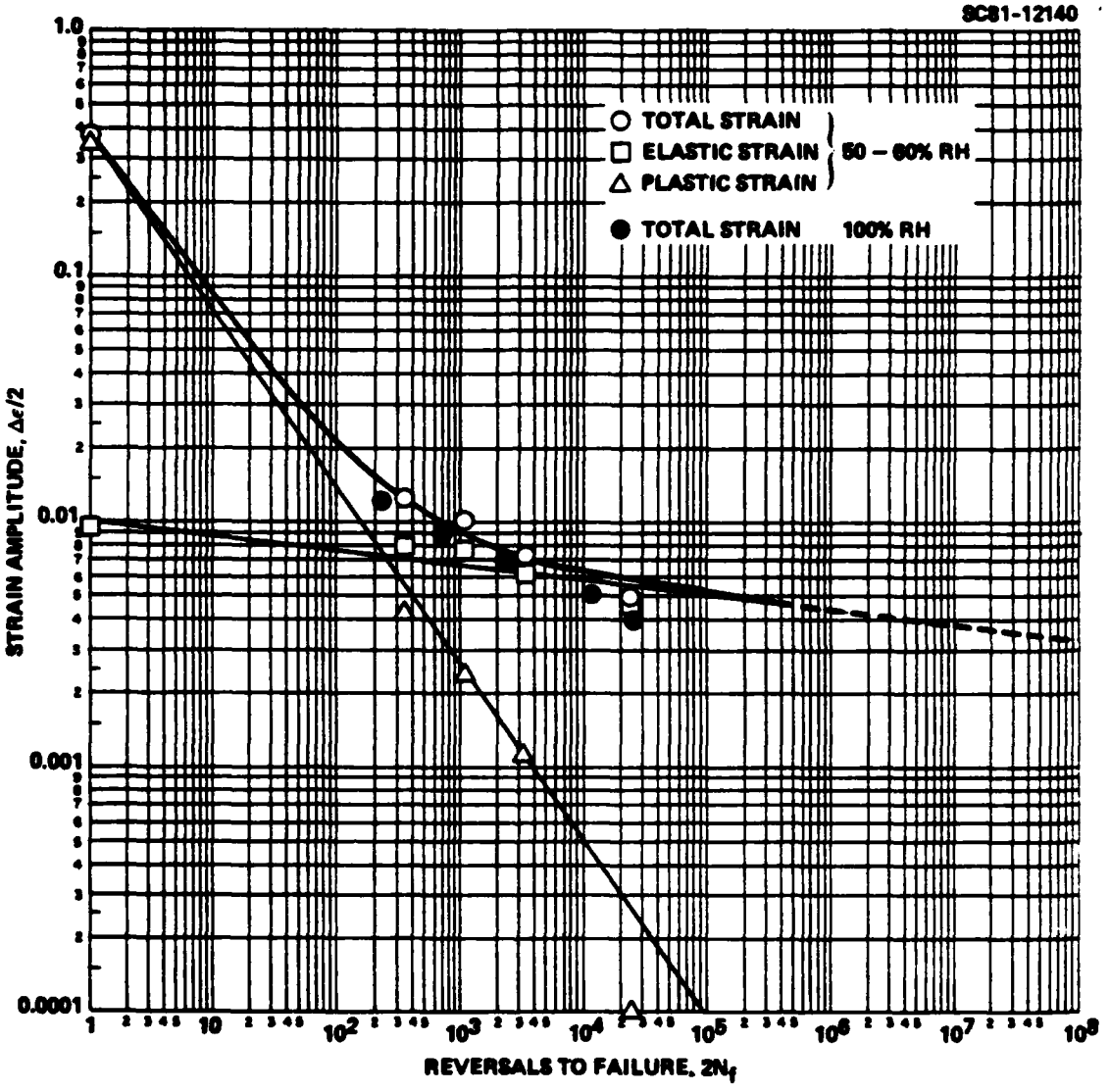

Fig. 26 Strain-life curve for Ti-6Al-4Vr, RA condition.

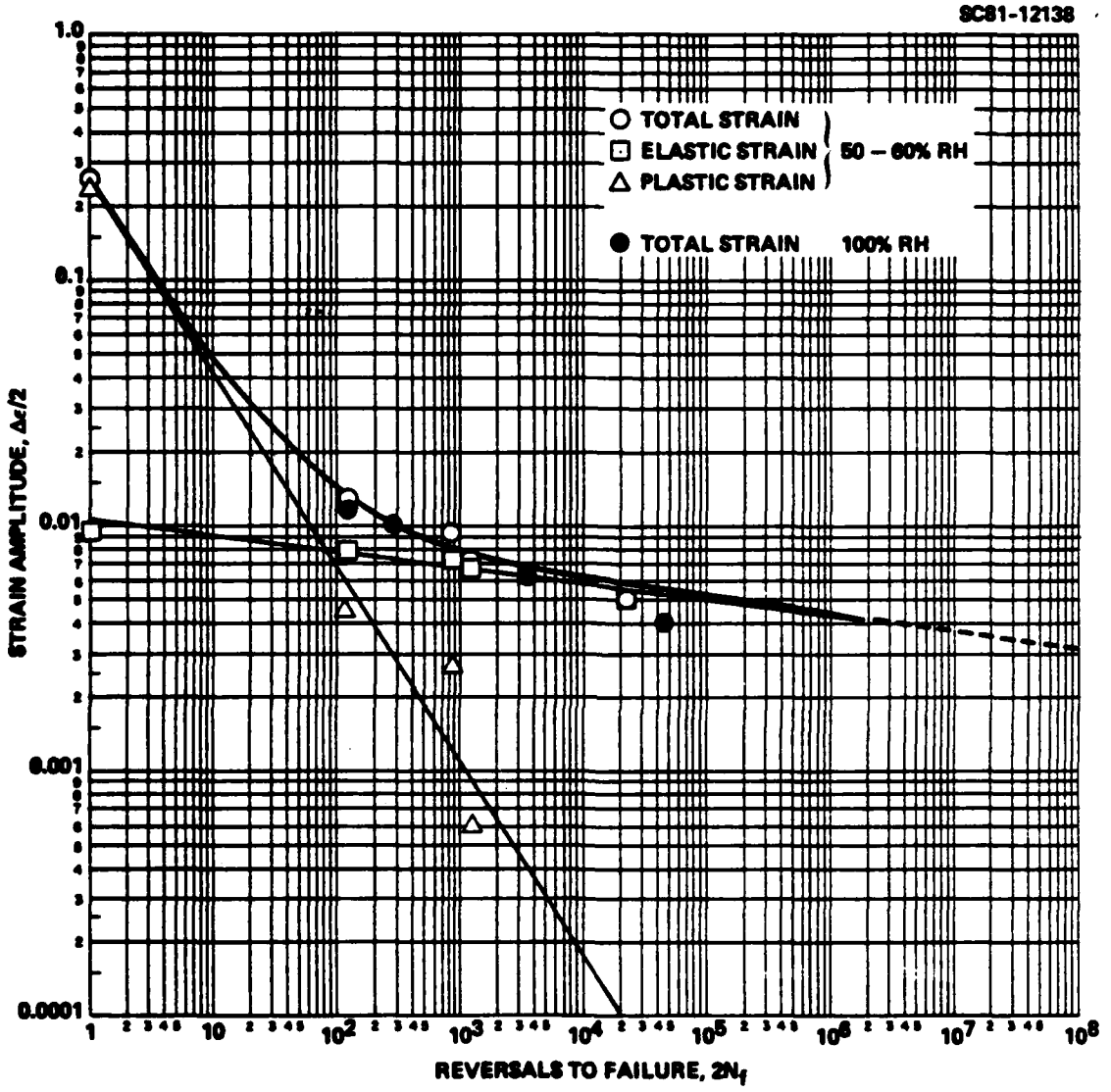

Fig. 27 Strain-life curve for Ti-6Al-4V, BA condition.

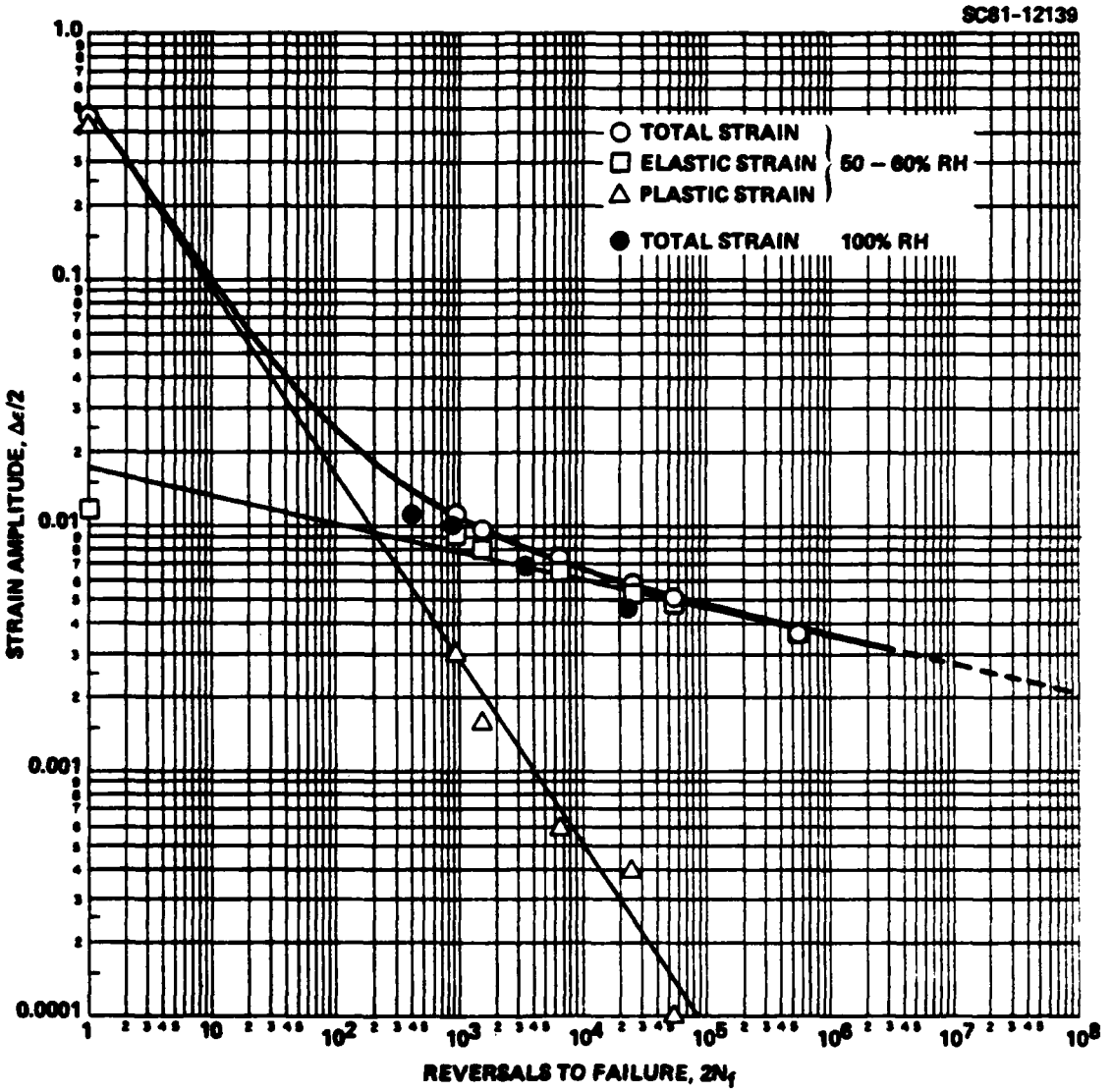

Fig. 28 Strain-life curve for Ti-6Al-4V, STOA condition.

$\Delta\varepsilon/2$ = total strain amplitude
$2N_f$ = reversals to failure
E = modulus of elasticity
σ_f' = fatigue strength coefficient
ε_f' = fatigue ductility coefficient
b = fatigue strength exponent
c = fatigue ductility exponent.

The elastic strain-life line has the slope b and an intercept σ_f'/E whereas the plastic strain-life line has the slope c and an intercept ε_f'. Values of these fatigue properties for the three microstructural conditions of Ti-6Al-4V are given in Table XII.

Table XII
Material Properties of Ti-6Al-4V

Microstructure	RA	BA	STOA
Modulus of Elasticity, E (GPa)	123.4	120.0	126.2
Cyclic Strength Coeff, K' (MPa)	1964.3	1801.6	2060.8
Cyclic Strain Hardening Exp., n'	0.14	0.14	0.14
Fatigue Ductility Coeff., ε_f'	0.40	0.27	0.52
Fatigue Ductility Exp., c	-0.76	-0.79	-0.75
Fatigue Strength Coeff., σ_f' (MPa)	1727.8	1499.6	1892.6
Fatigue Strength Exp., b	-0.106	-0.107	-0.097

Comparison of the total strain-life curves for each microstructural condition evaluated in laboraotry air (50 - 60% RH) and 100% RH shows that increased humidity decreases life to crack initiation. Although there is an effect on fatigue life of Ti-6Al-4V due to increased humidity there is little or no change in the cyclic stress-strain or deformation response of the Ti-6Al-4V, as shown in Figs. 23, 24 and 25. Similar behavior has been observed in aluminum

and steel alloys subject to fatigue and combined high humidity [24]. For the subject titanium alloys, a cumulative fatigue damage analysis was performed using laboratory air deformation response (i.e., cyclic stress-strain curve) while the fatigue-life behavior in an aqueous environment was described through a modification of the fatigue strength exponent, b. By such a modification to the strain-life curve, the longlife regime is most greatly affected. Using this technique and appropriate crack growth methodology predictions of the total life within a factor of three of actual life have been made for steel and aluminum components subject to alternate dry/humid environments and pseudo-random block loading histories.

Figures 29, 30 and 31 show the notched-bar, axial stress-life data for the three microstructural conditions tested in laboratory air, at 20 Hz and R = -1. The theoretical stress concentration factor, K_t, was 2.52 for the specimen geometry and loading mode used. From the notched fatigue strength at 10^7 reversals, and from the smooth bar fatigue strength at 10^7 reversals, the fatigue notch factor, K_f, was calculated. The smooth-bar (or unnotched) fatigue strength is calculated from the strain for 10^7 reversals from the unnotched, strain-life data and the Young's modulus. The unnotched fatigue strength for 10^7 reversals is also shown in Figs. 29, 30 and 31.

The unnotched fatigue strength and notched fatigue strength rankings along with the fatigue notch factor, K_f, for the three microstructural conditions are given in Table XIII, where 1 to 3 reflects most to least fatigue resistant.

Table XIII

Fatigue Rank and K_f for Ti-6Al-4V

Unnotched Rank	Notched Rank	K_f
1. STOA	1. BA	BA: 1.4
2. RA	2. RA	RA: 2.1
3. BA	3. STOA	STOA: 2.4

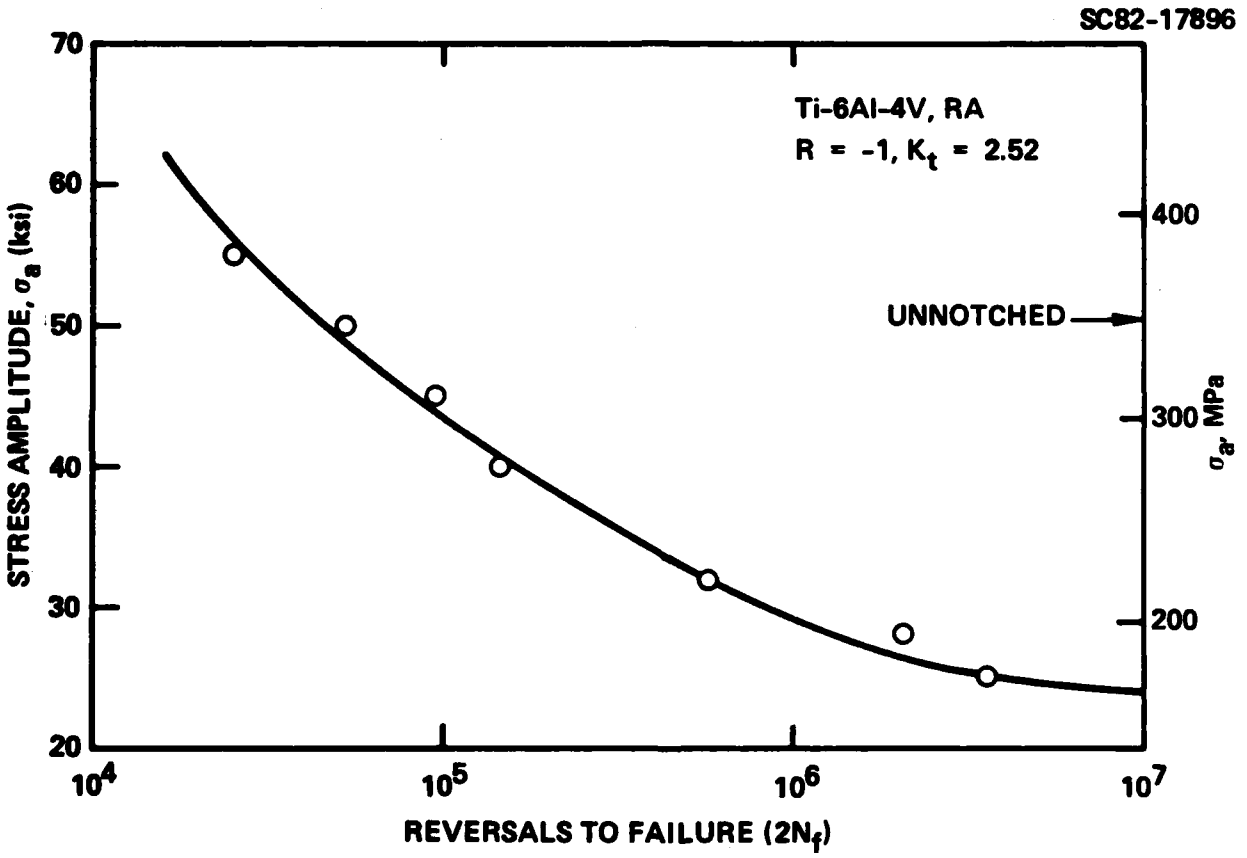

Fig. 29 Notched-bar fatigue-life data for Ti-6Al-4V, RA condition.

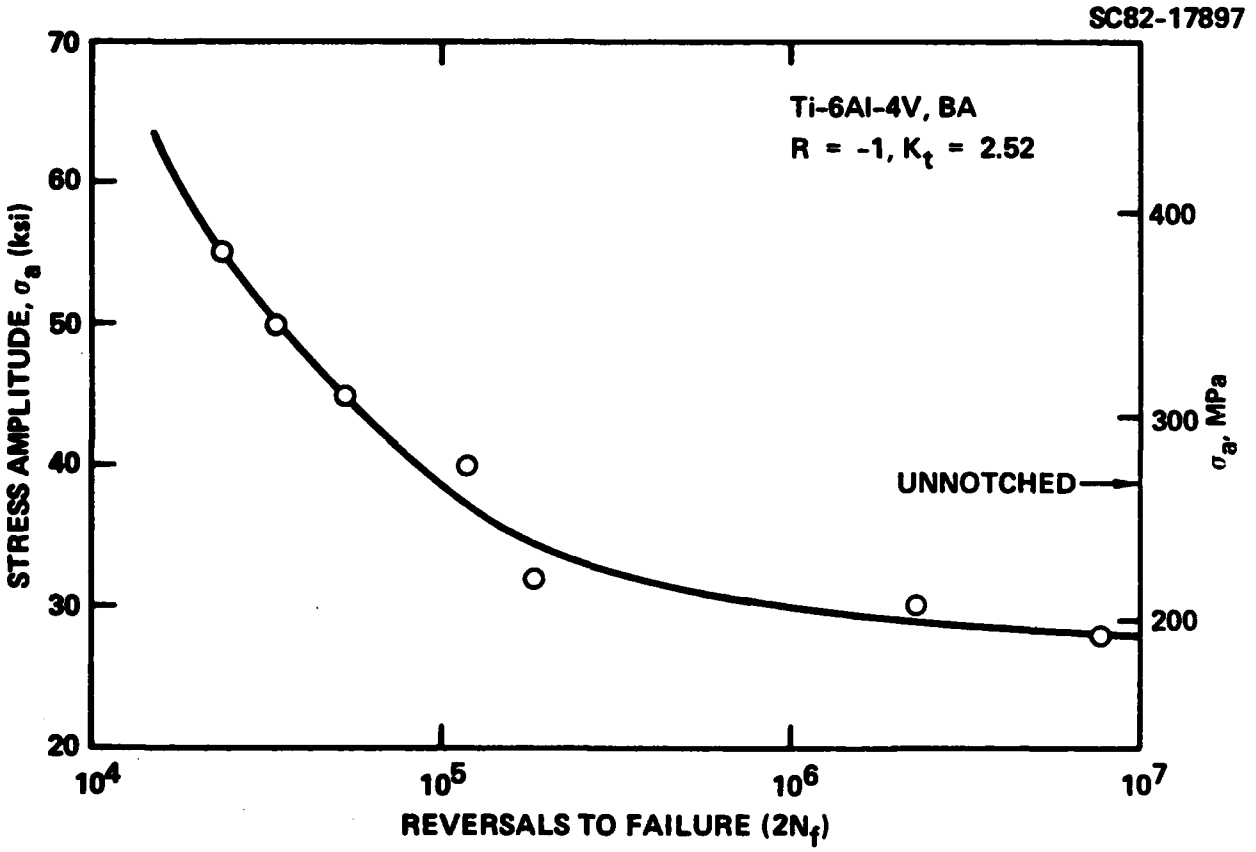

Fig. 30 Notched-bar fatigue-life data for Ti-6Al-4V, BA condition.

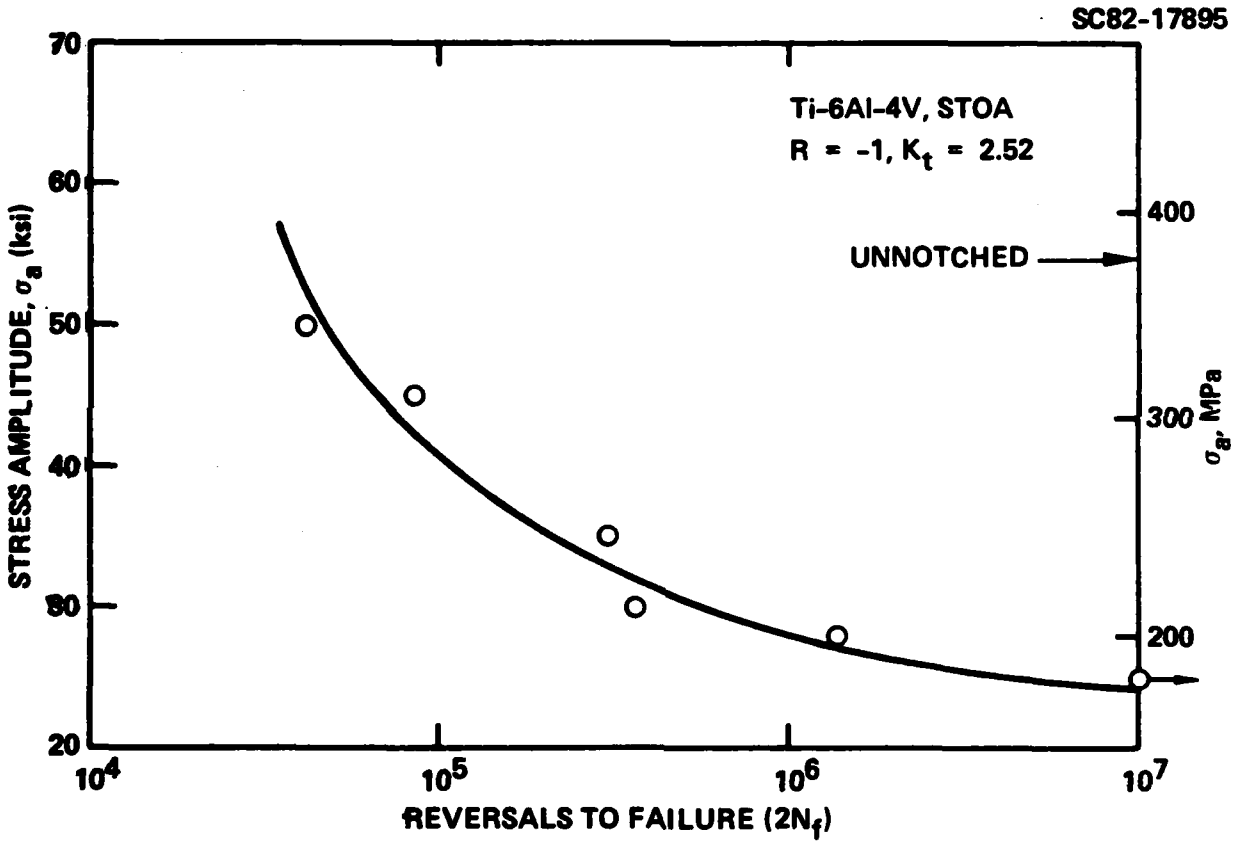

Fig. 31 Notched-bar fatigue-life data for Ti-6Al-4V, STOA condition.

4.3.4 Prediction of Fatigue Crack Growth Rates from LCF

A model, developed by Charkrabortty and Starke [30] and modified by Heikkenen [33] for near-threshold growth, can be used to predict fatigue crack growth behavior from low-cycle fatigue (LCF) properties and a characteristic microstructural parameter. This predictive model has been used to predict the near-threshold fatigue crack growth rate curve for each of the three microstructures tested in laboratory air. The results of the predictions along with the experimental data are shown in Figs. 32, 33 and 34. Figure 32 shows the data and prediction for two different microstructural parameters in RA microstructure, 1) the mean alpha phase grain size (λ = 12 μm) and 2) the alpha phase mean free path (λ = 24 μm). Figure 33 shows the case for the beta annealed (BA) condition with predictions for λ = 2 μm (the α plate thickness) and two colony size values. Lambda was initially set at 29 μm based on an estimate of the colony size. More accurate measurement of the Widmanstatten alpha colony size yielded a value of 40 μm. Figure 34 shows the case for the solution-treated and over-aged (STOA) microstructure with predictions for λ = 7.0 μm, the alpha-phase grain size, and λ = 14 μm, the mean free path in the transformed matrix.

In all three cases an excellent fit between a predicted curve and the experimental data was found for a sensible microstructural parameter. The significance of such microstructural parameters will be addressed in the discussion section.

4.3.5 Fatigue Damage Analysis

An improved computer program for cumulative fatigue damage analyses was developed. For understanding of the procedure employed in this damage analysis, an illustrative example follows.

Fatigue lifetime prediction techniques require basically three inputs (1) a description of material properties, namely the cyclic stress-strain and strain-life curve (2) the geometric effect in reducing the fatigue life of the component in question, for example, the fatigue strength reduction factor, K_f, and (3) the loading sequence applied to the component in actual service.

SC82-19485A

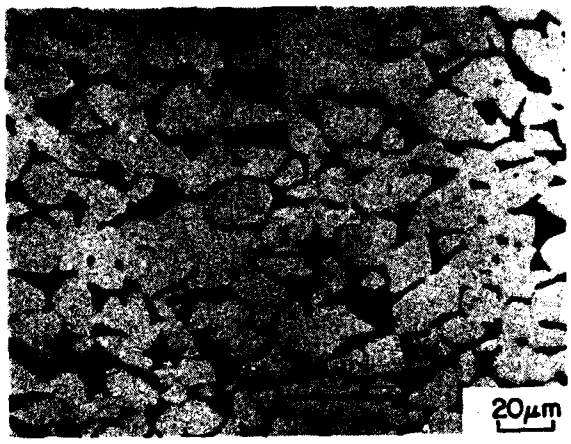

(a)

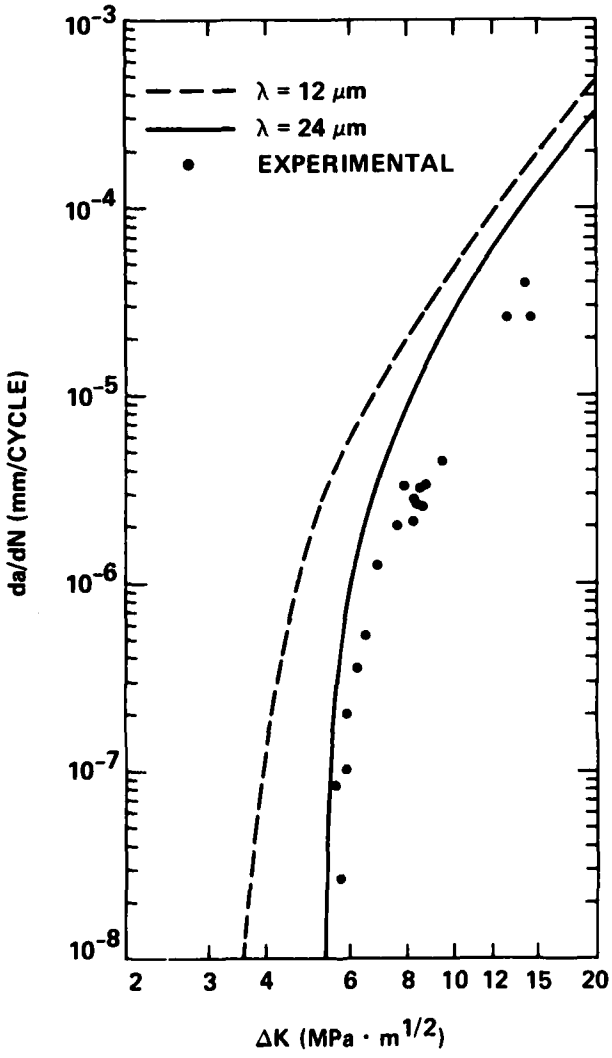

(b)

Fig. 32 Predicted FCP for Ti-6Al-4V, RA condition.

SC83-23119

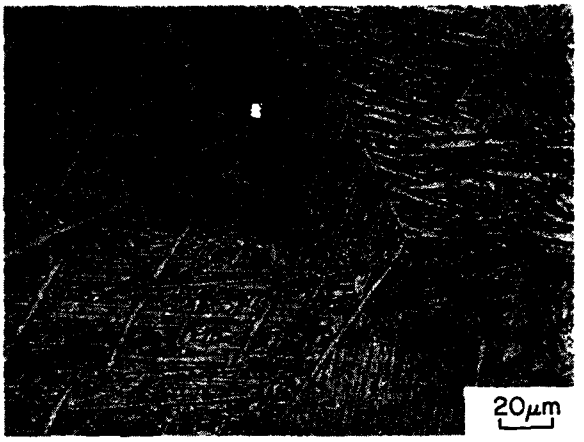

(a)

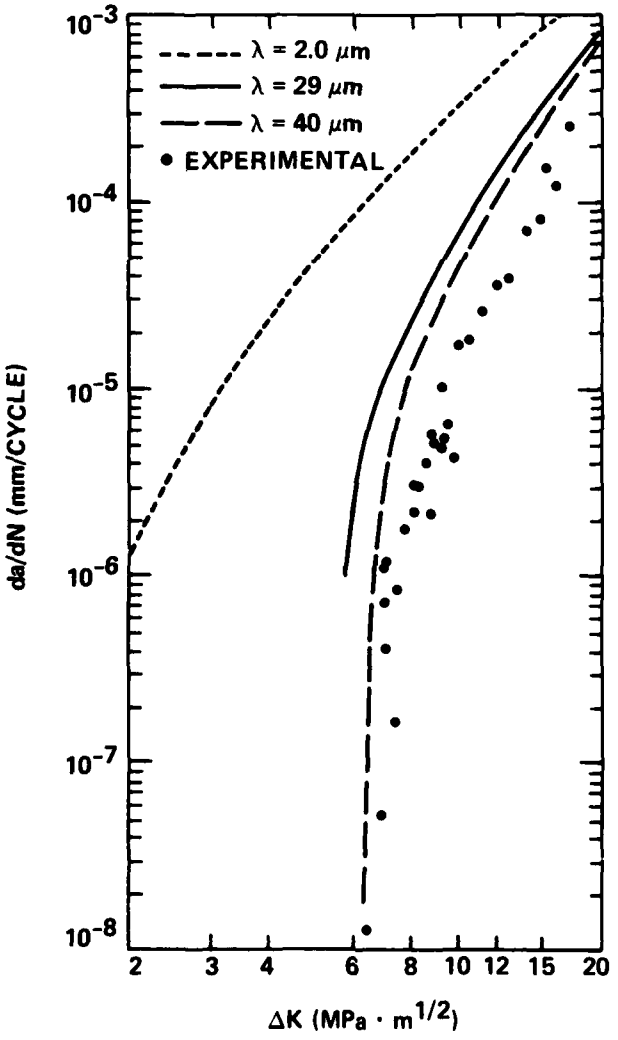

(b)

Fig. 33 Predicted FCP for Ti-6Al-4V, BA condition.

SC83-23118

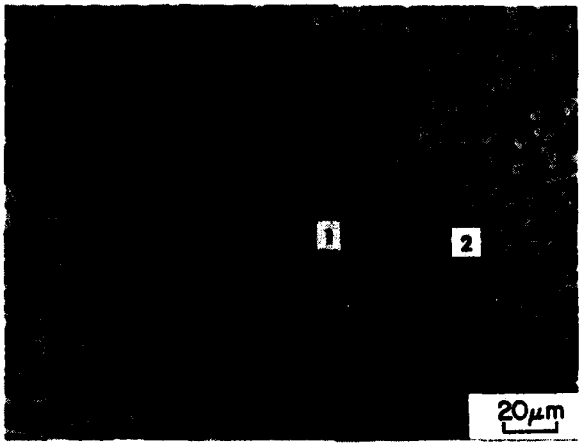

(a)

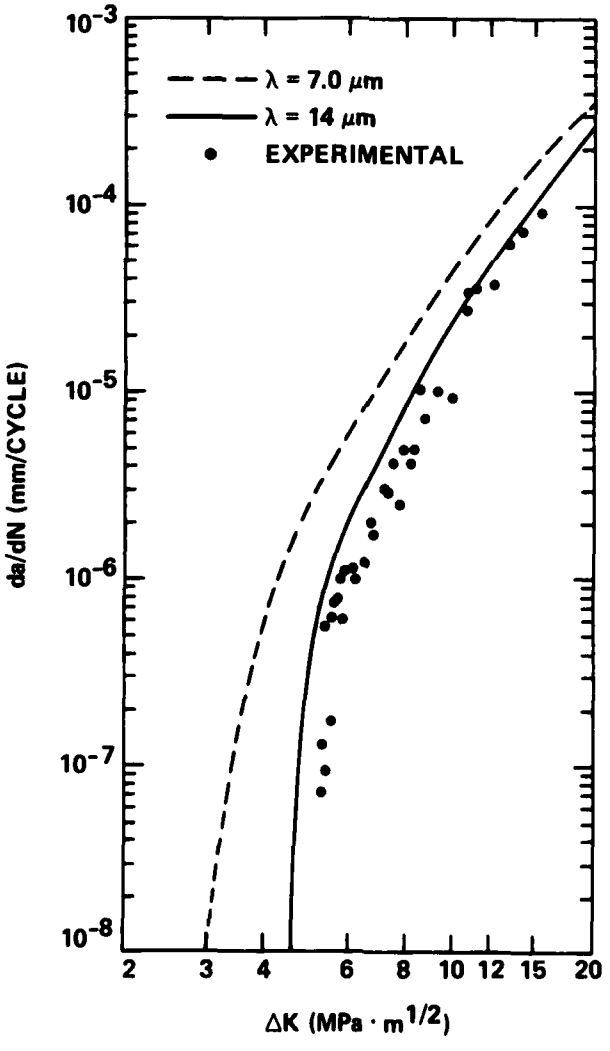

(b)

Fig. 34 Predicted FCP for Ti-6Al-4V, STOA condition.

Figure 35 illustrates a simple strain-time, pseudo-random history (or one block) from point A to point A. The cumulative fatigue damage program first accepts such a history and through constitutive relationships of stress and strain (the cyclic stress-strain relationships) "models" the stress-time response, Fig. 35b. The relationship employed is of the form

$$\varepsilon = \frac{\sigma}{E} + \left(\frac{\sigma}{K'}\right)^{1/n'} \tag{8}$$

where

ε = strain amplitude
σ = stress amplitude
K' = cyclic strength coefficient
n' = cyclic strain hardening exponent.

If strain is input, then an iteration for stress is necessary. If stress is input, the solution for strain is straightforward. Elimination of the time variable then produces the stress-strain response as shown in Fig. 35c. As can be seen there are a series of closed hysteresis loops in stress-strain space, namely loops A-D-A, D-E-D, B-C-B and F-G.F. Each loop has associated with it a strain amplitude, ε, and a mean stress, σ_0. Take, for example, loop A-D-A which is symmetric about zero stress and strain. Since A-D-A has no mean stress σ_0 is zero and the strain amplitude is half the strain range (i.e., $\varepsilon = \overline{AD}/2$). The "damage" associated with this excursion is determined by the reciprocal life, $1/2N_f$, at this strain amplitude found through iteration of the strain-life equation

$$\varepsilon = \frac{\sigma_f'}{E} (2N_f)^b + \varepsilon_f' (2N_f)^c \tag{9}$$

where

σ_f' = fatigue strength coefficient
b = fatigue strength exponent

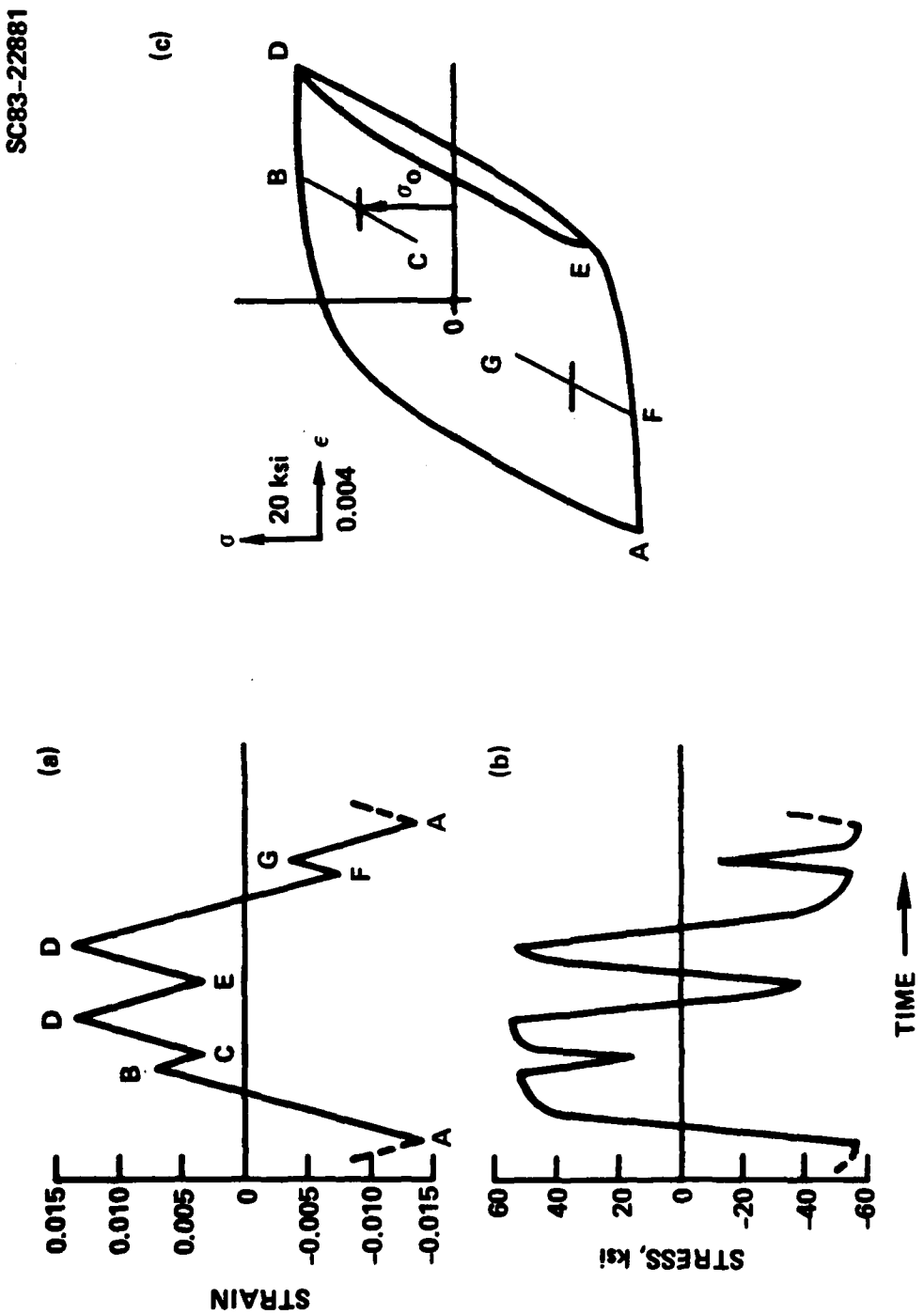

Fig. 35 Imposed variable-strain history and stress response.

ε_f' = fatigue ductility coefficient
c = fatigue ductility exponent
E = modulus of elasticity
$2N_f$ = reversals to failure

and solving for the value of $2N_f$. Had there been N_i-occurrences at this particular strain amplitude the "damage" is calculated as $d_i = Ni/2N_f$.

Now, consider the two closed loops B-C-B and F-G-F. B-C-B has a tensile mean stress, $+ \sigma_o$, while F-G-F has a compressive mean stress, $- \sigma_o$. The strain amplitude associated with both these loops is the same numerical value (e.g., $\varepsilon = \overline{CB}/2$, $\varepsilon = \overline{GF}/2$), however, there is an opposite effect of the mean stress. Compressive mean stresses tend to increase fatigue life while tensile mean stresses decrease fatigue life. This damage analysis program accounts for mean stress by iteration of the equation

$$\varepsilon = \left(\frac{\sigma_f' - \sigma_o}{E}\right)(2N_f)^b + \varepsilon_f'(2N_f)^c \qquad (10)$$

where σ_o = mean stress with appropriate sign (- = compression, + = tension). Again, after the life to failure at the strain amplitude, mean stress combination is determined, the damage associated with these events is the reciprocal life. This same sequence of events is employed for damage calculations in even more complex input histories as discussed later in this section for an F-15 navigation history containing 68 peak and valley stresses.

The previous example applies to a smooth sample without a stress concentration caused by a change in geometry. Let us now consider a notched member as shown in Fig. 36. Nominally, the stress, S, and strain, e, are applied to the sample. The geometry change concentrates the stress and strain at the root of the notch where the local stress and strain are respectively σ and ε. The fatigue strength reduction factor is used to relate nominal to local stresses and strains since

SC83-22880

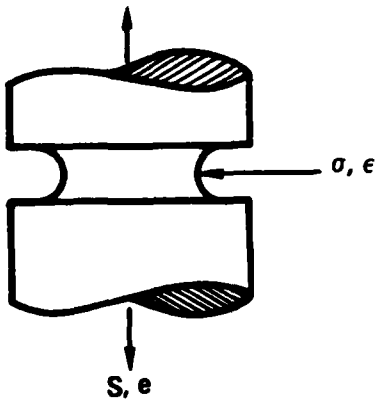

Fig. 36 Schematic of notch geometry and variables.

$$K_f = \left(\frac{\Delta\sigma\Delta\varepsilon E}{\Delta S \Delta e E}\right)^{1/2} \tag{11}$$

where Δ signifies ranges in stress or strain. Although the nominal stresses and strains may be plastic, for simplicity of illustration assume they are elastic. Since "elastically," stress and strain are proportional through the modulus of elasticity we have

$$S = Ee \tag{12}$$

and Eq. (11) is rewritten as

$$K_f \Delta S = (\Delta\sigma\Delta\varepsilon E)^{1/2} \tag{13}$$

or

$$\Delta\sigma\Delta\varepsilon = \frac{(K_f \Delta S)^2}{E} \quad . \tag{14}$$

The input strain- (or stress-) time history defines the value of ΔS. Since K_f and E are known, the right hand side of Eq. (14) is a constant for a given value of ΔS. Thus, $\Delta\sigma\Delta\varepsilon$ = constant is by definition, a rectangular hyperbola. There exists a family of values for both Δσ and Δε that will satisfy this relationship. However, if the cyclic stress-strain curve of the material of interest is traced in rectangular coordinate space, as illustrated in Fig. 37, there is a unique value of the <u>product</u> of stress and strain (point P) that satisfies the relationship. In a pseudo-random history each peak and valley of nominal strain (or stress) must be associated with a local value of strain (or stress) in order to to access "damage." This is accomplished in a point-to-point analysis by employing the relationship

$$\frac{(K_f \Delta S)^2}{E} = \Delta\sigma\Delta\varepsilon = \frac{(\Delta\sigma)^2}{E} + \Delta\sigma \left(\frac{\Delta\sigma}{K'}\right)^{1/n'} \tag{15}$$

for solution of the point-to-point products of local stress and strain. Once stored in an array within the damage analysis program, the "scaled," local

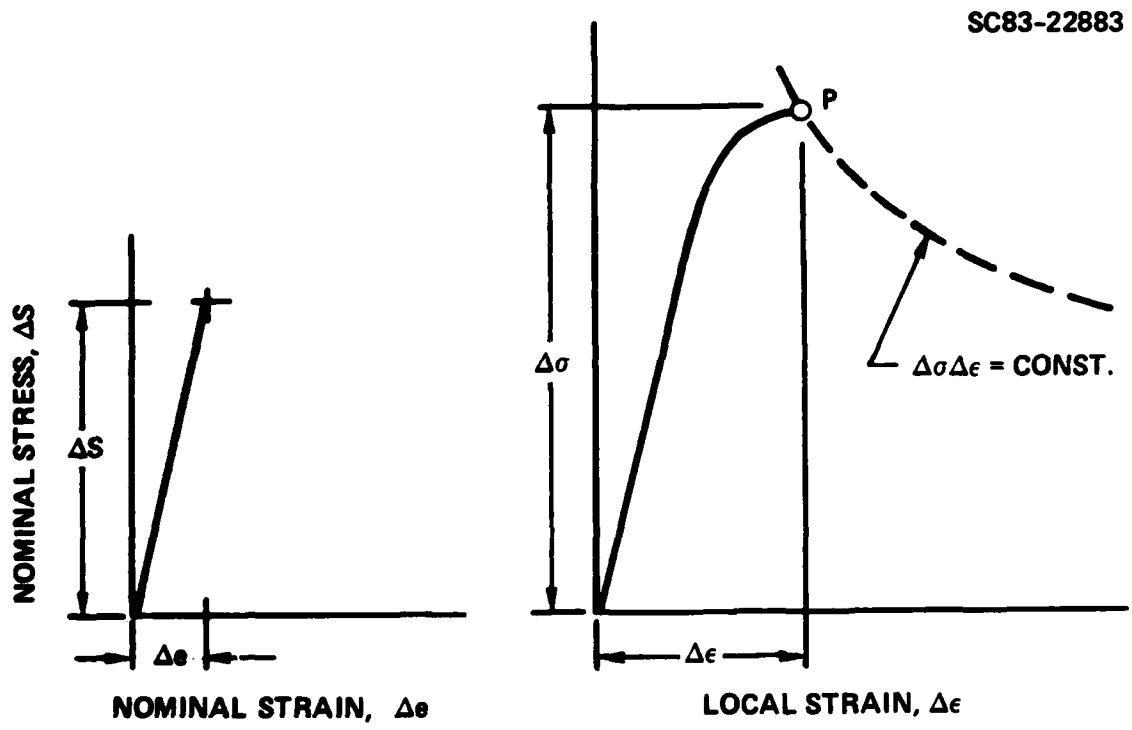

Fig. 37 Nominally imposed elastic stress and strain and local changes in stress and strain at a notch roof.

stress-strain response is analyzed for damage in the same way as for the smooth sample. That is, the "scaled" response is divided into closed hysteresis loops each being associated with a strain amplitude, mean stress combination and the damage assessed as the number of occurrences divided by the life to failure at each strain amplitude, mean stress combination. The total damage is then determined by algebraically adding the individual damages associated with closed loop events.

The material property data employed in the cumulative fatigue damage analysis for Ti-6Al-4V in various microstructural conditions is given in Table XII. Figure 38 shows a portion of the navigation history of an F-15 aircraft that was used as the pseudo-random, nominal stress-time history employed in the damage analysis program. For purposes of scaling the magnitude of peaks and valleys in the history, the maximum stress was selected as 827 MPa corresponding to the digitized event of +999 given in Table XIV. The results of

Table XIV

Series of 68 Digitized Events of F-15 Navigation History

Event #	Digitized	Event #	Digitized	Event #	Digitized	Event #	Digitized	Event #	Digitized
1	66	18	475	35	285	52	500	65	143
2	999	19	214	36	500	53	114	66	228
3	143	20	500	37	214	54	257	67	143
4	542	21	86	38	400	55	200	68	150
5	214	22	557	39	71	56	243	repeat block	
6	400	23	214	40	785	57	143		
7	357	24	500	41	143	58	285		
8	542	25	143	42	357	59	143		
9	214	26	400	43	214	60	642		
10	542	27	214	44	500	61	257		
11	143	28	500	45	143	62	400		
12	557	29	457	46	714	63	143		
13	157	30	571	47	214	64	285		
14	371	31	285	48	285				
15	114	32	357	49	143				
16	428	33	143	50	428				
17	214	34	357	51	357				

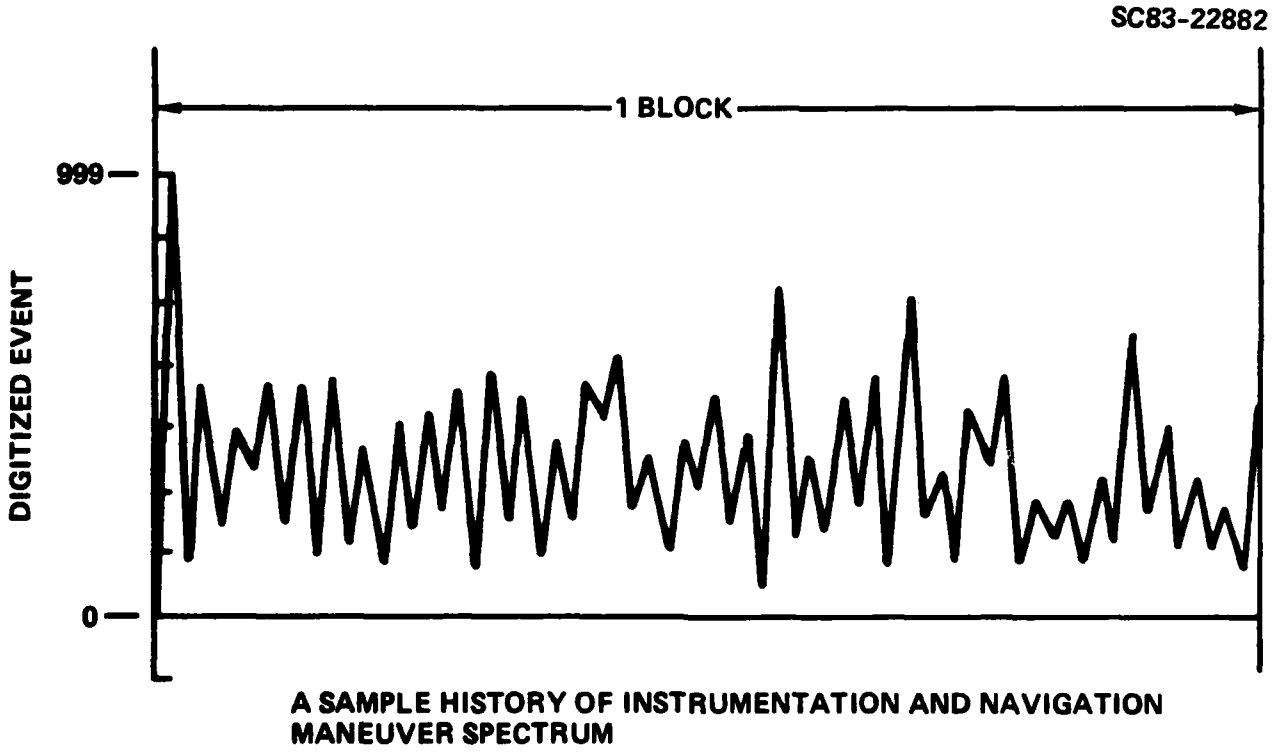

Fig. 38 A sample history of instrumentation and navigation maneuver spectrum.

the cumulative fatigue damage analysis for smooth specimens with maximum nominal stress of the navigation history scaled to 120 ksi are given in Table XV.

Fatigue life prediction for notched members was also performed, these results are also given in Table XVI. The STOA condition is most notch sensitive by virtue of its higher strength.

Table XV

Predicted Blocks to Crack Initiation Under F-15 Navigation History for Smooth and Notched Samples of Ti-6Al-4V in Various Microstructural Conditions

Specimen Geometry	RA	BA	STOA
Smooth	9850	18000	70000
Notched	33	105	45
K_f used for Predictions of Notched Specimen Life	2.1	1.4	2.4

4.4 Discussion

4.4.1 Fatigue Crack Propagation

The microstructures developed for the fatigue and fracture study were similar to those used in a previous study on pancake forgings of Ti-6Al-4V [28]. Although data for the plate material in this program and pancake forgings in the previous program cannot be compared directly, similar microstructural effects should be observed.

Fatigue crack propagation behavior produced no surprises, in that the plate material behaved similarly to the forging material from the previous study. For of the recrystallization annealed (RA) condition, the data in laboratory air correlated very well with the previous results as was shown in Figure 16. The dip in the FCP curve between ΔK of 8 and ΔK of 15 $MPa.m^{1/2}$ correlated well with the grain size spread which observed was in this material. The change in growth rate at ΔK levels representing a reverse plastic zone size equal the grain size

is in agreement with the results of Yoder, et al [32]. The ranking of the three microstructures in laboratory air at near-threshold growth rates is the same as the result ranking from other studies [28, 134], in that the STOA condition exhibits the fastest growth rate while the BA condition exhibits the slowest growth rate with the RA condition intermediate to the two. The lower growth rate of the RA microstructural condition with respect to BA microstructural condition at higher ΔK levels is probably associated with the dip in the curve for the RA material. Such behavior probably results from the combined effect of the grain size and texture on FCP affect. The material used in this study exhibited some texture as opposed to the weakly and uniformly pancake forgings used in the previous study. Beta annealed microstructures are generally found to exhibit the slowest growth rate of the three microstructural condition ratio at load ratios (R) of 0.1 to 0.3, in the absence of significant texture.

For the BA and STOA conditions, increased humidity had a negligible effect on fatigue crack propagation behavior. The increased crack growth rate at a given ΔK level in the case of the RA microstructural condition was larger than might be expected from the change in relative humidity from 50% to 100%. Examination of the fracture surfaces of the two specimens revealed more faceted fracture in the wet air test specimen than in the laboratory air test specimen. The faceted fracture and associated accelerated cracking can be related to the texture of this plate material. The recrystallization annealed (RA) microstructure consists of equiaxed primary alpha grains. If a significant degree of texture exists in the material, adjacent grains may be similarly oriented thereby presenting a longer unconstrained slip distance and reduced cracking resistance in a more aggressive environment.

4.4.2 Low Cycle Fatigue

The monotonic and cyclic stress strain properties from this study are in good agreement with previous results [28]. The RA microstructural condition cyclically softens at strains less than 0.009 and cyclically hardens at greater strains. The BA microstructural condition is essentially cyclically stable and

the STOA cyclically softens only slightly. The cyclic stress strain behavior of the three microstructural conditions was unaffected by humidity. The strain-life behavior of the three microstructural conditions produced a ranking which was comparable to that found for similar microstructures in stress controlled (S-N) tests. The STOA condition exhibited the best behavior, and the BA condition the worst, with the RA condition intermediate. Increased humidity tends to decrease the life-to-initiation as can been seen in Figures 26, 27, and 28, but the decrease is small for all three microstructural conditions.

The notched-fatigue ranking, shown in Table XIII, is changed from the unnotched ranking in that the BA condition is most fatigue resistant, the STOA the least resistant, and the RA, intermediate. This change in ranking relates to the strength of the various microstructural conditions and the attendant notch sensitivity. The highest-strength microstructural condition, STOA, has the largest fatigue notched factor and the poorest notched fatigue life ranking.

4.4.3 Prediction of Fatigue Crack Growth Rate from LCF Properties

Excellent results were obtained in predicting near-threshold fatigue crack growth behavior of all three microstructural conditions using the model of Charkrabortty and Starke [30] as modified by Heikkenen [33] suitable microstructural parameters. In all three cases, the microstructural parameter which resulted in the predicted curve being in excellent agreement with experimental data, could be rationalized in terms of a microstructural constituent which was important to the slip and cracking behavior of that microstructure. For the recrystallization annealed (RA) microstructure, the microstructural parameter was the alpha-phase, mean free path which was essentially two alpha grain diameters. In a material of this microstructural condition which has significant texture, two adjacent alpha grains can be considered to act as a single slip unit and therefore be the controlling microstructural constituent.

In the beta annealed (BA) microstructural condition, the controlling microstructural parameter was found to be the Widmanstatten-alpha colony size as indicated in Fig. 33. In a considerable amount of the literature concerning

AD-A133 947 DEFORMATION AND FATIGUE OF AIRCRAFT STRUCTURAL ALLOYS (U) ROCKWELL INTERNATIONAL THOUSAND OAKS CA SCIENCE CENTER J A WERT ET AL. JUL 83 SC5254.2FR 2/2

UNCLASSIFIED AFOSR-TR-83-0745 F49620-80-C-0030 F/G 11/6 NL

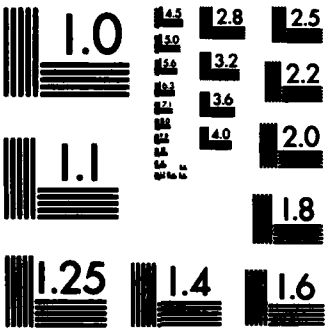

beta microstructures, the colony size is found to be a controlling feature for slip and cracking behavior. The alpha platelets in a single colony tend to act as a single slip unit especially in the absence of a significant amount of beta phase between the alpha platelets as shown by Hack and Leverant [35]. Thus, it is not surprising that excellent agreement between the predictive curve and the experimental data is seen to correlate with the Widmanstatten alpha colony size in this microstructural condition.

In the higher-strength, STOA condition, the controlling microstructural feature appears not to be the alpha grain but the transformed beta matrix. In Fig. 34 the mean linear intercept for the alpha phase particles is 14 μm. The predicted curve using this microstructural dimension showed excellent agreement with the experimental data. The use of the mean linear intercept through the transformed beta phase appears reasonable in terms of the relative strength and cracking resistance of the alpha phase and the transformed beta matrix. In the high-strength STOA condition, a considerable portion of the strength is derived from the fine transformed matrix, and this matrix is generally observed to crack in a flat, lower-energy mode when compared to the crack propagation through the alpha particles. Therefore, it seems reasonable that the overall growth rate is controlled by cracking of the matrix as opposed cracking of the primary alpha particles.

In summary, excellent predictive capability of the model has been demonstrated. Selection of the controlling microstructural constituent requires careful analysis in that fatigue crack propagation behavior of titanium alloys is a complex interaction of the imposed plastic zone at the crack tip and the microstructural constituents on several scales and can be affected strongly by the crystallographic texture that exists in the material. The controlling microstructural feature may not be the most obvious one, as illustrated by the case of the STOA condition previously described.

4.4.4 Fatigue Damage Analysis

The predicted fatigue life results for smooth specimens subjected to pseudo-random loading conditions (Table XV) rank the microstructural conditions slightly differently than they are ranked under constant amplitude loading. The STOA condition has the longest life under both constant amplitude and pseudo-random loading conditions. However, the predicted ranking of the RA and BA microstructural conditions subjected to pseudo-random loading is reversed from the ranking observed for constant amplitude loading. It is thought that the shorter life of the RA condition under pseudo-random loading is related to the cyclic softening observed at low strain amplitudes in the cyclic stress-strain results, see Fig. 23.

The predicted fatigue life results for notched specimens subjected to pseudo-random loading are different than the predicted lives of smooth specimens under the same loading conditions. The prediction for the notched specimens suggests that the BA microstructural condition would have the longest life, followed by the STOA and RA microstructures. The BA microstructure is by far the least notch sensitive because of its moderately low value of fatigue strength reduction factor (i.e., Kf = 1.4). The ranking of the STOA and RA microstructural conditions under pseudo-random loading conditions can be understood by considering the superior ductility of the STOA condition, see Table IX. Selection of 827 MPa as the maximum stress in the loading history causes considerable notch root plasticity for all three microstructural conditions. The higher ductility of the STOA condition compared with the RA condition provides greater resistance to the occasional high strain excursions in the selected load history.

4.5 Conclusions

1. The fatigue crack propagation behavior of all three microstructural conditions was consistent with previous results for both forgings and plate Ti-6Al-4V.

2. Increased humidity only affected the crack growth behavior of recrystallization annealed Ti-6Al-4V, causing an acceleration in crack growth rate. The accelerated crack growth rate was associated with cleavage of the alpha phase.

3. Monotonic and cyclic stress-strain properties of the three microstructural conditions are in good agreement with previous results.

4. Low cycle fatigue properties of the three conditions were well behaved. Increased humidity decreases the life to initiation for all three conditions, but only slightly. The notched low-cycle fatigue rankings of the three microstructures are different from the smooth-bar ranking primarily as a result of the notch sensitivity of the higher strength STOA condition.

5. Fatigue crack propagation predictions using the model of Charkrabortty and Starke as modified by Heikkenen were in excellent agreement with the experimental data. The controlling microstructural features were: 1) the mean linear intercept distance through the alpha-phase particles in the RA condition, 2) the Widmanstatten alpha colony size in the BA condition, and 3) the mean linear intercept distance through the beta phase in the STOA condition.

5. References

1. D. Lee and W.A. Backofen, Trans. AIME, 1967, vol. 239, pp. 1034-1040.

2. J.A. Wert, Superplastic Forming of Structural Alloys, N.E. Paton and C.H. Hamilton, eds., The Metallurgical Society of AIME, Warrendale, PA, 1982, p. 69-83.

3. J.J. Kearns, J.E. McCauley and F.A. Nichols, J. Nuclear Materials, 1976 61, pp. 169-184.

4. C. Hammond, Superplastic Forming of Structural Alloys, N.E. Paton and C.H. Hamilton, eds., The Metallurgical Society of AIME, Warrendale, PA, 1982, pp. 131-145.

5. D.J. Lloyd and D.M. Moore, Superplastic Forming of Structural Alloys, N.E. Paton andC.H. Hamilton, eds., The Metallurgical Society of AIME, Warrendale, PA, 1982, pp. 147-169.

6. N. Ridley, Superplastic Forming of Structural Alloys, N.E. Paton and C.H. Hamilton, eds., The Metallurgical Society of AIME, Warrendale, PA, 1982, pp. 191-207.

7. N.E. Paton and J.A. Hall, U.S. Patent 4,299,626, November 10, 1981.

8. C.H. Hamilton, A.K. Ghosh and M.W. Mahoney, Advanced Processing Methods for Titanium Alloys, D.F. Hasson and C.H. Hamilton, eds., The Metallurgical Society of AIME, Warrendale, PA, 1982, pp. 129-144.

9. T. Chandra and D.M.R. Taplin, J. Materials Science, 1975, vol. 10, pp. 1642-1643.

10. J.A. Wert and N.E. Paton, Proc. Sixth International Conference on the Strength of Metals and Alloys, R.C. Gifkins eds., Pergamon Press, Oxford, 1982, pp. 727-732.

11. N.E. Paton and C.H. Hamilton, Met. Trans. A, 1979, vol. 10A, pp. 241-250.

12. M.F. Ashby and R.A. Verrall, Acta Met. 1973, vol. 21, pp. 149-163.

13. F. Dyment, Proc. of the Fourth International Conference on Titanium, H. Kimura and O. Izumi, eds., The Metallurgical Society of AIME, Warrendale, PA, 1980, pp. 519-528.

14. Metals Handbook, Eigth Edition, 8, Metallography, Structure and Phase Diagrams, American Society for Metals, Metals Park, OH, 1973, pp. 252-340.

15. G.B. Gibbs, D. Graham and D.H. Tomlin, Phil. Mag. 1963, vol. 8, pp. 1269-1281.

16. J.F. Murdock, T.S. Lundy and E.E. Stansbury, Acta Met. 1974, vol. 12, pp. 1033-1039.

17. R.R. Wells, Welding Journal [Welding Research Supplement] 1976, vol. 55, pp. 20-s to 27-s.

18. J.A. Wert, J.C. Chesnutt and N.E. Paton, "Deformation and Fatigue of Aircraft Structural Alloys," Annual Report No. 1, Contract F49620-80-C-0030, March, 1981.

19. N. Furushiro, H. Ishibashi, S. Shimoyama and S. Hori, Proc. of the Fourth International Conference on Titanium, H. Kimura and O. Izumi, eds., The Metallurgical Society of AIME, Warrendale, PA, 1980, pp. 993-1000.

20. M.E. Rosenblum, P.R. Smith and F.H. Froes, Proc. of the Fourth International Conference on Titanium, H. Kimura and O. Izumi, eds., The Metallurgical Society of AIME, Warrendale, PA, 1980, pp. 1015-1024.

21. W.R. Cribb, Scripta Met. 1979, vol. 12, pp. 893-898.

22. A.K. Ghosh and C.H. Hamilton, Met. Trans. A, 1982, vol. 13A, pp. 733-743.

23. Y. Ito and A. Hasegawa, Proc. of the Fourth International Conference on Titanium, H. Kimura and O. Izumi, eds., The Metallurgical Society of AIME, Warrendale, PA, 1980, pp. 983-992.

24. M.R. Mitchell, M.E. Meyer, and N.Q. Nguyen, "Fatigue Considerations in Use of Aluminum Alloys," SAE Special Publication P-109, Proc. of SAE Fatigue Conference, Detroit, Mich., April, 1982, pp. 249-272.

25. M.R. Mitchell, "Fundamentals of Modern Fatigue Analysis for Design," Fatigue and Microstructure, American Society for Metals, Metals Park, OH, 1979, pp. 385-437.

26. L.F. Coffin, "Fatigue in High Temperature - Prediction and Interpretation," Proc. Inst. of Mech. Eng'rs. 188, pp. 109-127, Sept. 1974.

27. J.M. Potter, "The Effect of Load Interaction and Sequence on the Fatigue Behavior of Notched Coupons," in Cyclic Stress-Strain Behavior Analysis Experimentation and Failure Prediction, ASTM STP 519, Am. Soc. Test Mater. pp. 109-132, 1973.

28. J.C. Chesnutt, A.W. Thompson, and J.C. Williams, "Influence of Metallurgical Factors on the Fatigue Crack Growth Rate in Alpha-Beta Titanium Alloys, AFML-TR-78-68, Air Force Materials Laboratory, Wright-Patterson AFB, OH, May 1978.

29. S.B. Charkrabortty, "Cyclic Ductility, Cyclic Strength and Fatigue Crack Propagation in Metals and Alloys," Technical Report 78-2, ONR Contract N00014-75-C-0349, May 16, 1978.

30. S.B. Charkrabortty and E.A. Starke, Jr., "Fatigue Crack Growth Behavior of Metastable Beta Titanium-Vanadium Alloys," presented AIME Annual Meetings, New Orleans, February 19, 1979.

31. R.O. Ritchie, International Metals Reviews, Vol. 24, 1979, pp. 205-230.

32. G.R. Yoder, L.A. Cooley and T.W. Crooker, J. Engr. Mater. Tech. 101, 86-90 (1979).

33. H.C. Heikkenen, "A Study of the Fatigue Behavior of an Al-6Zn-2Mg-0.1Zr Alloys," M.S. Thesis, Georgia Institute of Technology, November 1981.

34. J.C. Chesnutt, C.G. Rhodes and J.C. Williams, ASTM STP 600, American Society for Testing and Materials, 1976, pp 99-103.

35. J.E. Hack and G.R. Leverant, Met. Trans. S. Vol. 13A, 1982, pp 1729-1738.

6. Acknowledgments

The authors are grateful to Dr. N.E. Paton, Dr. J. A. Hall, Dr. C.H. Hamilton, W.M. Parris and C.G. Rhodes for valuable discussions. The assistance of Dr. S.B. Charkrabortty in transfering the predictive FCP computer program was greatly appreciated. R.A. Spurling, M. Calabrese, P.Q. Sauers, A.R. Murphy, and F.N. Nevarez provided invaluable experimental assistance.

7. Personnel

Dr. J.A. Wert, Physical Metallurgy Group
Program Manager
Principal Investigator on Part I

Mr. J.C. Chesnutt, Manager, Physical Metallurgy Group
Co-principal Investigator on Part II.

Dr. M.R. Mitchell, Materials Characterization Group
Co-principal Investigator on Part II.

8. Publications and Presentations

1. "Fatigue Crack Initiation Properties of Ti-6Al-4V," J.C. Chesnutt and M.R. Mitchell, TMS-AIME Fall Meeting, Louisville, Oct. 1981.

2. "Enhanced Superplasticity in Modified Ti-6TAl-4%V Alloys," J.A. Wert and N.E. Paton, Sixth International Conference on the Strength of Metals and Alloys, R.C. Gifkins ed., Pergamon Press, Oxford, 1982, pp. 727-732.

3. N.E. Paton and J.C. Chesnutt, "Micromechanics of Crack Propagation in Ti-6Al and Ti-6Al-4V," in Micro and Macro Mechanics of Crack Growth, K. Sadananda, ed., TMS-AIME, New York (1982).

4. "Fatigue of Titanium Alloys," M.R. Mitchell and J.C. Chesnutt, TMS-AIME Fall Meeting, St. Louis, Oct. 1982.

5. "Enhanced Superplasticity and Strength in Modified Ti-6Al-4V Alloys," J.A. Wert and N.E. Paton, TMS-AIME Fall Meeting, St. Louis, Oct. 1982.

6. "Enhanced Superplasticity and Strength in Modified Ti-6Al-4V Alloys," J.A. Wert and N.E. Paton, submitted to Metallurgical Transactions, April 27, 1983.

7. "Effect of Microstructure and Load Ratio in Titanium Alloys," J.E. Chesnutt and J.A. Wert, TMS-AIME Fall Meeting, Philadelphia, Oct. 1983.

9. Coupling Activities

1. J.A. Wert has presented the work on Enhanced Superplasticity and Strength in Modified Ti-6Al-4V Alloys to AFWAL/MLLS and to NAVAIR personnel.

2. Potential applications for the lower temperature superplastically formable alloys have been discussed with North American Aircraft Operations, the Rockwell Division responsible for B-1B production.

3. The prediction of fatigue crack propagation from low cycle fatigue properties complements AFOSR-sponsored work at Georgia Institute of Technology. Extensive discussions have been held with Dr. S.B. Charkrabortty and Prof. G.E. Starke.

4. Discussions have been held with Dr. J. Lankford and Mr. J. Hack at Southwest Research Laboratory and with Prof. R.O. Ritchie of University of California, Berkeley, concerning near threshold fatigue crack propagation behavior.

5. The work on fatigue crack propagation complements a concurrent study of fatigue crack propagation in CORONA-5, sponsored by NAVAIR.

END

FILMED

11-83

DTIC